JOURNAL OF ADVANCES IN

ENGINEERING AND TECHNOLOGY

Civil Engineering Electrical and Electronic Engineering Materials Engineering Mechanical Engineering Mechatronics Engineering Quantity Surveying

About the Journal of Advances in Engineering and Technology

The Journal of Advances in Engineering and Technology (JAET) is an international, open access, double blind peer-reviewed journal. It is published by the Faculty of Engineering of Sri Lanka Institute of Information Technology (SLIIT). The JAET aims at fostering research and development work in Engineering and Technology and bringing researchers on to a common platform. Furthermore, JAET will also accept review articles on appropriate subject areas including concept papers of academic opinions, book reviews, etc. for publication therein.

All correspondence should be addressed to:

Contents

Journal of Advances in Engineering and Technology (JAET)

Volume 1 Issue (2)-2023

Sri Lanka Institute of Information Technology
Malabe, Sri Lanka

Faculty of Engineering

Sri Lanka Institute of Information Technology (SLIIT)

Malabe, 10115, Sri Lanka

Notes to the Authors

Journal of Advances in Engineering and Technology (JAET) is a biannual peer review journal which aims at publishing original, theoretical and practice-oriented research papers related to Engineering and Technology. This journal provides a forum for researchers, scholars, academicians, and practitioners in the field of Engineering at international level to discuss and disseminate their findings in advanced and emerging technologies in Engineering.

Articles/ contributions should be sent to:

Editor-in-Chief
Journal of Advances in Engineering and Technology (JAET)
Faculty of Engineering
SLIIT, New Kandy Road, Malabe, Sri Lanka
E – mail: jaet@sliit.lk

- Your article will be subjected to a double-blind review process by two reviewers who are experts in their relevant field. In order to facilitate anonymous review process, you are requested to provide the title page separately.
- The title page should include the title of the article, your full name, affiliation, address, email and telephone/ mobile number.
- Recommendations of two reviewers are necessary for the publication of your article.
- The article should not exceed 6,000 words.
- Abstract should be between 150-200 words with 4-5 keywords.
- Article should include the following:
- Introduction to the research statement/ background to the research/ rationale
- Methods and Material
- Results and Discussion
- Conclusions and Recommendations
- References
- Footnotes can be numbered and given at the end of the article.
- Referencing should conform to the APA style.
- Tables/ graphs should be included in the appropriate places. Longer tables should be added at the end of the article as annexes.
- Use Times New Roman Fonts - Abstract 11pt; Article 11pt; Spacing Single

Evaluating the Effectiveness of Speed Humps Related to Speed Profile and Noise Profile

K.G. Dilanka Gamlath, Niranga Amarasingha
Faculty of Engineering, Sri Lanka Institute of Information Technology,
New Kandy Road, Malabe, 10115, Sri Lanka
dilankaseniya@gmail.com, niranga.a@sliit.lk

Vasantha Wickramasinghe
Faculty of Engineering, University of Peradeniya
Peradeniya, Sri Lanka.
vskw@eng.pdn.ac.lk

ABSTRACT

Speed humps are an effective traffic calming measure to improve the safety of road users. On the other hand, speed humps have certain drawbacks, such as increasing emergency response time, causing damage to cars, and high noise levels due to excessive traffic. These impacts further vary with different hump profiles. Thus, the primary objective of this research is to investigate how the geometric profile of speed humps affects vehicle speed and noise level. The secondary objective is to find the Level of Service in the presence and absence of a speed hump by using VISSIM microsimulation. In this study, Lake Drive Road, Nawala, was selected with four different speed hump profiles. The Sound Meter smartphone application was used for noise monitoring. A drone camera footage was utilized to capture vehicle flows while speed trajectories of each vehicle were developed using tracking software. The developed speed profiles were used for the simulation purpose. Then, a Multiple Linear Regression (MLR) model was developed and validated to predict the hump height for the desired speed reduction and desired noise level for each selected four-vehicle category. Further, the average noise levels were found to be higher than the Central Environmental Authority's permissible noise level, and it increases with the height of the hump. It was also observed that as the height of the hump increases, vehicle speed decreases. The largest speed reduction, 42.13 %, was observed in passenger cars, while the lowest speed reduction, 23.5 %, was observed in motorcycles. Therefore, speed analysis findings reveal that passenger cars have a significant speed reduction when compared to other categories. However, the average speed reduction for all vehicles was identified as 33.85 %, and VISSIM simulations revealed that the average Level of Service (LOS) drops to LOS C from LOS A due to the presence of the speed hump.

KEYWORDS: *Level of Service, Speed hump profile, Speed hump, VISSIM*

1   INTRODUCTION

Traffic calming devices play a prominent role in the present day. With the rise in the preference of private vehicles, it is necessary to implement traffic calming devices to increase safety of road users. These devices are used to maintain a balance between road traffic and other road users. Placing a traffic calming device in an inconvenient position would not solve the problem of roadways. It can reduce human efficiency and have several negative consequences for road users, such as car damage and wear and tear over time, a delay in emergency response time, and increased road noise (Kiran et al., 2020). Therefore, the main objective of the study is to build two regression models to predict the vehicular speed and the noise level as a function of hump characteristics. Then, using a simulation model, the LOS due to the presence and absence of the speed hump is measured. Since limited research on the impact of hump characteristics on driver behavior has been conducted in Sri Lanka, the created model may serve as a guide for the future development of speed humps.

2   LITERATURE REVIEW

2.1 Literature study of speed analysis

Numerous implementations and attempts at speed analysis for various hump profiles have been made by previous researchers. The main distinguishing feature among these studies is the method used to detect the speed of the vehicle. The findings of the speed analysis literature are summarized in Table 1.

Table 1: Summary of the previous speed analysis studies

Author	Method Used	Gap
Kiran et al., 2020	-A speed radar gun was utilized - Measured speed range: -100m to 80m from the speed hump. -Vehicle categories: two-wheelers, four-wheelers, and multi-axle vehicles, light commercial vehicles, and auto vehicles	Incapable of measuring the speed of the same vehicle at several points.
Mustafa et al., 2019	- A speed radar gun was utilized - Measured speed range: -20 m to 20m from the speed hump - Vehicle categories: motorcycles, cars, buses and lorries.	Incapable of measuring the speed of the same vehicle at several points.
Rosli and Hamsa, 2019	- A speed radar gun was utilized - Six identical hump profiles were selected - Speed measured at the speed hump	Unable to analyse the speed hump effect on vehicular speed whereas it can only be compared with the different speed profile characteristics.
Arthanayake et al., 2020	- A drone camera was used to capture the footage, and Tracker software was used to extract the speed measurements	The study was conducted for only one specific speed hump.
Gupta, 2014	- A speed radar gun was utilized - Measured speed range: 10m, 7m, 5m, and 2m (left and right side of the hump).	Data has been collected for only two vehicle categories.
Kadar et al., 2013	-Only the vehicle count was observed. - Data processing has been done at 30-minute intervals over a 12-hour duration, from 7:00 am to 7:00 pm. - They have collected data for four categories.	There is no speed analysis. Only the traffic volume was considered.
Antić *et al.*, 2013	- A speed radar gun was utilized - Speed measurements were taken before speed bump installation, one day and one month after the installation of the speed bump. - Measured speed range: 40 meters before, after, and at the speed bump.	Installation is more expensive and requires approval from several departments.
Teja et al., 2017	- Video camera technique was used to measure the vehicle speed. - Every 15 minutes, volume counts have been obtained. - Measured speed range: 10 m, 7 m, 4 m, and 1 m before and after the speed breaker.	This approach is ineffective when compared to the speed gun measurement.

Source: (Literature Sources)

2.2 Literature study of noise level analysis on speed humps

Previous researchers have attempted and implemented several noise analysis methods for different hump characteristics. The technique they utilized to determine the vehicle's noise level is the primary feature that differentiates them from one another. The findings of the noise analysis literature are summarized in Table 2.

Table 2: Summary of the previous noise analysis studies

Author	Method Used	Gap
Mustafa et al., 2019	- The noise level meter was placed at an elevation of 1.2m from the ground level. - Every 15 minutes, the noise level, has been recorded. - Used a comparison with average speed.	No comparison with the speed measurement.
Kadar et al., 2013	- Noise level meter placed at 1m depth from the ground level. - For about 12 hours, the noise intensity was calculated at 15-minute intervals. - A comparison was made with traffic volume	The average noise level was not measured.
Wewalwala et al., 201	- The sound level meter has been installed on a stand 1.5 meters from the ground floor, 1.0 meters from the outer driving lane side. - Two different sets of measurements were used. - Vehicle categories: Passenger cars, passenger vans, three-wheelers, bicycles, and lorries	Only one road was selected for noise measurement. No comparison was made with speed measurement.

Source: (Literature Sources)

2.3 Literature study of speed hump models

Several speed hump models have been developed and utilized in the past for a variety of objectives. The majority of studies simulated the speed hump using VISSIM software. Table 3 summarizes some of the previous literature related to speed hump simulations.

Table 3: Summary of the previous simulation models

Author	Method Used	Gap
Chimba et al., 2019	- VISSIM microsimulation was used to simulate individual vehicle motions to measure traffic efficiency. - Reduced Speed Area (RSA) tool was used to simulate the speed hump.	The model has not been calibrated.
Kiran et al., 2020	- VISSIM microsimulation was used to simulate individual vehicle motions to measure traffic efficiency. - RSA tool was used to simulate the speed hump. - Two models (with humps & without humps) were developed for each stretch and results were tabulated	The study was conducted only for a one-speed hump.
Nair et al, 2013	-In this study, the impact of speed restriction measures on road safety and level of service has been measured. -RSA tool has been used to simulate the Speed hump	Use of the speed gun to measure the speed is not effective when compared to the video camera technique.

Source: (Literature Sources)

3   METHODOLOGY

In the modern world, with the growing population and advancements in the transportation field, the use of private vehicles for mobility has become very common. In this situation, traffic calming devices play a prominent role in the present day. Traffic calming devices such as road humps contribute to the enhancement of living conditions by reducing vehicle accidents and ensuring the surrounding environment is safe from possible collisions. However, placing a speed hump in a random location does not resolve the issue of highways entirely. It may have downsides such as increasing emergency response time, causing damage to cars, increasing noise levels, and causing discomfort for drivers (Tester *et al.*, 2004). Therefore, the main objective of the study is to perform a speed analysis and obtain a regression model to predict the profile of the speed hump for the desired speed reduction as well as

the desired noise level for each of the selected four vehicle categories. Furthermore, the Level of Service in the presence and absence of a speed hump was observed using VISSIM modeling software. Lake Drive Road in Nawala has been chosen for this study. For speed observation, all the vehicles have been categorised into four vehicular categories like category A for two-wheelers, category B for three-wheelers, category C for passenger cars, and category D for MSVs. For noise observation, all the vehicles have been categorised into five vehicular categories like category A for motorcycle, category B for three-wheelers, category C for passenger cars, category D for MSVs, and category E for MGVs. For the speed data collection, several methods had been adopted by past researchers such as speed measuring through speed guns (Kiran, Kumar, et al, 2020), analyzing traffic speed patterns using a video camera (Teja et al, 2017), and utilizing a drone camera (Arthanayake et al, 2020). By considering the pros and cons of such methods, the droner camera has been chosen as the best method for data collection. Therefore, a video camera mounted on a drone was utilized for the primary data collection. The "Tracker" application was used to obtain the speed data, and the VISSIM modeling software was used to demonstrate the presence and absence of the speed hump. The noise level was determined using the "Sound Meter" application, which rated 4.8 out of 5 in Google Play Store. Here, a selected road section is required to reduce external factors that led to the decrease in vehicular speed. Therefore, by considering several factors Lake Drive Road was selected with varying speed hump profiles for the primary data collection in the Western Province, Sri Lanka.

3.1 Selection of the location

The major purpose of site selection was to reduce external factors that led to the reduction of the vehicular speed. The Lake Drive Road, Nawala route was selected for this study since this road has an average traffic density during off-peak hours, ensuring that a vehicle's motion is not disrupted by other cars. Here four different hump profiles were selected as shown in Figures 1-4 for speed measurements and three different hump profiles were selected for noise level measurement. The characteristics of those different hump profiles are shown in Table 4.

Figure 1: Seed Hump 1

Figure 2: Speed Hump 2

Figure 3: Speed Hump 3
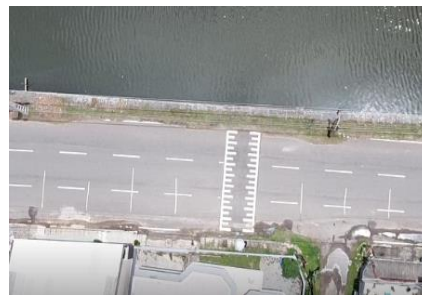
Figure 4: Speed Hump 4

Table 4: Speed Hump Characteristics

No	Height(mm)	Width (m)
Hump-1	70 mm	8.75 m
Hump-2	85 mm	9.21 m
Hump-3	100 mm	7.31 m
Hump-4	90 mm	8.46 m

3.2 Collection of speed measurement data

A drone camera was used to measure the speed of the vehicles since it can be used to determine the speed of a vehicle at any point utilising Tracker software, whereas a speed gun is only capable of determining the speed of a vehicle at one location. Here data were collected on Saturday from 11.00 am to 12.30 pm. Firstly, 5m markings were labelled on the road with a range of 30m as shown in Figure 5.
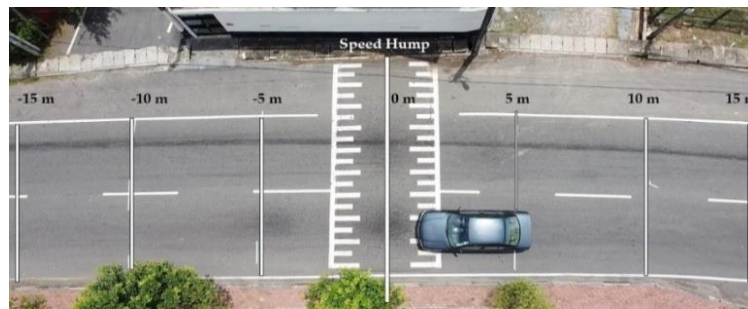
Figure 5: Labelled 5m markings before and after the speed hump

After, using a drone camera, video footage was recorded for four different hump profiles. Then, using the Tracker software, the speed for each of the four vehicle categories (bikes, three-wheelers, cars, and Medium Size Vehicles (MSV)) was extracted.

3.3 Collection of Noise measurement

For the Noise measurement, the "Sound Meter" application which has 4.8 ratings out of 5 was used. Here a smartphone was placed 1m above the ground level and 7m apart from the hump to capture the noise level as shown in Figure 6.

Figure 6: Smartphone placed on a tripod to obtain the noise level

3.4 Develop a simulation model

Two models were developed using the microsimulation program VISSIM which were created to demonstrate the real-time behaviour of vehicles in the presence of humps as well as

to understand the behaviour of vehicles in the absence of speed humps. The Speed hump with a height of 90mm was selected for the VISSIM simulation. Vehicle behaviour in this region was calibrated in terms of delays and queue length. Those values were taken from a study done by Gunarathne et al. (2021) in the same area. Figure 7 depicts the outcome of the simulation.

3.5 Data analysis

Two multiple linear regression models were developed to predict the speed reduction and the noise level as a function of the height of the speed hump. The dependent variable was speed reduction (%) for the first model, whereas the independent variables were hump height, hump width, and vehicle type. Noise level (dB(A)) was used as a dependent variable in the second model, whereas hump height, hump width, and vehicle type were used as independent variables. SPSS software was used for data analysis. For the speed data analysis, 320 vehicles were considered, whereas 225 vehicles were considered for the noise data analysis. Both the noise and speed reduction models were validated primarily by verifying the assumptions. The equation for multiple linear regression is similar to that of basic linear regression, except for the additional terms.
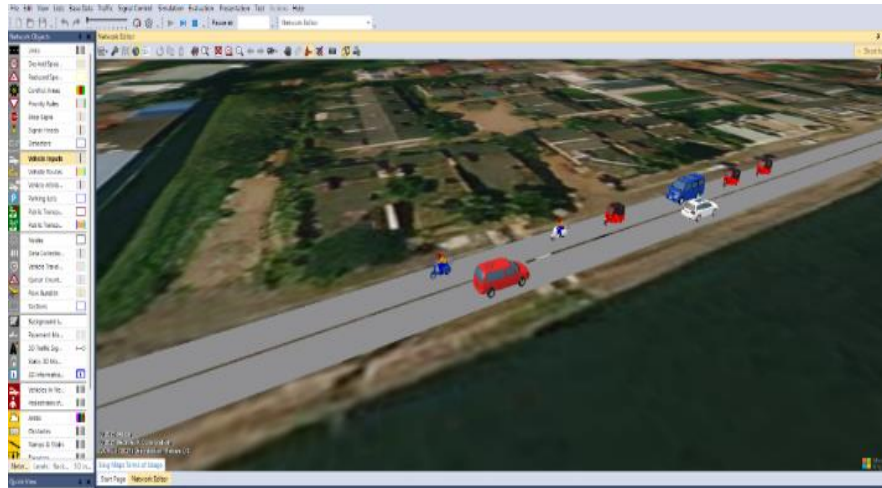
Figure 7: 3D view of the simulation

4 RESULTS AND DATA ANALYSIS

4.1 Findings of speed measurements

Figure 8 shows the average vehicle speed for each vehicle category between -15m and 15m from the speed hump. Here the yellow line on the graph represents the vehicle's speed variation on the highest hump height, which is 100mm, and the green line represents the vehicle's speed variation on the lowest hump height, which is 70mm. As shown in Figure 8, for all the four vehicle types, the height of the hump rises, while the speed of each vehicle decreases. Here, for motorbikes, the speed reduction percentages for hump heights of 70mm, 85mm, 90mm, and 100mm are 13.6 %, 14.08 %, 20.73 %, and 22.04 %, respectively. Therefore, it is clear that as the height of the hump rises, the speed reduction is increased. Also, the average speed reduction for motorcycles, three-wheelers, cars, and MSVs are 17.62 %, 22.67 %, 34.38 %, and 30.64 %, respectively. Therefore, it can be observed that cars have a higher speed reduction which is 34.38% while motorcycles have the lowest speed reduction which is 17.62 % owing to the speed hump. Then, the average speed reduction due to all four humps was identified as 26.33 %. Further, cars have the highest speed regain percentage which is 34.38%, whereas motorcycles have the lowest speed regain percentage, which is 17.62%. Finally, based on observed data, none of the vehicles exceeded the allowed speed limit of 40 km/hr due to the presence of the speed hump. As a result of the hump's placement, it will become more secure for both residents and drivers.
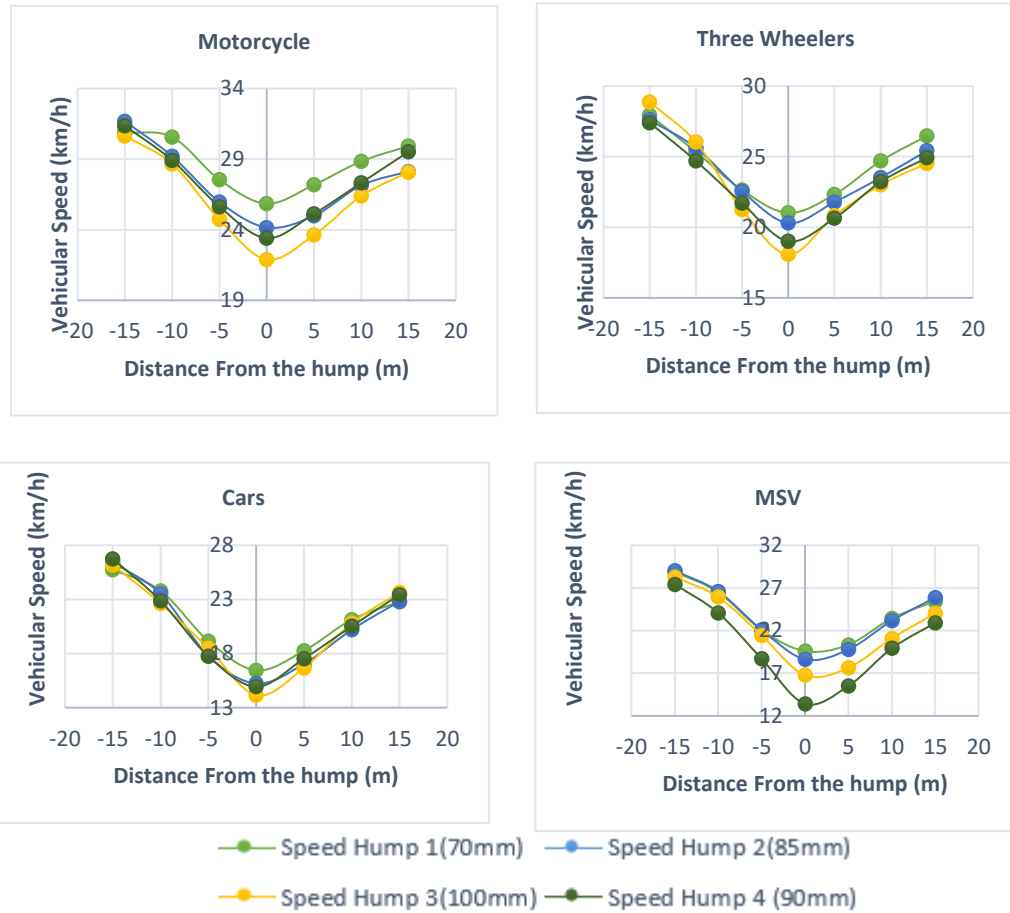
Figure 8: Speed Variation due to different hump profile for the four vehicle categories

4.2 Findings of the noise measurements

Figure 9 represents the average noise level variations derived by observing three different hump profiles.

It clearly shows that when the height of the hump increases, the noise level also increases. Further, it was observed that Medium Good Vehicles (MGV) have the highest average noise level, which is 78.82 dB(A) for the hump-1, 78.59 dB(A) for the hump-2, and 80.63 dB(A) for the hump-3. At the same time, the passenger cars have the lowest average noise level, which is 71.06 dB(A) for the hump-1, 71.98 dB(A) for the hump-2, and 72.81 dB(A) for the hump-3. The maximum allowable noise level established by the Central Environmental Authority is shown in Table 5 (Srimani, 1996). Here, it was identified that the measured average noise level for these five vehicle categories exceeded the Central Environmental Authority's permissible noise level.

Table 5: Maximum permissible noise level (Srimani, 1996)

LAeq, T (Average of the total sound energy (Leq) measured over a specified period of time (T)		
Areas	Day Time	Night-time
Rural Residential Area	55	45
Urban Residential area	60	50
Mixed Residential Area	63	45
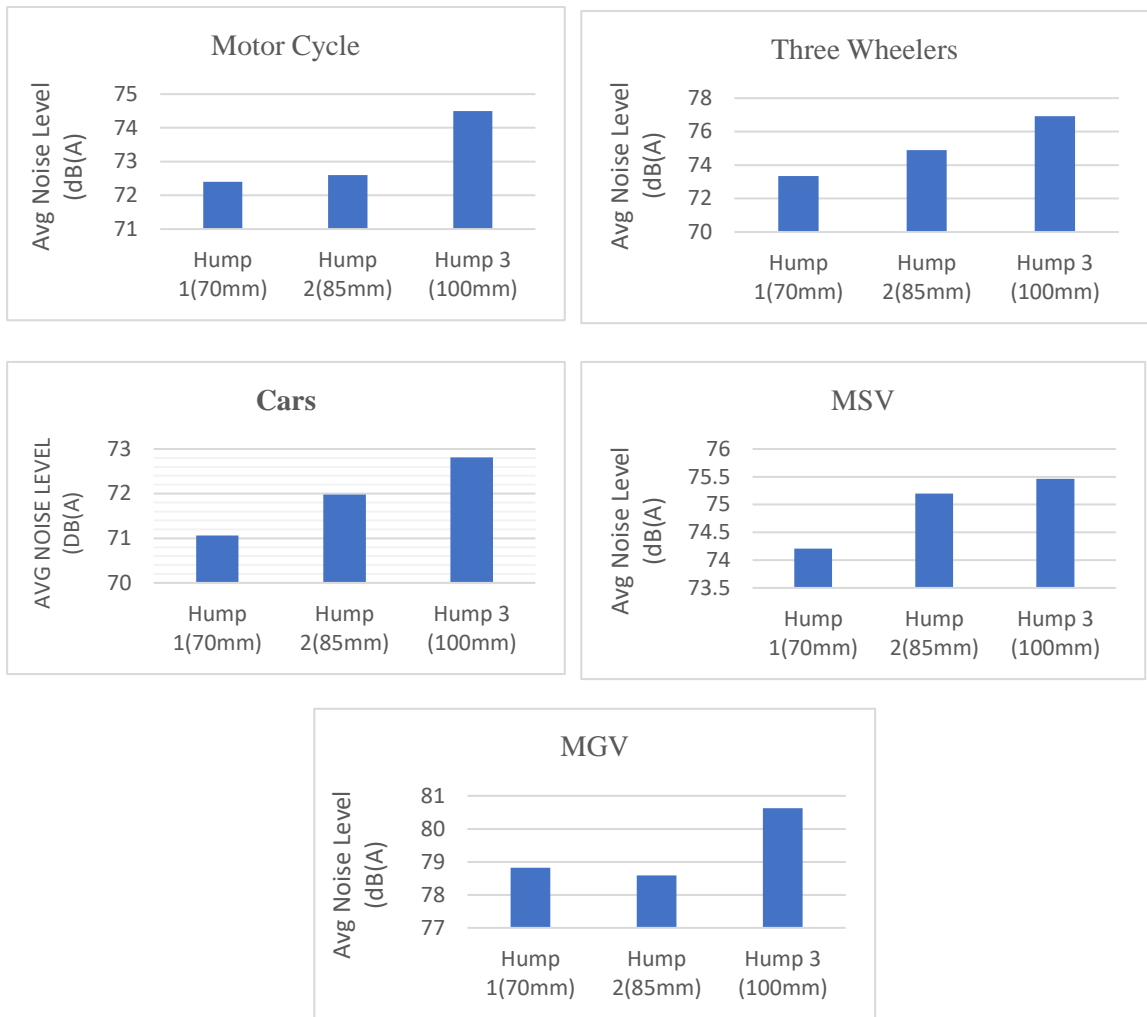
Figure 9: Average Noise level on the hump in different vehicles categories

4.3 Findings of the VISSIM simulation

In this instance, two models were developed for the presence and absence of the speed hump in order to identify the driving behaviour influenced by the speed hump. The model was calibrated using the queue length of the selected area. The existence of the speed hump indicates that LOS C is for Westbound and LOS B is for Eastbound, which has a lower degree of freedom as shown in Table 6.

Table 6: Existence of speed hump

Link No	QLen	QLenMax	Vehicles	LOS
Westbound	5.36 m	66.13 m	477	LOS C
Eastbound	2.70 m	72.20 m	465	LOS B
Average	403 m	72.20 m	942	LOS C

The absence of a speed hump, Both Westbound and Eastbound have LOS A, which is an excellent road operating condition as shown in Table 7.

Table 7: Absence of speed hump

Link No	QLen	QLenMax	Vehicles	LOS
Westbound	0.0 m	0.0 m	479	LOS A
Eastbound	0.0 m	0.0 m	467	LOS A
Average	0.0 m	0.0 m	946	LOS A

According to the acquired data, the presence of a speed hump has a detrimental effect when compared to its absence because it increases traffic congestion and decreases the degree of freedom on the road. In conclusion, the existence of the speed hump has increased the safety of the drivers and residents. However, the effect of noise and driver delay time have increased. Thus, prior to constructing the speed hump, it is recommended to determine the desired speed of the road and the noise limit. In this instance, the noise emission model and the speed reduction model will aid future designers in designing the road humps.

4.4 Data Analysis

Here, two distinct multiple linear regression models were developed for speed reduction as well as the noise level. Table 8 shows the variables that were collected. In this section, the development of those two models is discussed. SPSS software was utilized to conduct the analysis since it was recommended in previous literature.

Table 8: Collected variables

Factors	Type of variable
Type of vehicle	Independent
Height of the speed hump	Independent
Width of the speed hump	Independent
Speed Reduction %	Dependent
Noise Level dB(A)	Dependent

4.4.1 Noise data analysis

The parameter estimates summarize the effect of each predictor. Here for covariates (B), Positive coefficients show positive correlations between predictors and outcome for covariates. Here, the p-value was 0.287 (> 0.05) for the width of the hump, it denotes that it is not Statistically significant and indicates strong evidence for the null hypothesis. Therefore, the model was refitted by removing the width of the speed hump. The fitted model result is listed in Table 9.

Table 9: Parameter estimation of Noise Analysis

Parameter	B	std Error	Lower	Upper	Wald Chi-Square	df	Sig.
(Intercept)	67.228	1.1318	65.010	69.446	3528.534	1	.000
MGVs	6.191	.4908	5.229	7.153	159.099	1	.000
MSVs	1.800	.4908	.838	2.762	13.449	1	.000
Cars	-1.207	.4908	-2.169	-.245	6.044	1	.014
Three wheelers	1.899	.4908	.937	2.861	14.963	1	.000
Bikes	0^a	.	.	.	.	.	.
Hump height(mm)	.070	.0127	.045	.095	30.276	1	.000
(Scale)	5.421^b	.5111	4.506	6.521			

Then, the following equations (Equations 1-5) were obtained from the model. Here, NL denotes the noise level in decibels (A), while H denotes the speed hump height in millimeters.

$$\mathbf{NL_{MGVs}} = 6.191\,(1) + 0.07\,(H) + 67.288 \tag{1}$$

$$\textbf{NL}_{\textbf{MSVs}} \quad = 1.80 \ (1) + 0.07 \ (H) + 67.288 \qquad (2)$$
$$\textbf{NL}_{\textbf{Cars}} \quad = -1.207 \ (1) + 0.07 \ (H) + 67.288 \qquad (3)$$
$$\textbf{NL}_{\textbf{TW}} \quad = 1.899 \ (1) + 0.07 \ (H) + 67.288 \qquad (4)$$
$$\textbf{NL}_{\textbf{Bikes}} \quad = 0.07 \ (H) + 67.288 \qquad (5)$$

4.4.2 Speed data analysis

Here the p-value is 0.775 (> 0.05) for the width of the hump indicates that it is not statistically significant and denotes strong evidence for the null hypothesis. Therefore, a refitted model was developed by removing the width of the speed hump. The fitted results are listed in Table 10.

Table 10: Parameter estimation of Speed Analysis

Parameter	B	Std Error	Lower	Upper	Wald Chi-Square	df	Sig.
(Intercept)	-9.680	5.6935	-20.839	1.479	2.891	1	.089
MSVs	16.300	1.9725	12.433	20.166	68.281	1	.000
Cars	17.465	1.9539	13.635	21.294	79.889	1	.000
Three wheelers	6.070	1.9600	2.229	9.912	9.592	1	.002
Bikes	0ª	.	.	.	.	.	.
Height of the Hump	.388	.0640	.263	.514	36.747	1	.000
(Scale)	153.665ᵇ	12.1673	131.576	179.462			

Then, using the created model, the following equations (Equations 6-9) were obtained. Here, SR denotes the speed reduction %, while H is the height of the speed hump in millimeters.

$$\textbf{SR}_{\textbf{MSVs}} \quad = 16.3 \ (1) + 0.388 \ (H) - 9.680 \qquad (6)$$
$$\textbf{SR}_{\textbf{Cars}} \quad = 17.465 + 0.388 \ (H) - 9.680 \qquad (7)$$
$$\textbf{SR}_{\textbf{TW}} \quad = 6.070 \ (1) + 0.388 \ (H) - 9.680 \qquad (8)$$
$$\textbf{SR}_{\textbf{Bikes}} \quad = 0.388 \ (H) - 9.680 \qquad (9)$$

4.5 Checking Model Assumptions

In this section, the assumptions of the developed multiple regression model are tested. Then the model was validated using sample data by comparing the obtained sample values to the model predicted values. The following assumptions were tested.
1. The dependent variable is normally distributed, and it is a continuous variable
2. Contain two or more independent variables
3. Independence of observations
4. The variance of the residuals is constant
5. A linear relationship between the dependent and the independent variable
6. This test does not have any multicollinearity
7. Check the significant outliers and highly influential points
8. The residuals are approximately normally distributed

As a result, the dependent variable is normally distributed, then the first assumption is satisfied. Also, there are three independent variables included in the test; therefore, it satisfies the second assumption of the multiple linear regression. Additionally, the residuals are independent in this model, and the Durban Watson values obtained were 2.172 and 2.086 for noise analysis and speed analysis,

respectively, which are closer to 2. Therefore, the third assumption was satisfied. Here, the relationship between the independent and dependent variables is linear; additionally, the plot of standardized residuals vs. standardized predicted value shows no apparent signs of funneling, and the VIF score is well below 4, indicating that there are no issues with multicollinearity in the model, implying that the fourth, fifth, and sixth assumptions were met. Finally, no significant outliers were identified, and the residuals are approximately normally distributed. Thus, all MLR assumptions were satisfied for the obtained two models.

5   DISCUSSION

After collecting the data, two MLR models were created to predict the speed reduction and noise level, as a function of the hump height, and all assumptions were checked. Subsequently, the obtained regression models were validated.

Here, it was observed that, when the height of the hump increases, there is a decrement of vehicular speed but an increasement in the noise level. Also, it was observed that average speed reduction for the motorcycle, three-wheelers, cars, and MSVs are 17.62 %,22.67 %, 34.38 %, and 30.64 %. Therefore, passenger cars have a more significant speed reduction when compared to other vehicles. Further, it was identified that the noise level at the speed hump exceeded the permissible noise level according to the Central Environmental Authority guidelines, Sri Lanka, and also it was observed that MGVs have the highest average noise level, whereas passenger cars have the lowest average noise level for each selected hump profile. Finally, the VISSIM simulation shows that the existence of the speed hump reduces the average level of the service of the road from LOS A to LOS C. Therefore, it was identified that the presence of a speed hump has a detrimental effect compared to its absence.

6   LIMITATION AND RECOMMENDATIONS

The experimental findings indicate that the hump's height substantially impacts both speed reduction and noise levels around the hump. This research examined about 30m range while speed data collecting. To obtain the maximum reduction in speed, it is recommended to utilize a larger area. Additionally, vehicle speeds may vary significantly depending on road conditions as well as the time of day. Also, the speed of the vehicle could also vary depending on the signboard prior to the speed hump and the presence of speed hump markings. For this study, there were no signboards identified before the speed hump, and only markings were present on the speed hump. In general, the differences in hump profiles have a substantial effect on vehicle speed. Here the average noise level was found to be greater than the permitted level. It caused a serious issue for those who live near the road. However, the noise level measurement method using a smartphone is not very accurate. Further corrections for background noise and vehicle engine noise need to be done in future studies. Therefore, a proper investigation is recommended prior to installing speed humps. Since limited research on the impact of hump characteristics on driver behavior has been conducted in Sri Lanka, the created model may serve as a guide for future improvements of the speed hump.

7   CONCLUSIONS

This research was conducted in the residential area of Lake Drive, Nawala. A drone camera was used to gather speed data, and vehicular speed was measured between -15m and 15m from the speed hump's center. The spotted speed was extracted using a tracker software, and the noise level was measured using a smartphone application. Then, two MLR models were created to predict the vehicle's desired speed reduction and noise level in terms of hump height. These connections offer field engineers with a valuable tool for designing hump shapes for speed control as well as noise control. The paper's primary results revealed that the vehicle speeds decreased as vehicles reached each road hump. Also, the average speed observed was less than the permissible speed limit on this road. Additionally, the observation showed that passenger cars had a higher percentage of speed decrease than other vehicles. Here it was identified for all categories, a 10mm increase in the height of the speed hump reduces the speed by 3.88 % as well as for all categories, a 10mm increase in the height of the speed hump increases the noise level by 0.7 dB(A). Moreover, MGVs generate the highest noise level on average, while

passenger vehicles generate the least noise level on average for each of the chosen hump profiles. Additionally, it was observed that the noise level surpassed the acceptable limit set by the Sri Lanka Central Environmental Authority. Consequently, it will cause long term harm and disruptions to the people who live near the residential road in the long run. Finally, it was observed that the average LOS dropped to LOS C from LOS A due to the presence of the speed hump. Also, it was observed, a minor difference in hump height, increases the driver's delay time and the noise level near the speed hump significantly. Therefore, it is suggested to follow a guideline prior to constructing a speed hump. Finally, it can be concluded that the objectives of the research were accomplished.

8   ACKNOWLEDGEMENT

REFERENCES

Antić, B. et al. (2013) 'The influence of speed bumps heights to the decrease of the vehicle speed - Belgrade experience', *Safety Science*, 57, pp. 303–312. doi: 10.1016/j.ssci.2013.03.008.

Arthanayake, C. and Wickramasinghe, V. (2020) 'Effects of speed humps on driver behaviour'.

Chimba, D. and Mbuya, C. (2019) 'Simulating The Impact of Traffic Calming Strategies final report', TRCLC 17-10, Transportation Research Center Reports. 42. Available at: https://scholarworks.wmich.edu/transportation-reports/42.

Gunarathne D., Amarasingha N., and Wickramasinghe V., (2021) *Effect of the Traffic Flow with Change in Time on Driver Behavior Parameter Values in Micro-Simulation*. The 14th International Conference of Eastern Asia Society for Transportation Studies (EASTS) in Hiroshima, Japan.

Gupta, A. (2014) 'Study on Speed Profile Across Speed Bumps', Doctoral dissertation, National Institute of Technology Rourkela, pp. 1–43.

Kadar, H. and Rosli, N. (2013) 'Evaluating The Effects of Road Hump on Traffic Volume And Noise Level At Taman Keramat Residential Area, Kuala Lumpur', Journal of the Eastern Asia Society for Transportation Studies, 10, pp. 1171–1188. doi: 10.11175/easts.10.1171.

Kiran, K. R., Kumar, M. and Abhinay, B. (2020) 'Critical Analysis of Speed Hump and Speed Bump and Geometric Design of Curved Speed Hump', Transportation Research Procedia, 48(2018), pp. 1211–1226. doi: 10.1016/j.trpro.2020.08.144.

Kiran, K. R., Molugaram, K. and Sandeep, M. (2020) 'Analysis of Speed Profiles at Speed Hump under Various Dimensions & Simulating their LOS Using VISSIM', *Transportation Research Procedia*, 48, pp. 1200–1210. doi: 10.1016/j.trpro.2020.08.143.

Mustafa, N. A, and Kadar Hamsa A.A. (2019) 'Evaluating the Effects of Road Hump on Speed and Noise Level at a University Setting', In *Proceedings of the Eastern Asia Society for Transportation Studies*, 12.

Nair, P. M., Bindhu, B. K. and Elangovan, T. (2013) 'Impact analysis of speed restriction measures using VISSIM 5.40', 2(1), pp. 303–310.

Rosli, N.N.A. and Hamsa, A.A.K., (2019) Evaluating the Effects of Road Hump on The Speed of Vehicles in an Institutional Environment. In Proceedings of the Eastern Asia Society for Transportation Studies 12.

Srimani, A. (1996) 'The National Enviornment Al Act, No. 47 Of 1980 Regulations', Modern at

large: Cultural dimensions of globalization, (47). Available at: http://dx.doi.org/10.1016/j.cirp.2016.06.001%0Ahttp://dx.doi.org/10.1016/j.powtec.2016.12.05 5%0Ahttps://doi.org/10.1016/j.ijfatigue.2019.02.006%0Ahttps://doi.org/10.1016/j.matlet.2019. 04.024%0Ahttps://doi.org/10.1016/j.matlet.2019.127252%0Ahttp://dx.doi.o.

Teja, T. and Jyothi, M. (2017) 'Speed Profile Analysis at Speed Breakers on An Urban Road', i-manager's Journal on Civil Engineering, 7(1), p. 25. doi: 10.26634/jce.7.1.10370.

Tester, J. M. *et al.* (2004) 'A Matched Case-Control Study Evaluating the Effectiveness of Speed Humps in Reducing Child Pedestrian Injuries', American Journal of Public Health, 94(4), pp. 646–650. doi: 10.2105/AJPH.94.4.646.

Wewalwala, S. and Sonnadara, U. (2012) 'Traffic Noise Enhancement due to Speed Bumps', Sri Lankan Journal of Physics, 12(0), p. 1. doi: 10.4038/sljp.v12i0.3155.

Strategies Used by the Sri Lankan Construction Industry to Overcome the Challenges Posed by the Covid-19

Piyumi Fernando
Liverpool John Moores University, United Kingdom
piyumifernando230@gmail.com

Nishanthi Gunarathna
Sri Lanka Institute of Information Technology, Malabe, Sri Lanka
nishanthi.g@sliit.lk

ABSTRACT

The global outbreak of the COVID-19 pandemic has thrown the world's political, social, economic, religious, and financial structures into disarray. COVID-19 has a broad range of effects on numerous industries, including construction. Sri Lanka as a developing country is also affected by the pandemic and many sectors of the Sri Lankan economy such as construction, education, tourism, imports and exports, agriculture, and health etc are experiencing negative consequences of the pandemic, Construction industry as one of the key sectors of the economy was also severely affected by the COVID-19 global pandemic in various ways. Construction companies and government institutes are taking action to face these challenges. This study describes how COVID-19 impacts the local construction industry throughout the construction process. Furthermore, the impact was evaluated with regard to several aspects namely, financial, human resources, supply chain and logistics, legal, and completion and handover of the project. The strategies which are used by the construction industry participants to face the challenges of the pandemic are also discussed. A mixed research approach was used in the study and questionnaires which comprised of both qualitative and quantitative questions were used as a data collection tool. This research revealed new knowledge about the construction industry in relation to the COVID-19 pandemic. The study's most important finding was that the spread of the virus influenced the entire construction process. The pandemic had a major impact on the construction stage as well as the human resources aspect of the industry.

KEYWORDS: *COVID-19, Construction Industry, Sri Lanka, Strategies*

1   INTRODUCTION

The COVID – 19 epidemic has been the world's most serious health emergency in the recent past. Many nations have entered deep recessions, and many global value chains have been severely disrupted as a result of demand and, in some cases, supply shocks, which have sent reverberations across supply chains with negative multiplier and accelerator effects (Tumwesigye et al., 2020). According to Tumwesigye et al., 2020 current economic recession is the most catastrophic synchronized global economic downturn since the Great Depression, which extended over 216 nations and territories worldwide. As of 12th October 2021, there have been 237,655,302 confirmed COVID-19 cases, with 4,846,981 deaths worldwide (World Health Organization, 2021).

The virus's influence on society and the economy can be seen in the worldwide lockdowns, labour mobility restrictions, travel bans, airline suspensions, and, most notably, the economic slowdown (Shafi et al., 2020). Three transmission channels are predicted to account for economic losses in the global economy: supply chain, demand, and the financial sector. Businesses, local consumption, and foreign commerce will all suffer as a result of these channels (Aladejebi, 2020).

Global economy relies heavily on construction. The impact of COVID-19 pandemic on the construction industry is unprecedented (Fairlie, 2020), regardless of the scale of its operation. The construction industry, which has always been a major contributor to the local economy, was also forced

to slow down. It is evident that, almost every construction project got delayed or disrupted as a direct result of the pandemic. All plans and projects have been postponed until further notice (Gamil and Alhagar, 2020). According to Shibani et al., 2020, in the UK, COVID-19 has had a considerable impact on the construction sector, resulting in the cancellation of several projects and the extension of others. As a result, building businesses have suffered significant losses due to people's unwillingness to invest in residential construction or commercial development. Furthermore, Shibani et al., 2020 claimed that due to a shortage of funds from clients and banks, construction companies are experiencing financial difficulties and the pandemic has caused several projects to be halted owing to the scarcity of building supplies because of the lockdown, which rendered supply chain bottlenecks.

According to the Central Bank of Sri Lanka (CBSL), COVID-19 posed a considerable impediment to the delivery of services and development activities related to the country's economic and social infrastructure. The island-wide lockdown had a significant impact on public transportation and the ports sector was also damaged by the global logistics chain difficulties that resulted from the global adoption of lockdown measures (Central Bank of Sri Lanka, 2020). Despite having a negative Gross Domestic Product (GDP) growth rate of 3.6 % in 2020, Sri Lanka slowly and steadily recovered from the adverse scenario. The country has managed to secure a GDP growth rate of 4.3% in the 1st Quarter of 2021 (Department of Census and Statistics, Sri Lanka, 2021). However, once again with the sudden outbreak of the 3rd wave in late April 2021, the construction industry began to contract towards the 3rd Quarter of 2021. As per the recent statistics, GDP from the Construction Industry decreased to 137,391 LKR million in the 2nd Quarter of 2021 from 154,286 LKR million in the 1st Quarter of 2021. This illustrates the downfall of the country's economy due to the impact of the pandemic.

To contain the spread of the virus, several government restrictions and laws have been implemented, which unfortunately have a negative influence on the construction sector. Interruption of the supply chain and resources, project quarantine because of positive cases, project delays, and terminations are only a few of the consequences (Hansen, et al., 2021). Significant delays and disruption of construction activities have a negative impact on both the contractor and the client. Many labourers had to abandon construction sites and look for other sources of income. Contractors now have an extra burden ensuring workforce safety, while maintaining the smooth flow of work. In relation to the adverse economic impact, cash inflows to the contractors were restricted, leading to more financial issues. Also, many small-scale construction sites came to a standstill. Even though many sectors have embraced online job execution, building projects cannot be completed online since employees must be present on-site to achieve productivity (Amoah, et al., 2021). According to Pathirana, 2021, most existing projects have been suspended or postponed, and local clients and contractors are operating their companies with insufficient financial reserves, positioning them in difficult situations and exposing their market shares to rivals. It is critical that debts to suppliers are paid on time to maintain an uninterrupted supply chain and continue the work process.

To overcome this situation many regulations have been newly imposed on construction projects by the Construction Industry Development Authority (CIDA), which is the industry regulator in Sri Lanka. According to this, social distancing, dividing shifts, disinfecting the premises, working from home, limiting non-essential activities, monitoring people's health, and quarantine are newly added precautions and unfortunately, those measures are not favorable for the construction sector (Vithana et al., 2020). Maintaining a minimal carder on-site with required distances, accommodations, and spending on additional Personal Protective Equipment (PPE) drain contractors' finances and keeping a sizable carder on site with no work in progress is a challenge for construction companies (Pathirana, 2021). Construction projects require a constant supply of resources and an intake of workers at various phases of the project (Vithana et al., 2020). Also, the industry has traditionally had the largest payment waiting lines, which will be further aggravated due to economic instability (Kawmudi et al., 2021). Pathirana, (2020), states that the substantial depreciation of the local currency against the US dollar signaled the economic impact of the pandemic on Sri Lanka. This has negatively affected the industry because it has added an extra cost.

Given the above backdrop, only a limited number of studies have been conducted on the impact of the pandemic on the construction industry, particularly in the Sri Lankan context. Contractors, material suppliers, and clients play important roles in the industry, and the current situation has forced all three parties to deal with issues such as completing projects on time, expecting supplies on time at

the right price, and, most importantly, ensuring that the final product or completed project meets set goals (Pathirana, 2020). Therefore, this research is focused on identifying the existing situation in the Sri Lankan construction industry with respect to the Covid-19 pandemic. This paper will be beneficial to the stakeholders in the construction industry to identify the impact of the pandemic on the Sri Lankan construction industry, the strategies which are used in the construction industry to overcome the challenges posed by the pandemic, and to explore the effectiveness of the existing strategies.

2   METHODOLOGY

Research design comprised of both qualitative and quantitative approaches. A questionnaire was used as the data collection tool, which contained both open-ended and closed-ended questions. The study sample comprised of forty (40) participants from the local construction industry, representing the key professional segments namely Architects, Engineers, Project Managers, Quantity surveyors, and senior employees of technical grades. The sample represented a random segment of the construction industry in terms of stakeholders such as consultancy organizations, contractor organizations, interior design offices, and specialized sub-contractor organizations. Selective sampling techniques were used to decide the participants for the study focusing on all the professional categories who are currently engaged in the local construction industry. The criteria for selecting participants for the study were based on research findings by Fei and Khan, (2015) who listed the following qualities and tangible criteria for experts:

I. Age should be 19-60 years.

II. A minimum 1 year of experience and participation in the construction industry is needed.

Based on that scenario, participants were selected above the age of 19 years and more than 1 year of experience in the construction industry.

Statistical techniques were used to analyze quantitative data. Since advanced data analysis functions of Microsoft Excel have proven their robustness as a useful tool in data analysis, this study has utilized the features of the same to perform relevant calculations. The qualitative data was evaluated using thematic content analysis. Thematic analysis is a popular method for evaluating qualitative data on unexplained phenomena (Maguire and Delahunt, 2017; Creswell and Poth, 2018). It is a technique for defining and analyzing data based on themes and relative frequency. It is also a platform for organizing and analyzing data in order to come up with clear conclusions and outcomes (Vaismoradi, Turunen and Bondas, 2013). Accordingly, thematic content analysis was performed under five main themes.

3   RESULTS

The impact of the COVID-19 pandemic on the Sri Lankan construction industry was evaluated in two aspects; (1) Construction process perspective (2) Other aspects related to the construction industry.

3.1   Impact of Covid -19 Pandemic

Every participant acknowledged that there was an impact on the construction industry due to the pandemic. 73.8% (n=31) acknowledged that there was a major impact, 23.8% (n=10) acknowledged that there was a moderate impact and 2.4% (n=1) acknowledged that there was a moderate to minor impact on the industry.

In order to get first-hand experience on the impact level of the COVID-19 pandemic, the participants were asked whether their company was affected by the pandemic. 95.2% (n=40) of the participants responded positively and only 4.8% (n=2) of the participants said that their companies were not affected by the pandemic. The responses from the latter group of participants were again excluded from the study.

Out of the first group of participants, 47.6% (n=20) said that there was a major impact, 31% (n=13) said that there was a moderate impact, 16.7% (n=7) said that there was a moderate to minor impact and 4.8% (n=2) said that there was a minor impact due to the COVID-19 pandemic.
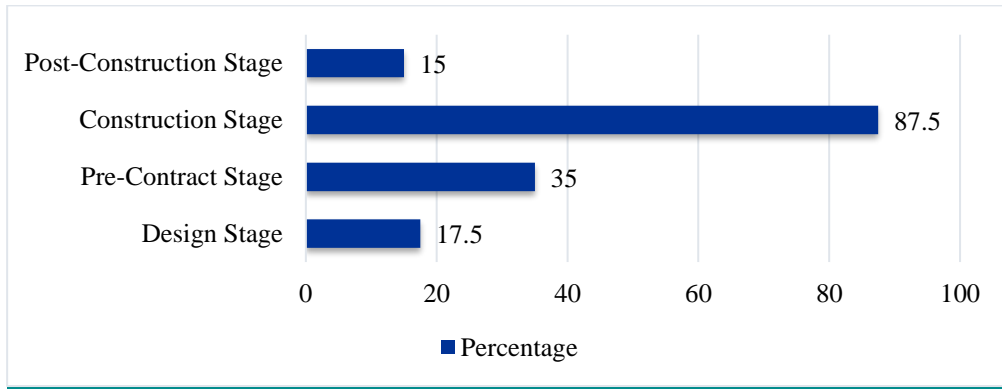
Figure 1: Impact level of COVID-19 in different stages of construction
Source: Analysis of the research findings

According to the respondents' point of view, when considering the construction process, the construction stage was severely affected by the pandemic. Pre-contract, designing, and post-contract stages were affected in descending order.
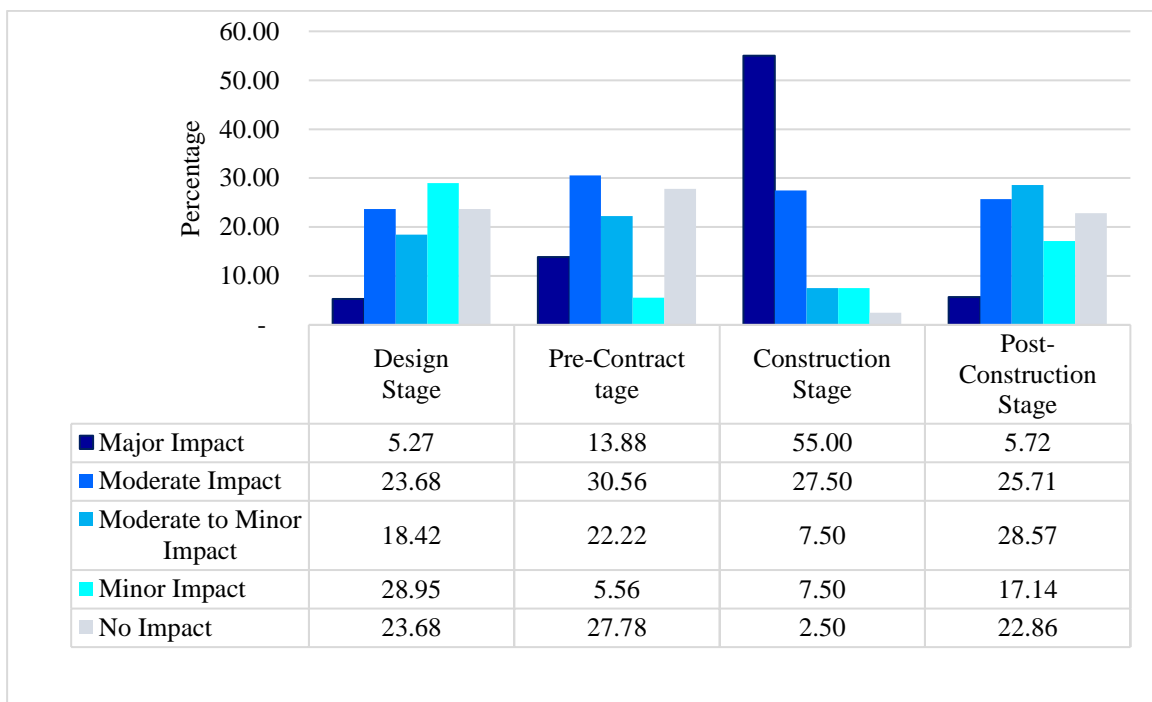

	Design Stage	Pre-Contract tage	Construction Stage	Post-Construction Stage
■ Major Impact	5.27	13.88	55.00	5.72
■ Moderate Impact	23.68	30.56	27.50	25.71
■ Moderate to Minor Impact	18.42	22.22	7.50	28.57
■ Minor Impact	28.95	5.56	7.50	17.14
No Impact	23.68	27.78	2.50	22.86

Figure 2. COVID – 19 Impact level analysis based on the construction stages
Source: Analysis of the research findings

3.1.1 Impact level of the design stage:

As per figure 2, the impact level on the design stage of a construction project reveals that the majority of the respondents claimed that there was a "minor impact" (28.95% responses), while an equal number of respondents claimed, a "moderate impact" and "no impact" (23.68% responses), followed by 18.42% claiming "moderate to minor impact", while 5.27% claimed a "major impact" due to the pandemic on the design stage of a construction project. All the descriptive answers of the responses above were thematically summarized into the following facts: Design stage of construction was impacted due to 1) Inability to attend pre-bid meetings, meet clients in person due to travel bans, curfew,

isolations, and lock down, 2) Unable to proceed with design development and finalize designs due to communication difficulties and architectural designers affected by the virus.

3.1.2 Impact level of the pre–contract stage:

According to figure 2, the impact level on the pre-contract stage of a construction project reveals contradictory results, while the majority claimed that there was a "moderate impact" (30.56% responses), followed by 27.78% of respondents who claimed, "no impact". The rest of the respondents claimed, "moderate to minor impact" (22.22% responses), followed by 13.88% claiming "major impact", while 5.56% claimed "minor impact" due to the pandemic on the pre-contract stage. Thematic analysis revealed the following key points on the impact level of the pre-contract stage of construction such as 1) Difficulties in meeting with relevant parties to get approvals, 2) Fluctuations in the material prices and doubtful market conditions in terms of materials. 3) Necessary documents (such as BOQs) could not be finalized on time, 4) The Government and most of the companies were not working smoothly, 5) Official staff was affected by the virus and it caused delays in the tender process.

3.1.3 Impact level of the construction stage:

According to figure 2, the impact level on the construction stage of a construction project shows consistency in the study results, while the majority claimed, a "major impact" (55% responses), followed by 27.50% claiming a "moderate impact". The rest of the respondents claimed, "moderate to minor impact" (7.50% responses), followed by the same level of responses for a "minor impact", while 2.50% claimed "no impact" due to the pandemic on the construction stage of a construction project.

Major issues described in the descriptive question could be divided into two (2) main parts as workforce issues (related to labourers) and material supply difficulties. With respect to labour issues, construction sites were unable to manage their work due to the lack of labourers. Considerable numbers of labourers were either being quarantined or affected by the disease, while others were not reporting to work at sites that were in locked-down areas.

Material acquisition issues were encountered due to late or postponed shipments and transportation issues occurred when transporting through lockdown areas. Shutting down of construction sites to contain the spread of the virus and delays in the construction period were due to some axillary issues mentioned by the participants which occurred mainly from the above two main reasons.

3.1.4 Impact level of the post-contract stage:

According to figure 2, the impact level on the post-contract stage of a construction project also showed some contradictory results in the study, while the majority of the respondents claimed that there was a "moderate to minor impact" (28.57% responses), followed by 25.71% respondents claiming that there was a "moderate impact". The rest of the respondents claimed that there was "no impact" (22.86% response), followed by 17.14% responses for a "minor impact" while 5.72% claimed that there was a "major impact" due to the pandemic on the post-contract stage of a construction project. As per the participants' responses, descriptive answers given by the participants on the impact level of the post-contract stage revealed that deliver bills and the invoices were taking time to process due to work schedule delays and construction time delays in projects, and clients took more time to settle bills.

3.1.5 Impact of COVID-19 on other aspects of the construction industry:

Another set of questions was posted for the participants from another point of view to identify the impact of the COVID-19 pandemic on the Sri Lankan construction industry. Here the impact was evaluated in the financial aspect, human resources aspect, supply chain and logistics aspect, legal aspect, and completion and handover of project aspect.

Figure 3 clearly portrays a significant impact on the financial aspect of the pandemic, which was followed by the human resources aspect, supply chain and logistics aspect, completion and handover of projects, and legal aspects in descending order.
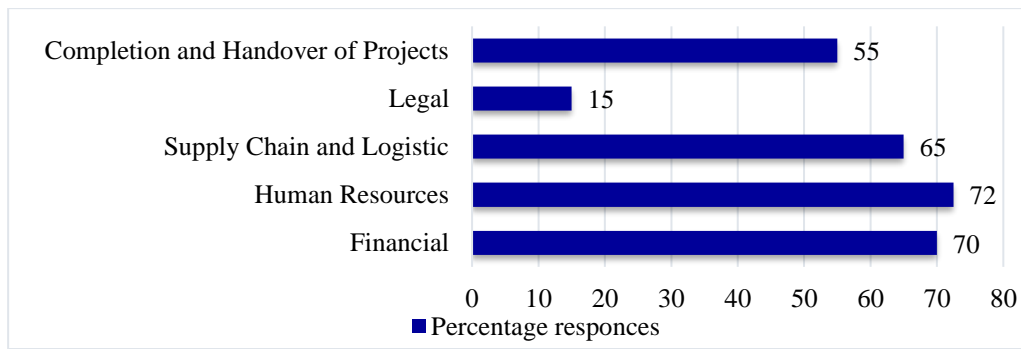
Figure 3. Impact levels of other aspects
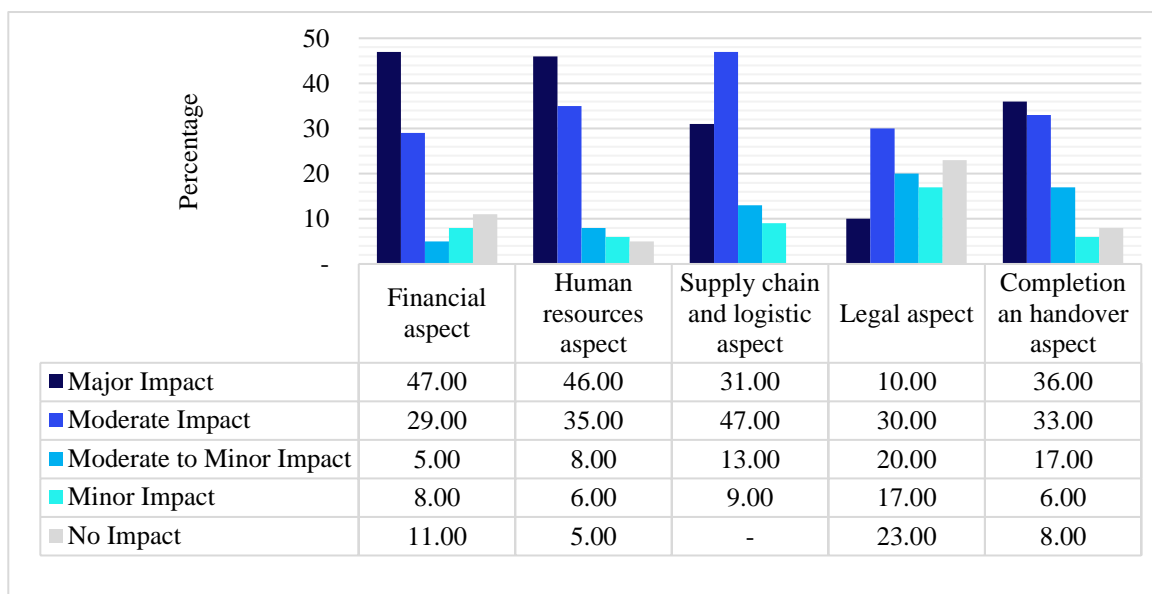Source: Analysis of the research findings

	Financial aspect	Human resources aspect	Supply chain and logistic aspect	Legal aspect	Completion an handover aspect
Major Impact	47.00	46.00	31.00	10.00	36.00
Moderate Impact	29.00	35.00	47.00	30.00	33.00
Moderate to Minor Impact	5.00	8.00	13.00	20.00	17.00
Minor Impact	8.00	6.00	9.00	17.00	6.00
No Impact	11.00	5.00	-	23.00	8.00

Figure 4. COVID-19 impact level analysis based on other aspects
Source: Analysis of the research findings

3.1.6 Impact level of financial aspects:

The thematic analysis performed on the impact level of the above responses on the financial aspects of the construction industry highlights the following areas: clients not paying bills on time due to project delays, cost overruns due to time delays, cash flow interruptions in the companies, the sudden increase in material prices and labour charges, delays and deductions in staff salaries and delays in other payments.

3.1.7 Impact level of human resources aspect:

Thematic analysis done on the human resources aspects of the construction industry highlight the following areas: labourers and the other staff were not able to report to construction sites and offices due to lockdowns and travel bans (like travel restrictions across districts) and only limited staff was allowed to report to work to minimize the spread of the virus. Most companies had introduced shift-based working hours to reduce the number of workers and staff gatherings. Due to the minimum number of workers in workplaces, projects could not be managed within the original timeline. Due to the disturbances in their personal cash flows, most workers showed a lack of motivation and did not report to work. On the other hand, several construction companies reduced the number of workers to control

expenses, while others introduced work from home concept for office workers, and these initiatives also did not work well in many instances in terms of construction companies. Despite all attempts to prevent the virus spread, many construction workers and staff members were affected by the virus.

3.1.8　　Impact level of supply chain and logistic aspect:

Thematic analysis of the supply chain and logistics aspects of the construction industry revealed the following areas: price increase due to less availability and high demand for materials, country regulations on importing foreign luxury items, import bans, shipment, and delivery delays as problems by supply chain and logistic divisions of construction companies.

3.1.9　　Impact level of legal aspect:

Thematic analysis performed on the legal aspects of the construction industry highlight the following areas: while the delays in the tendering process due to the non- functioning of government and private sector companies were the main reason, normal construction work could not be carried out smoothly by adhering to new regulations as claimed by other participants; necessary approvals from various authorities could not be obtained in a timely manner, whereas many construction companies had to renegotiate with banks about the existing loan schemes and other financial problems.

3.1.10　　Impact level of completion and handover of projects aspect:

The thematic analysis done on the impact level on the completion and handover of project aspects also highlight the previously mentioned reasons to have impacted the completion and handover of projects aspect as well.

4　　DISCUSSION

4.1　　Strategies and methods currently used to mitigate the adverse impacts of the COVID-19 pandemic

Unlike previous studies performed on the same subject domain, this research was focused mainly on the identification of the impact of the COVID – 19 pandemic on the local construction industry in two main aspects namely, the construction process perspective and six other aspects related to the construction industry namely, financial, human resources, supply chain and logistics, legal aspect and completion and handover of project aspect. The results of those two aspects complement each other. In terms of the construction process perspective, research focused mainly on four stages of the construction process namely, design stage, pre – contract stage, construction stage, and post–construction stage. Results proved that the construction stage of the construction process was heavily impacted by the pandemic, while the design stage, the pre – contract stage and the post–construction stage were also impacted in descending order.

During the construction stage, all the companies encouraged workers and staff members to strictly follow the government regulations (COVID-19 rules and regulations) on health and safety to prevent the spread of the disease. Companies provided accommodation and other facilities to the workers including transportation for the staff, shift-based, and roster-based work schedules were implemented to reduce worker gatherings. Several companies encouraged staff to work additional - hours to cover the targets.

The introduction of online meeting platforms with clients, consultants, and staff members to make decisions in the design stage and encouraging work-from-home concepts were the methods used by many construction companies in their design stage. Occasionally, some companies tend to store materials beforehand in the pre-contract stage to avoid delays during construction and purchasing materials from proximity was the other option adopted by the companies in the pre-contract stage. As the strategies utilized in the post-construction stage, contractor and sub-contractor bills were settled electronically through various online and fund transfer platforms.

When analyzing the impact level on all other aspects of the construction industry, study results proved that the human resource aspect created a major impact on the construction industry (72%), while the financial aspect (70%), supply chain, and logistics aspects (65%), completion and handover of

project aspect (55%), and legal aspect (15%) also created a considerable impact. The following strategies were utilized by the responding companies to mitigate the effect of the pandemic in terms of all other previously discussed aspects of construction projects. In terms of the human resource aspect, construction companies tried to safeguard the human resources of their organizations by establishing work from home concept, reducing the number of workers at a time, implementing shift-based and roster-based work schedules, and providing transport and other facilities to workers. With respect to the financial aspect, obtaining financial facilities from banks to stabilize the cash flow, reducing the labor force, and deducting salaries and other allowances of the staff members were the strategies utilized by many. Under the supply chain and logistic aspect, companies consider strategies such as advancing material imports, maintaining buffer stocks, minimizing the transportation of materials, and using alternate materials available at the market. In terms of the legal aspect of the construction companies, securing relevant approvals to travel across districts, negotiations with banks for rescheduling of existing financing facilities, negotiating with clients and other relevant parties on time extensions, and tender document clearance at the earliest possibility were the steps taken by many participants. Further, construction companies had negotiations with clients on the tenor of the project and processed on-time extension requests as well.

Apart from these, participants proposed new strategies which could be used to overcome the effects of the pandemic. Implementing Building Information Modelling (BIM) designs for the projects, carrying out accurate estimations and forecasting of the material requirement to store construction materials in buffer quantities, and carrying out off-site pre-fabrication activities to prevent delays were among those proposals.

The findings of this research further strengthen the results of previous studies and proved that the construction stage of the construction project was severely hampered due to the pandemic in the Sri Lankan construction industry. It also reinforces the previous knowledge on the fact that human resource and financial aspects of the local construction industry were mostly impacted while supply chain and logistic aspects closely followed the same.

5   CONCLUSION

The study identified the ways in which the COVID-19 global pandemic affected the construction industry in Sri Lanka which was evaluated in two ways: construction process point of view and the whole construction industry perspective. In terms of the construction process point of view, it could be concluded that the construction stage of the construction process is severely affected by the pandemic. Workforce issues and material supply interruptions were the main reasons. Pre-contract, designing, and post - construction stages were also affected in descending order. When considering the other aspects pertaining to the entire construction industry, results statistically proved that the human resources aspect was severely affected due to the pandemic. This was due to many reasons including lockdowns, travel bans, quarantine of labourers, the limited number of labourers and staff, shift-based working hours etc. The financial aspect, supply chain and logistics, completion, and handover of projects, and the legal aspect of the construction industry were also affected due to the pandemic. The results of these two ways of evaluation tally with each other and this confirms the validity of the results.

Existing strategies used by the construction industry participants to overcome the challenges posed by the pandemic were also identified broadly. The Analysis proved that most construction organizations implement various strategies to face the challenges posed by COVID-19. Several construction companies introduced online working platforms such as Zoom® and Microsoft Teams® meetings. While many promoted the work from home concept for their executive staff, some companies provided staff transportation facilities. Few others appointed designated staff members to visit construction sites occasionally to minimize social gatherings. With respect to the labour force, strategies such as reduction of the number of workers in the sites, shift-based, and roster-based working systems, and offsite pre-fabrication systems were introduced. To eliminate project delays, some companies-maintained buffer stocks to manage material requirements. Survey participants also suggested that the measures like proper costing, estimation, and accurate forecasting of material requirements, and proper storage facilities could prevent wastages. The use of BIM designs by the construction project

participants to disseminate information among relevant stakeholders was also suggested, while this could also be used to identify risks of the projects in advance.

Due to the prevailing pandemic situation in the country, physical interviews with survey participants could not be utilized as a data collection tool. Meeting research participants on their own sites was impossible and meeting them via online meeting platforms could not be done since most of the professionals experience tight working schedules. If an opportunity prevailed, physical interviews might clarify matters more clearly with more justifications. This could be highlighted as the main limitation of this study.

In conclusion, the study has vividly found the impact of the COVID-19 pandemic on the Sri Lankan construction industry, the strategies which are currently used by the companies to minimize the effects, and the effectiveness of these strategies in a descriptive manner.

The results of the study would help private and government sector organizations and future entrepreneurs to easily identify the impact of the COVID -19 pandemic on the construction industry in Sri Lanka and methods that could be used to mitigate the impact today and to lessen any detrimental effects in the future. Furthermore, novel research could be carried out to find more effective strategies which could be used by the construction industry stakeholders when facing a pandemic. Case-control studies, and simulation studies can also be explored as optimum methods for this kind of research.

6   ACKNOWLEDGEMENT

REFERENCES

Aladejebi, O., 2020. Managing Small Businesses in Nigeria during Covid-19 Crisis : Impact and Survival Strategies. *Journal of Business and Management*, [online] 228, 24–34. Available at: www.iosrjournals.org.

Central Bank of Sri Lanka., 2020. *Economic and social infrastructure. In: Recent Economic Developments : Highlights of 2020 & Prospects for 2021. Colombo. 39–60.*

Creswell, J.W. and Poth, C.N., 2018. *Qualitative inquiry & research design: choosing among five approaches*. 4th ed. Los Angeles: SAGE.

Department of Census and Statistics, Sri Lanka., 2021. [online] Available from*: http://www.statistics.gov.lk/.*[Accessed 12 October 2021].

Fei, X. and Khan, T., 2015. Identifying Attributes for Expert Construction Project Managers in the Context of China. *International Journal of Asian Social Science*, 5, 407–418. doi:10.18488/journal.1/2015.5.7/1.7.407.418.

Fairlie, R.W., 2021. The Impact of COVID-19 on Small Business Owners: The First Three Months after Social-Distancing Restrictions. *SSRN Electronic Journal*.

Gamil, Y. and Alhagar, A. 2020. The Impact of Pandemic Crisis on the Survival of Construction Industry: A Case of COVID-19. *Mediterranean Journal of Social Sciences*, 11(4), 122. doi:10.36941/mjss-2020-0047.

Hansen, S., Rostiyanti, S.F., Rizaldi, R. and Andjarwati, C., 2021. Quantity Surveyors' Response to the COVID-19 Outbreak: A Mixed Method Approach. *Journal of the Civil Engineering Forum*, 72, 177.

Kawmudi, W.N., Jayasooriya, S.D., Rupasinghe, A.R. and Ariyarathna, K.C., (2021) Identification of the Challenges Imposed by COVID-19 Pandemic on Sri Lankan Construction Projects. *13th International Research Conference of General Sir John Kotelawala Defence University*, Sri Lanka January 2021, 35–44.

Maguire, M. and Delahunt, B. 2017. Doing a thematic analysis: A practical, step-by-step guide for learning and teaching scholars. *All Ireland Journal of Higher Education*, 9(3). Available at: https://ojs.aishe.org/index.php/aishe-j/article/view/335 (Accessed: 10 April 2021).

Pathirana, L.P.D.S., 2021. Construction Industry and Factor Condition Prospective of Sri Lanka: A Special Reference to Skill Labour Shortage. *Journal of Business and Management*, 232, 35–41.

Shafi, M., Liu, J. and Ren, W., 2020. Impact of COVID-19 pandemic on micro, small, and medium-sized Enterprises operating in Pakistan. *Research in Globalization*, 2, 100018.

Shibani, A., Hassan, D. and Shakir, N., 2020. The Effects of Pandemic on Construction Industry in the UK. *Mediterranean Journal of Social Sciences*, 116.

Tumwesigye, N.M., Biribawa, C., Jackline, M.N., Namanda, C., Atukunda, G. and Ayebale, L., 2020. Introduction. In: COVID-19 in the Global South. [online] Bristol University Press. 1–4. Available at: <https://www.jstor.org/stable/j.ctv18gfz7c.21%0D>.

Vaismoradi, M., Turunen, H. and Bondas, T. 2013. Content analysis and thematic analysis: Implications for conducting a qualitative descriptive study: Qualitative descriptive study, *Nursing & Health Sciences*, 15(3), 398–405. doi:10.1111/nhs.12048.

Vithana, N.D.I., Bandara, K. and Jayasooriya, S.D. 2020. Impact of Covid -19 Pandemic to Construction Industry in Sri Lanka, in *Built Environment and Spatial Sciences Sessions*. *13th International Research Conference General Sir John Kotelawala Defence University*, 161–166. Available at: http://ir.kdu.ac.lk/handle/345/3267 (Accessed: 16 April 2021).

World Health Organization, 2020. COVID - 19 Strategy Update. [online] Available from: https://www.who.int/docs/default-source/coronaviruse/covid-strategy-update-14april2020.pdf?sfvrsn=29da3ba0_19[Accessed 15 December 2020].

World Health Organization, 2021. WHO Coronavirus(COVID-19) Dashboard. [online] Available from: https://covid19.who.int/.[Accessed 12 October 2021].

A Review on Sub-Synchronous Resonance Damping with Thyristor Controlled Series Compensators

D. R. Weerakoon, U. D. Annakkage
University of Manitoba
75 Chancellors Cir., Winnipeg, Canada.
rathnayd@myumanitoba.ca, Udaya.Annakkage@umanitoba.ca

C. Karawita
Trans Grid Solutions (Pvt.) ltd.
100-78 Innovation Drive, Winnipeg, Canada.
ckarawita@tgs.biz

ABSTRACT

Over many years, the power industry has used series compensation with fixed series capacitors for long-distance ac power transmission. With the availability of Thyristor Controlled Series Compensators (TCSC), utilities have the option of using them instead of fixed series capacitors to exploit the advantage of their flexibility and controllability. The use of TCSCs for damping electro-mechanical oscillations and Sub-Synchronous Resonance (SSR) has been investigated and reported over the years. This paper presents a review of those techniques to damp SSR problems associated with conventional multi-mass turbine generator systems in series compensated networks. This paper also demonstrates that SSR can be damped out with the proper choice of TCSC parameters and/or control strategies even without an auxiliary damping controller. Sub-synchronous behavior of the TCSC is simulated in both open loop and closed loop controls in the time domain through Electro-Magnetic Transient (EMT) simulations. IEEE 1st Benchmark model for SSR studies is used in this paper to demonstrate the effect of TCSC parameters and control methodology in damping SSR.

KEYWORDS: *Thyristor Controlled Series Compensators (TCSC), Sub-Synchronous Resonance (SSR), time-domain analysis, IEEE 1st Benchmark model for SSR studies.*

1   INTRODUCTION

Series compensation has long been in use to overcome limitations of long-distance bulk ac power transmission. The use of Fixed Series Compensators (FSC) is an economical solution to improve power transfer capability and stability. However, the potential risk of Sub-Synchronous Resonance (SSR) associated with FSC (Anderson, Agrawal, & Van Ness, 1999) makes it undesirable to be used widely in the system. SSR occurs due to the interaction between the generator electrical system and/or torsional system against the network at a frequency below the synchronous frequency. SSR is not limited to series compensated networks or conventional generators but also exists in power electronic-based systems such as HVDC terminals and wind farms, even in the absence of series capacitors (Xu, Zhao, Cao, & Sun, 2019; Karawita & Annakkage, 2009). The first incident of SSR in a series compensated network is reported in 1970 at the Mohave generating station in Southern Nevada which resulted in severe damage to two turbine shafts (Walker, Bowler, Jackson, & Hodges, 1975). A conventional technique to mitigate SSR is to bypass some or all series capacitors. There are many techniques to counteract SSR in FSC networks such as supplementary excitation controls, static filters, dynamic filters etc. (Kundur, 1994).

TCSC is a Flexible AC Transmission Systems (FACTS) device that allows fast and flexible control of transmission line reactance. It is known to mitigate SSR problems and damp power system oscillations (Joshi & Kulkarni, 2009; Nyati, et al., 1994; Piwko, Wegner, Kinney, & Eden, 1996; Urbanek, et al., 1993). However, due to the complexity and costs associated with TCSCs, utilities have the option of placing full or partial TCSCs at optimal locations to exploit the advantages of TCSC after

thorough investigations not limited to SSR. Sometimes, it can be for the sole purpose of avoiding SSR issues. This paper reviews SSR damping methodologies with TCSC reported in the literature and explores the inherent damping capability of TCSC with proper choice of TCSC parameters through time domain simulations.

The organization of this paper is as follows: Section 2 reviews SSR damping techniques and TCSC structure and its operation is discussed in section 3. Section 4 demonstrates the inherent damping achieved with the appropriate choice of TCSC parameters when the TCSC is operated in open loop and closed loop configuration with EMT simulations followed by the conclusion in section 5.

2   REVIEW ON SSR DAMPING

SSR damping techniques associated with TCSCs mainly fall under two categories which are, active damping techniques and passive damping techniques. SSR damping with basic TCSC controls such as current and power controls and damping SSR with auxiliary controllers such as Sub-Synchronous Damping Controllers (SSDC) fall under active damping techniques. SSR damping can be achieved with the inherent nature of the TCSC as shown in Piwko, et al,1996; and Nyati, et al., 1994, and this paper includes how inherent damping of TCSC can be utilized in open loop configuration and closed loop current control mode to avoid SSR with the proper choice of parameters.

2.1   SSR damping with basic TCSC controls

The impact of TCSC control methodologies such as constant current, constant power, and constant impedance control on damping of SSR is presented in (Pilotto, Bianco, Long, & Edris, 2003). Simple PI regulators have been used in all control techniques and local feedback signals have been used. Constant current controller with a derivative line current feedback is effectively used to damp all SSR torsional modes in IEEE 1st benchmark model for SSR studies at different compensation levels. It is shown that fast power controllers induce large electromechanical and sub-synchronous oscillations. Therefore, the authors have proposed an enhanced power control methodology where a fast current controller is used in the main control loop and a slower secondary loop is used for power control. It is claimed that the constant impedance control where TCSC operates in an open loop configuration can successfully damp certain torsional modes but is not robust over the range of series compensation levels and may excite other torsional modes.

2.2   SSR damping with auxiliary controls

A supplementary damping controller "TCSC-DC" for TCSC operating in open loop constant impedance control mode is proposed in (Zheng, Xu, & Zhang, 2009, July). This technique uses generator speed deviation which is a remote signal as the input to the damping controller. The damping controller is designed based on wide bandwidth phase compensation technique. An auxiliary signal is added to the original firing angle order as shown in Figure 1. Auxiliary signal will add a supplementary electric torque component so that the net electrical damping torque becomes positive and thus the torsional mode damping is improved. However, controller gain, and phase compensator time constants must be tuned to get the optimal damping effect according to the operating condition. A similar approach has been used in (Dey, Das, & Kulkarni, 2021) along with an eigenvalue analysis, validating the performance of SSDC.
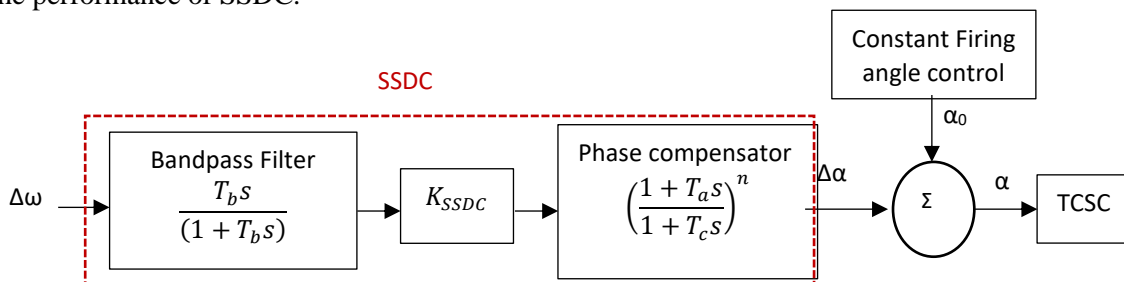

Figure 5: Sub Synchronous Damping Controller block diagram

A novel discrete control strategy based on phase unbalanced concept is introduced in (Subhash, Sarkar, & Padiyar, 2001,November) and applied to IEEE 1st benchmark model. The original phase unbalance concept in (Edris, 1990) which is introduced in FSC networks has been extended to TCSC systems. The basic concept is to have three different inductive-capacitive combinations in each phase so that they produce equal reactances at the power frequency and unequal reactances at the other frequencies. The purpose of having unbalanced reactances is to prevent balanced sub-synchronous currents from entering the generator stator during transients and producing a pure rotating MMF. Phase unbalance is achieved by either inserting or bypassing TCSC modules during a disturbance.

2.3   Passive damping of SSR

Field tests at the SLATT substation demonstrated that the use of TCSCs instead of FSC in vernier control mode avoids possible SSR (Piwko, et al.,1996). In (Nyati, et al., 1994), it is shown that electrical damping of the SLATT system with a TCSC is almost the same when there is no series compensation, claiming that the TCSC is SSR neutral. Although TCSC is known to inherently damp SSR, it is shown in (Pilotto, et al., 2003) that the TCSC is not always SSR neutral especially when the line is composed of both FSC and controlled series compensation. The effect of TCSC parameters on its inherent damping capability is further explored through time domain simulations in section 4.

3   TCSC STRUCTURE AND OPERATION

TCSC is composed of a fixed capacitor in parallel with a Thyristor Controlled Reactor (TCR) as shown in Figure 2. Thyristors are switched at supply frequency (50/60Hz) according to the firing angle delay (α) to control the equivalent reactance of the TCR. The equivalent impedance of the TCSC at a certain firing delay is the parallel combination of the fixed capacitor and equivalent inductance. Firing angles can be synchronized to the zero crossing of either the line current or capacitor voltage. But synchronization to line current zeros is the most effective as the line current is almost sinusoidal.
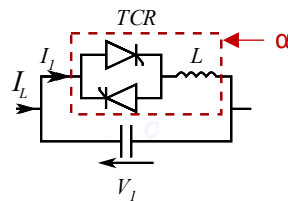

Figure 6: Structure of the TCSC

TCSC can be operated in open loop configuration which is the constant firing angle control mode or in closed loop configuration. In closed loop configuration, the firing angles are generated by upper layer controls such as constant current or power controllers. On top of basic controllers, auxiliary controls such as SSDCs and power oscillation damping controllers will play a role in generating the firing angle orders.
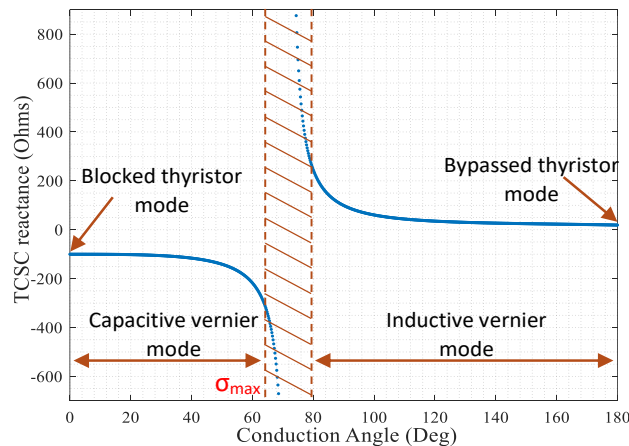

Figure 7: Impedance characteristics of the TCSC

26

TCSC can be operated in vernier mode, blocked thyristor mode or in bypass thyristor mode. In blocked thyristor mode, the TCSC appears as a fixed capacitor and in bypass thyristor mode it appears as the parallel combination of the fixed inductor and capacitor. When operated in vernier mode, the TCSC can offer either an inductive reactance or capacitive reactance according to the firing angle as shown by the impedance characteristics in Figure 3. TCSCs are generally designed to be operated in capacitive vernier mode with a maximum conduction angle ($\sigma = 2(\pi - \alpha)$) limit to avoid instabilities near the parallel resonance point.

When the required total series compensation level of the transmission line is known, the TCSC inductance and capacitance can be chosen based on three parameters which are, the level of controllable series compensation, boost factor, and the characteristic factor as given in Equations (1) to (3), respectively.

$$X_{FSC} + X_{TCSC} = X_{C,TOT} \tag{1}$$

$$K_b = \frac{X_{TCSC}}{X_C} \tag{2}$$

$$\lambda = \frac{\omega_0}{\omega_N} = \sqrt{\frac{X_C}{X_L}} \tag{3}$$

The total series compensation ($X_{C, TOT}$) is composed of both fixed series capacitive reactance (X_{FSC}) and controllable series capacitive reactance (X_{TCSC}) by the TCSC as in Eq. (1). Once the level of controllable series compensation is decided, TCSC fixed capacitive reactance (X_C) can be selected based on Eq. (2) with the proper choice of boost factor (K_b). A high boost factor implies that the TCSC is operating very close to the resonant point. Therefore, even small distortions can change the TCSC impedance drastically, leading to instabilities. Thus, the boost factor is typically chosen to be less than 3 (Zheng, Li, & Liang, 2015). The value of the reactor can be determined by the characteristic factor (λ) defined in Eq. (3). The characteristic factor must be chosen to avoid multiple resonant conditions, limiting to only one resonant point between 0^0 to 180^0 of the firing angles. Typical values of λ are in the range between 2 to 4 (Vuorenpää, Rauhala, Järventausta, & Känsälä, 2007,June).

4   INHERENT DAMPING OF TCSC

IEEE 1st benchmark for SSR studies (IEEE SSR working group, 1977) has been used to demonstrate how the inherent SSR damping capability of TCSC can be achieved with the proper choice of its parameters. Figure 4 shows the IEEE 1st benchmark test system with closed loop current control of TCSC. The generator is modelled with four turbine masses ignoring the exciter. Mechanical damping of turbine masses is ignored to obtain the worst-case scenario.
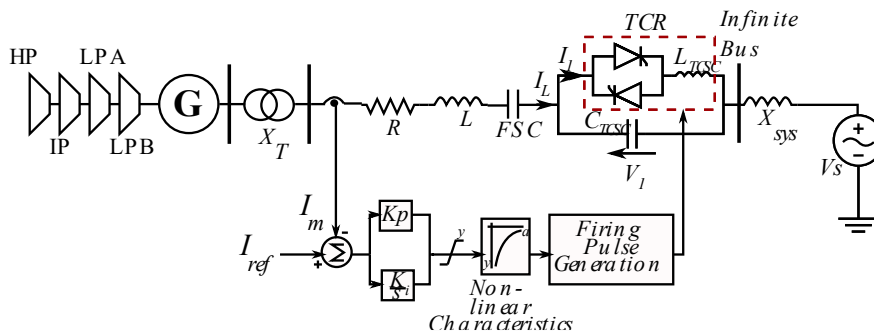

Figure 8: IEEE 1st benchmark test system with TCSC

The generator is operated at 1 pu terminal voltage, 0.9 pu active power and 0.9 power factor at the terminal. Small signal stability analysis of the above system with FSC corresponding to 66% of

series compensation reveals four torsional modes, an electromechanical mode, and a sub-synchronous network mode as shown in Table 1.

Table 1: Oscillatory modes in IEEE 1st benchmark test system with 66% FSC

Mode	Frequency	Damping
Torsional mode 1	16.25	-0.12%
Torsional mode 2	25.43	-0.009%
Torsional mode 3	32.19	0%
Torsional mode 4	47.45	0%
Electromechanical mode	1.7	4.7%
Network mode	20.6	2.24%

The most dominant unstable torsional mode is the 16 Hz mode with all turbine masses and generators participating and it is observable in generator speed deviations. Thus, the effect of three TCSC parameters, discussed in Section 3, in damping this 16 Hz torsional mode is explored with time domain simulations.

The level of controllable series compensation is varied in the range from 10% to 100% with TCSC operating in an open loop configuration. The boost factor (K_b) and the characteristics factor (λ) are maintained constant at 1.3 and 2.5, respectively. The proportional and integral gains of the PLL are set to 25 and 900, respectively in all test cases. Table 2 shows the TCSC parameters for each scenario. The firing angle order is maintained to get the same level of series compensation (66%).

Table 2: TCSC parameters for different levels of controllable series compensation

TCSC percentage	C_{TCSC}	L_{TCSC}	Firing angle
10%	285.7 µF	3.9 mH	156.6^0
30%	95.23 µF	11.8 mH	156.6^0
50%	57.14 µF	19.7 mH	156.6^0
70%	40.81 µF	27.6 mH	156.6^0
80%	35.713 µF	31.5 mH	156.6^0
100%	28.57 µF	39.4 mH	156.6^0

Figures 5-7 shows the generator speed variation for a small disturbance of 5% increment to the generator excitation voltage for a period of 1 ms. The unstable 16 Hz mode is clearly visible in Figure 5 when the TCSC compensation level is as low as 10%.
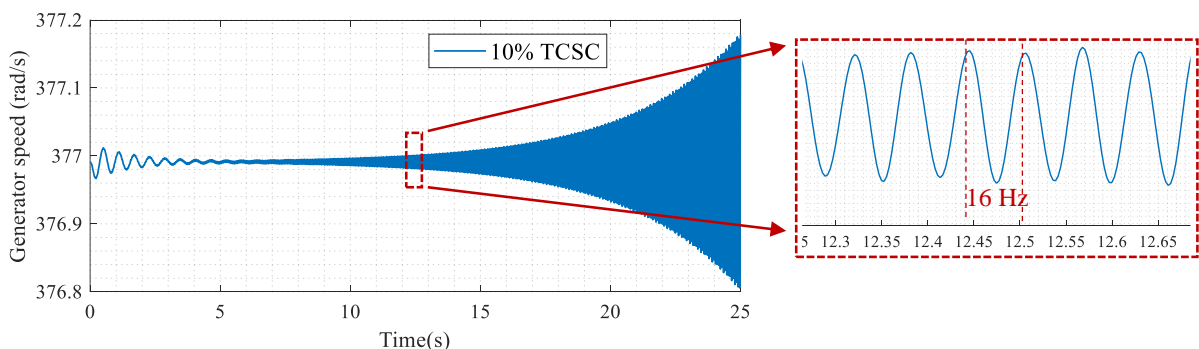

Figure 9: Generator speed variation for a small disturbance when TCSC corresponds to 10% of the total series compensation level

However, it is seen from Figure 6 that, damping of 16 Hz torsional mode is increasing with the increasing levels of controllable series compensation. Even though the torsional mode is fully damped beyond 70% TCSC level in Figure 7, the damping of the electromechanical mode is decreasing with the increasing level of TCSC when the TCSC is operating in constant firing angle control.
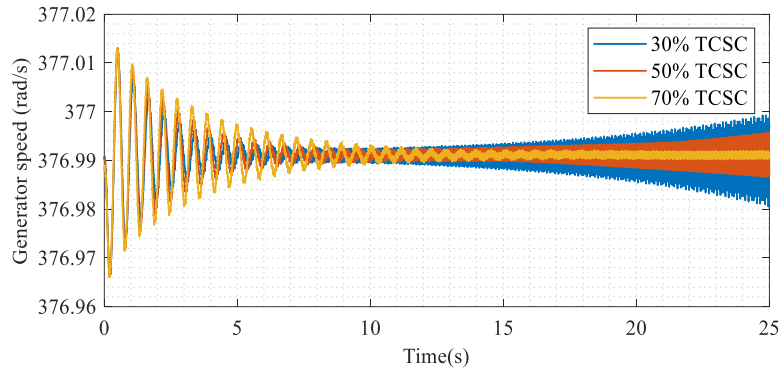
Figure 10: Generator speed variation for a small disturbance when TCSC corresponds to 30%, 50% & 70% of the total series compensation level
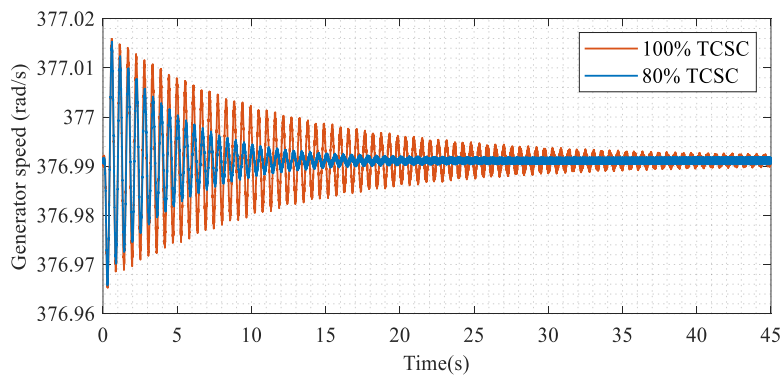

Figure 11: Generator speed variation for a small disturbance when TCSC corresponds to 80% & 100% of the total series compensation level

Figures 8-10 show the generator speed variation when the TCSC is operated in constant current control mode at 70%, 80%, and 100% of TCSC levels, respectively. Current is controlled to maintain the same level of compensation (66%) as in open loop configuration. The proportional and integral gains of the current controller are maintained as 5 and 160, respectively. The damping of electromechanical mode is improved in closed-loop current control mode. However, the controller action did not improve the damping of the unstable 16 Hz torsional mode.
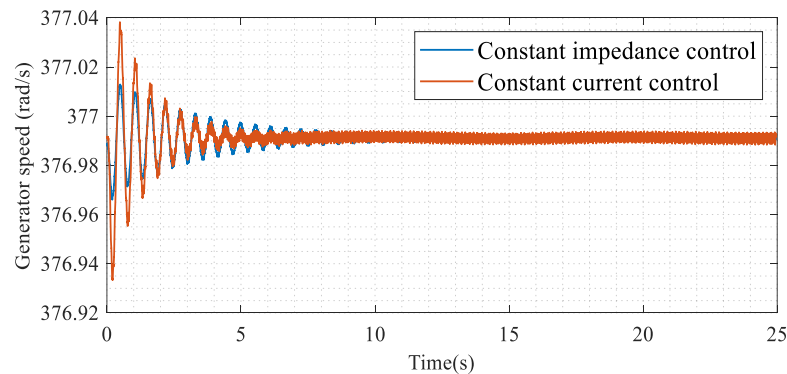

Figure 12: Comparison of generator speed with constant impedance control and constant current control when TCSC corresponds to 70% of the total series compensation level

Figure 13: Comparison of generator speed with constant impedance control and constant current control when TCSC corresponds to 80% of the total series compensation level
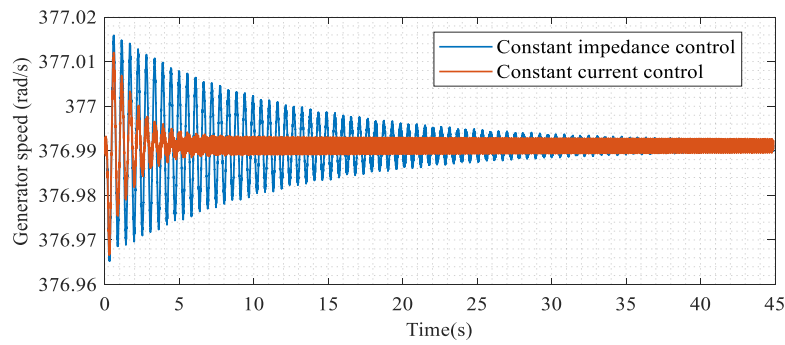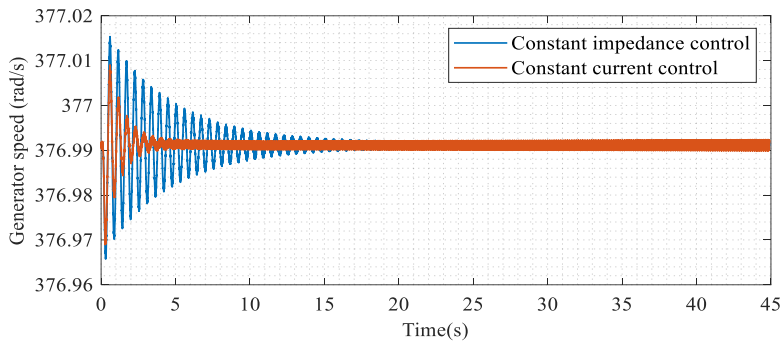

Figure 14: Comparison of generator speed with constant impedance control and constant current control when TCSC corresponds to 100% of the total series compensation level

The effect of operating TCSC at high boost factors (K_b) in open loop configuration is illustrated in Figures 11-13. TCSC parameters for each boost factor are shown in Table 3. TCSC contributes to 80% of the total series compensation level and the characteristic parameter (λ) is maintained constant at 2.5. Firing angles are adjusted to maintain the same total series compensation level of 66%.

Table 3: TCSC parameters for different boost factors

Boost Factor (K_b)	C_{TCSC}	L_{TCSC}	Firing angle
1.1	30.218 µF	37.3 mH	162.3^0
1.15	31.592 µF	35.6 mH	160.3^0
1.2	32.966 µF	34.2 mH	158.8^0
1.3	35.713 µF	31.5 mH	156.6^0
1.5	41.207 µF	27.3 mH	153.9^0

As seen from Figure 11, torsional mode damping is improved with increasing boost factor. Boost factor of 1.3 completely damps out the unstable 16 Hz torsional mode as evident from Figure 12, but the electromechanical mode damping is reduced to undesirable values and is almost unable to operate the TCSC at a boost factor as high as 1.5 as seen from Figure 13.
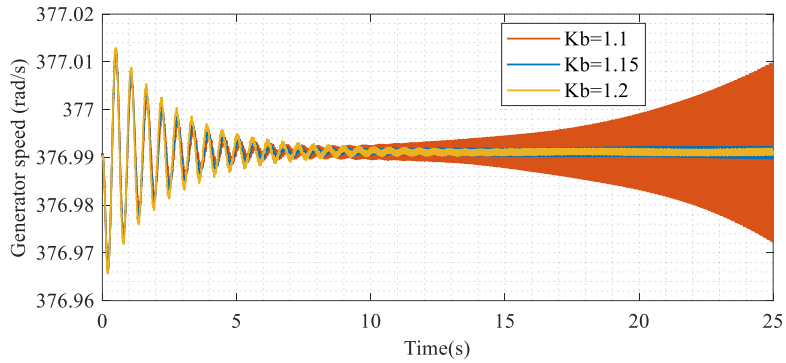
Figure 15: Generator speed variation for a small disturbance when TCSC boost factor =1.1, 1.15 & 1.2
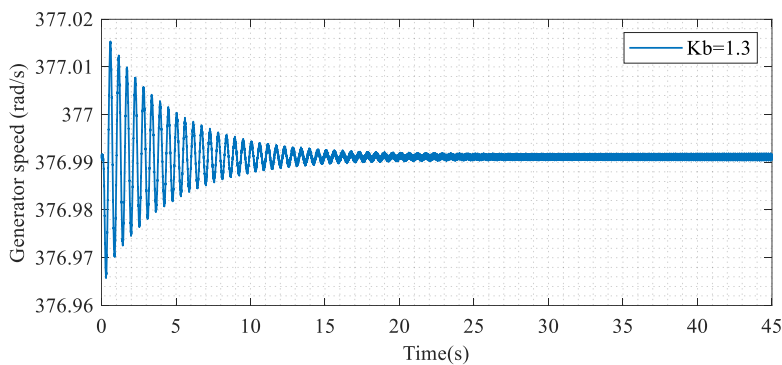
Figure 16: Generator speed variation for a small disturbance when TCSC boost factor =1.3
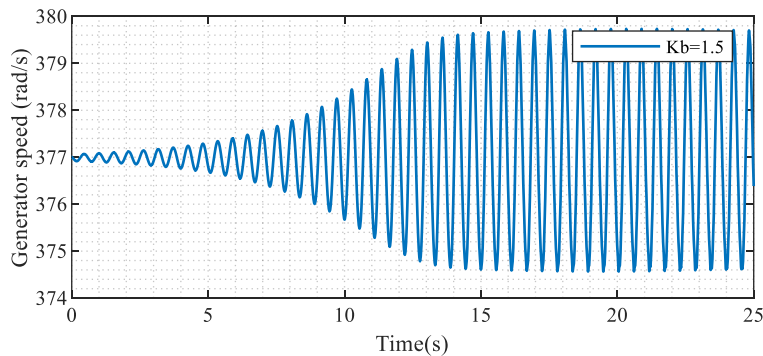
Figure 17: Generator speed variation for a small disturbance when TCSC boost factor =1.5

The impedance characteristics of the TCSC for each scenario in Table 3 are shown in Figure 14. The parallel resonant point is the same in all cases as the characteristic factor is a constant. But the TCSC operating point is moving towards the highly non -linear region with increasing boost factors. The closer the operating point is to the resonant point, the higher the conduction angle and thus better the damping of torsional modes. As seen in Figure 15, electromechanical damping is improved with the addition of closed-loop current control and therefore, high boost factors can be realized in closed-loop control.
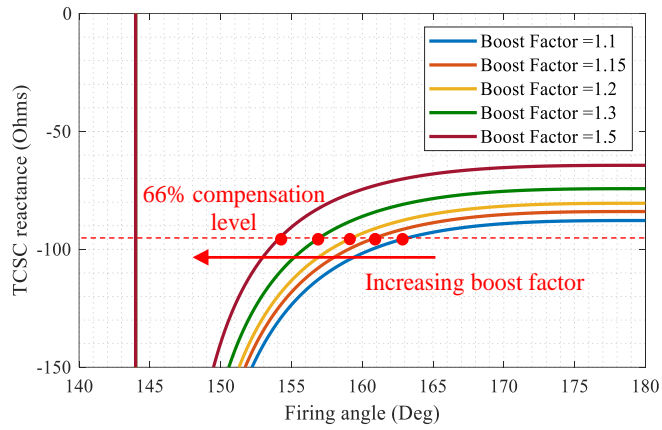
Figure 18: Effect of increasing boost factor on TCSC impedance characteristics
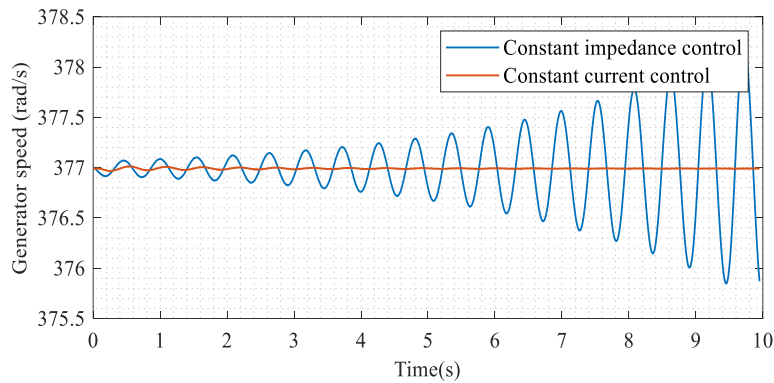
Figure 19: Comparison of generator speed with constant firing angle control and constant current control for a small disturbance when TCSC boost factor = 1.5

Finally, the effect of different characteristic factors on the inherent damping is explored. The TCSC is responsible for 80% of the total compensation level and the boost factor is maintained constant at 1.3. TCSC is fired to maintain a total of 66% series compensation level, all the time. Table 4 shows the TCSC parameters according to characteristic factors.

Table 4: TCSC parameters for different characteristic factors

| Characteristic Factor (λ)	C_{TCSC}	L_{TCSC}	Firing angle
2	35.713 µF	49.3 mH	152.2^0
2.5	35.713 µF	31.5 mH	156.6^0
3	35.713 µF	21.9 mH	159.8^0
3.5	35.713 µF	16.1 mH	162.1^0

Figure 20: Generator speed variation for a small disturbance when TCSC characteristic factor =2,2.5 and 3

Figure 21: Generator speed variation for a small disturbance when TCSC characteristic factor =3.5

It is seen from Figure 16 that there is no significant effect of changing characteristic factors on torsional mode damping. It only destabilizes the electromechanical mode at high characteristic factors. Therefore, a characteristic factor of 2 or 2.5 is sufficient for most operating conditions.

5   CONCLUSION

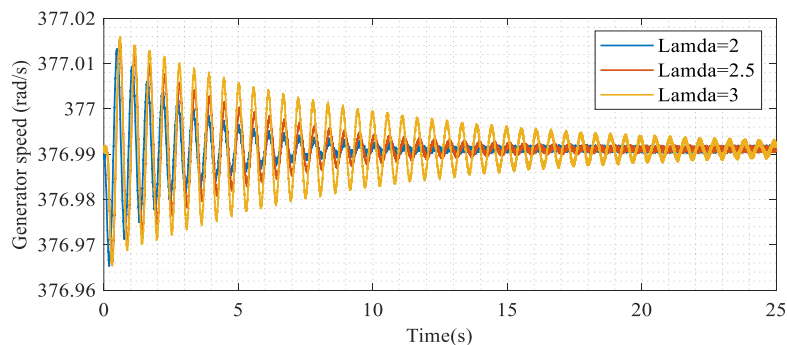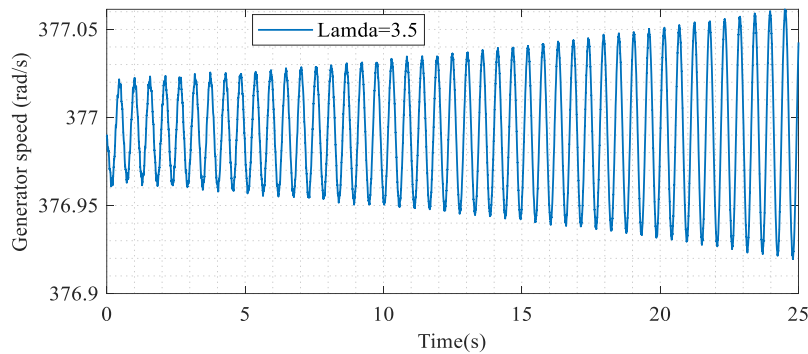SSR damping techniques associated with TCSC are reviewed in this paper. SSR damping can be achieved with basic control topologies such as current and power controllers, or auxiliary controllers such as SSDC or the TCSC can be designed to inherently damp out potential SSRs. It is shown with time-domain simulations that with the proper choice of controllable series compensation level and a boost factor, torsional mode damping could be improved without auxiliary controls. Electromechanical mode instability which occurs in TCSC open loop control is eliminated in closed loop constant current control, which allows a high level of controllable series compensation and boost factors to be realized.

REFERENCES

Anderson, P. M., Agrawal, B. L., & Van Ness, J. E. (1999). *Subsynchronous resonance in power systems* (Vol. 9). John Wiley & Sons.

Dey, K., Das, M. K., & Kulkarni, A. M. (2021). Comparison of dynamic phasor, discrete-time and frequency scanning based SSR models of a TCSC. *Electric Power Systems Research, 196*, 107237.

Edris, A. A. (1990). Series compensation schemes reducing the potential of subsynchronous resonance. *IEEE Transactions on Power Systems, 5*(1), 219-226.

IEEE SSR working group. (1977). First benchmark model for computer simulation of subsynchronous resonance. *IEEE Transactions on Power Apparatus and Systems, 96*(5), 1565-1572.

Joshi, S. R., & Kulkarni, A. M. (2009). Analysis of SSR performance of TCSC control schemes using a modular high bandwidth discrete-time dynamic model. *IEEE Transactions on Power Systems, 24*(2), 840-848.

Karawita, C., & Annakkage, U. D. (2009). Multi-infeed HVDC interaction studies using small-signal stability assessment. *IEEE Transactions on Power Delivery, 24*(2), 910-918.

Kundur, P. (1994). *Power System Stability and Control.* New York: McGraw-Hill.

Nyati, S., Wegner, C. A., Delmerico, R. W., Piwko, R. J., Baker, D. H., & Edris, A. (1994). Effectiveness of thyristor controlled series capacitor in enhancing power system dynamics: an analog simulator study. *IEEE Transactions on Power Delivery, 9*(2), 1018-1027.

Pilotto, L. A., Bianco, A., Long, W. F., & Edris, A. A. (2003). Impact of TCSC control methodologies on subsynchronous oscillations. *IEEE Transactions on Power Delivery, 18*(1), 243-252.

Piwko, R. J., Wegner, C. A., Kinney, S. J., & Eden, J. D. (1996). Subsynchronous resonance performance tests of the Slatt thyristor-controlled series capacitor. *IEEE Transactions on Power Delivery, 11*(2), 1112-1119.

Subhash, S., Sarkar, B. N., & Padiyar, K. R. (2001, November). A novel control strategy for TCSC to damp subsynchronous oscillations. *In Seventh International Conference on AC-DC Power Transmission* (pp. 181-186). IET.

Urbanek, J., Piwko, R. J., Larsen, E. V., Damsky, B. L., Furumasu, B. C., Mittlestadt, W., & Eden, J. D. (1993). Thyristor controlled series compensation prototype installation at the Slatt 500 kV substation. *IEEE Transactions on Power Delivery, 8*(3), 1460-1469.

Vuorenpää, P., Rauhala, T., Järventausta, P., & Känsälä, T. (2007, June). On effect of TCSC structure and synchronization response on subsynchronous damping. *In Proc. International Conference on Power system Transients.*

Walker, D. N., Bowler, C. E., Jackson, R. L., & Hodges, D. A. (1975). Results of subsynchronous resonance test at Mohave. *IEEE Transactions on Power Apparatus and Systems, 94*(5), 1878-1889.

Xu, Y., Zhao, S., Cao, Y., & Sun, K. (2019). Understanding subsynchronous oscillations in DFIG-based wind farms without series compensation. *IEEE Access, 7*, 107201-107210.

Zheng, R., Li, G., & Liang, J. (2015). Capability of TCSC on SSR Mitigation. *Journal of Power and Energy Engineering, 3*(04), 232-239.

Zheng, X., Xu, Z., & Zhang, J. (2009, July). A supplementary damping controller of TCSC for mitigating SSR. *In 2009 IEEE Power & Energy Society General Meeting* (pp. 1-5). IEEE

Neural Network based automated hot water mixture

F.N.M. Firsan[1], G. M. Herath[2], T.D.Thilakanayake[3]
[1]School of Civil and Mechanical Engineering, Curtin University Kent
St,Bentley WA 6102, Australia

[2,3]Faculty of Engineering, Sri Lanka Institute of Information
Technology, New Kandy Rd., Malabe, 10115, Sri Lanka
madhawa.h@sliit.lk

ABSTRACT

In the present day and age, most residential spaces comprise a shower system and generallya conventional system of hot water showers. Throughout history, showering has developed as an essential need in a person's life. Nevertheless, a typical hot water shower system comprises delays in hot water mixing and usually requi res an average of 2 to 4 minutes to mix the cold and hot water to deliver the appropriate shower temperature. The delay in mixing provides less comfort and poor satisfaction affecting people's lifestyles. Due to these disadvantages, a system incorporating artificial Intelligence can be utilized to enhance the performance of mixing which can offer an automated hot watermixture system with improved efficiency and effectiveness. Recently, significant research has been focusedon utilizing deep learning technology due to its multiple breakthroughs in fabricating a broad range of automated novel applications since Neural Networks comprise the capacity to learn from data to offerefficient and accurate systems. In this research project, the hot water mixture is employed by an ArtificialNeural Network model integrated with the combination of an embedded system of the proposed systemof hot water mixture. Furthermore, the proposed system comprises temperature and flow sensors along with controllable flow valves. The tested system indicated acceptable accuracy between the actualand desired output flow rate and temperature.

KEYWORDS: *neural networks, deep learning, hot water mixture, embedded system*

1 INTRODUCTION

Throughout history, showering has evolved into an essential need for people. The primary reasonshowering was considered a fundamental need is to maintain a satisfactory degree of hygiene and other positive effects with respect to people's health. Hot shower systems have developed and improvedthroughout history to improve the quality of showering. However, the existing conventional hot water shower control systems cause a delay of approximately 1 to 2 minutes in hot water mixing.

In general, there are two fundamental shower control systems. The pressure balance shower system comprises one lever which performs the on/off function, and the water temperature can be regulated even though the volumetric flow of water cannot be controlled with this type of system (Shower Systems Explained). When the valve of this system is turned on, it cannot be adjusted to the desired position since the valve can only function in completely open or closed positions. Moreover, the output volume of water cannot be regulated, nevertheless, an adjustable shower head may be employed to alterthe pressure. On the other hand, the thermostatic shower system comprises two levers, where one leveris capable of controlling the water temperature (thermostatic valve) and the other lever regulates the volume of water with the inclusion of an on/off function (volume control valve). This system enables the userto set the temperature permanently so that whenever the shower functions it provides the water temperature to the given value. However, when both basic shower systems are analyzed it can be said that they comprise drawbacks and lack versatility.

Therefore, this study offers a system of Artificial Intelligent hot water mixture that provides an improved duration of hot water mixing and a reliable system with increased versatilityto improve

the lifestyles of people by delivering a comfortable shower experience. The study prioritizes the development of a hot water mixture system providing people with an easy-to-use and versatile system to bring comfort to their lifestyle. The primary objective of this study is to fabricate an automated hot water mixture system by implementing Neural Networks to provide the user the ability to input the desired shower temperature and flow rate to the automated hot water mixture system. In addition, a good automatic control mixture must be established, in simple terms, the proposed system must be an advanced and user-friendly system. Moreover, the secondary objectives were to construct a comparison utilizing learning strategies of Artificial Neural Networks (ANN), collect data to train the ANN model, develop the script of data collection and ANN model, and lastly develop the overall algorithm to function the automated system. Furthermore, utilizing Deep Neural Network technology provides a faster rate of hot water mixing as computations occur rapidly to provide the best possible results and since this technology comprises the capacity to learn, the hot water mixing system can be improved over time by integrating more features and functions to the system. Hence, when constructing a comparison between Neural Network and conventional methods, Neural Network offers more advantages to the system. Therefore, the study examined the ways of utilizing current shower control systems to introduce an innovative and novel approach.

The study design comprises implementing a Neural Network based system by utilizing a significant amount of dataset to train the Neural network model successfully to acquire the best-performing model by employing several techniques, particularly hyperparameter optimization. The results of the best-performing models were then utilized by the microcontroller to provide the necessary instructions to the controllable flow valve when the user inputs the desired temperature and flow rate. This enables good automatic control and versatility for the user to insert the desired temperature and flow rate.

1.1   Literature background

Artificial Neural Networks (ANN) contain units of computation called neurons (Charu C. Aggarwal, 2018). Every input to a neuron consists of a scaled weight that affects the unit computation of that function. The propagation of computed values is transferred from the input to output neurons utilizing weights as the intermediary parameter in an ANN which evaluates the function of inputs. The learning process generally occurs by adjusting the weights connected with the neurons and these weights are adjusted in an ANN in response to errors from predicted results.

The objective of adjusting the weights was to reshape the computed function in order to secure more accurate predictions in future iterations. Hence, weights are altered delicately in a mathematically validated pathway to minimize the error in the particular computation of a model. With successful alterations to the weights between a myriad of input and output pairs of neurons, the function computed by ANN gets refined over a period of time to provide further accurate predictions. For example, in this research project, the ANN was trained with a significant amount of datasets, as eventually, it will be able to predict and provide the desired output flow rate and temperature accurately when a user inputs his desired temperature and flow rate whereas in most situations the desired values are outside the dataset provided to the model that has been trained. This key ability to accurately evaluate or compute functions of concealed inputs by training with a specific dataset which consists of a finite collection of input and output pairs is known as *model generalization.* The prime effectiveness of all deep learning models is acquired by their potential to generalize their learning process from visible training data to concealed examples or situations.

The experiments and computations for a particular fine-tuned neural network will not be suitable for another neural network. This is because it may consist of different input and output parameters, and a distinct complexity, and the objective of the results required may vary. Hence, for a given neural network, many parameters exist that are in need of optimization to acquire the best solution. A few of the common parameters to be tweaked in the neural network are, the number of hidden layers, number of neurons, batch size, and epoch number (Antonio Guili et.al, 2019). These listed parameters are limited as the number of parameters to be optimized will vary significantly, depending on the complexity of the neural networks. Furthermore, these parameters that are to be optimized in the neural network are defined as hyperparameters. This term is provided in order to distinguish between the system parameters of the network such as weights and biases. During the

process of training, Hyperparameter tuning is the approach of discovering the optimal set of hyperparameters used to obtain improved cost functions (reduced cost functions). There are several hyperparameter tuning methods offered by Python in the form of libraries that may beutilized to fine-tune the hyperparameters of an ANN model such as Hyperband, Keras Tuner and Scikit optimize. These libraries aid in tuning the hyperparameters to obtain a set of best models thatcan be utilized to train the ANN model with the relevant dataset.

In any Hyperparameter tuner, the initial hyperparameter that will be considered is the number ofhidden layers, and by constructing more layers the depth of the neural network may increase and eventually form a deep neural network that provides the ability to further examine complex features (Agrawal, 2021). Therefore, for simple problems, one or two hidden layer networks will work relatively well whereas for more complicated problems the number of hidden layers can be increased until the point of overfitting the training dataset is reached. Following this hyperparameter, the number of neurons in each existing hidden layer must be considered. The number of neurons is typically determined by the sort of input and output task required. In general, a fundamental size isto establish a pyramid-like pattern of neuron numbers, that is fewer neurons in each adjacent layer (Geron, 2019). However, this concept was discarded as utilizing the same number of neurons in each hidden layer performs fairly well or even better in the majority of the cases. Nevertheless, all of this depends on the dataset as it can provide an idea to construct the neurons in the hidden layers.Similar to the number of layers, the number of neurons may also be increased gradually to the point where the network begins to overfit, but this approach may be tedious and it is more efficient and straightforward to survey a model with more hidden layers and neurons first and thereafter to utilize options such as early stopping and regularization strategies to avoid overfitting. A scientist named Vincent Vanhoucke called this approach the "stretch pants approach" (Vanhoucke et al., 2011). This indicates that, instead of spending time to examine pants that precisely match the size, utilizing large stretch pants which will narrow down to the required size is more efficient. This approach avoids bottlenecking layers which can possibly ruin the model architecture and performance.

Likewise, the hyperparameter called learning rate is a salient hyperparameter that controls how one regulates variations of the model with respect to the computed error each time the weights of the model are updated (Patterson, Josh, and Gibson, 2017). The basic concept of identifying a reasonable learning rate is to train the network for several hundred iterations, initially with a low learning rate and slowly increasing it to a larger value. Subsequently, the best learning rate discoveredthrough this process can be utilized to train the network again whereas, the Optimizer dictates howthe network may be updated such as weights depending on the loss function (Chollet François, 2019). Several optimizers are available to offer high-performance to train models of deep learning. For example, stochastic gradient descent, AdaGrad, Adam, and AdaDelta (Soydaner, 2020).

Batch size may also have a substantial impact on the performance and time taken for the training of the model. A paper by Dominic Masters and Carlo Luschi in 2018, deduced that utilizing small batches typically between 2 to 32 was recommended since small batches supported providing better models in a short training period (Masters & Luschi, 2018). Nevertheless, a paper written in 2017 by Elad Hoffer et al. and Priya Goyal et al. illustrated a high probability of utilizing large batch sizes typically up to 8192, employing a variety of techniques such as increasing the learning rate, by warming it up from low to high learning rate value which is guided to a short period of training and without any generalization gaps. (Hoffer et al., 2017). Hence, two approaches are available either to utilize a large batch by warming up the learning rate and afterward if the training seems to be unstable or the performance of the model is unacceptable then it is recommended to try utilizing a smaller batch size instead.

Lastly, the objective of the activation function is to introduce nonlinearity to each neuron. Many activations functions are available for selection such as ReLU, Sigmoid, and variants of ReLU (such as Leaky ReLU). Moreover, it is important to choose the ideal activation function for the neural network model since they are used on all neurons available in the neural network of the given model and backpropagation utilizes their derivates. Consequently, the function and its derivative must comprise less computational complexity (Agrawal, 2021).

2   EXPERIMENTAL PROCEDURE

2.1   Development stage

The primary phase of the study was to perform an in-depth and detailed study of research findings related to the topic. The discovered research was then examined carefully to obtain a fundamentalunderstanding and visual of the study. The research sources comprised books, articles, or papers thatprovide principal ideas, designs, and novel strategies and how engineering techniques are employed to overcome the complications that emerge in the existing research findings. The priority of the findings was mainly on the shower control systems, Neural networks, and microcontrollers.

The research findings were then utilized to develop ideas on constructing the hot water mixture system design by employing existing components and technologies, particularly from previous related works. The design was developed employing AUTOCAD software and Figure 1 illustrates the design of the automated hot water mixture system.
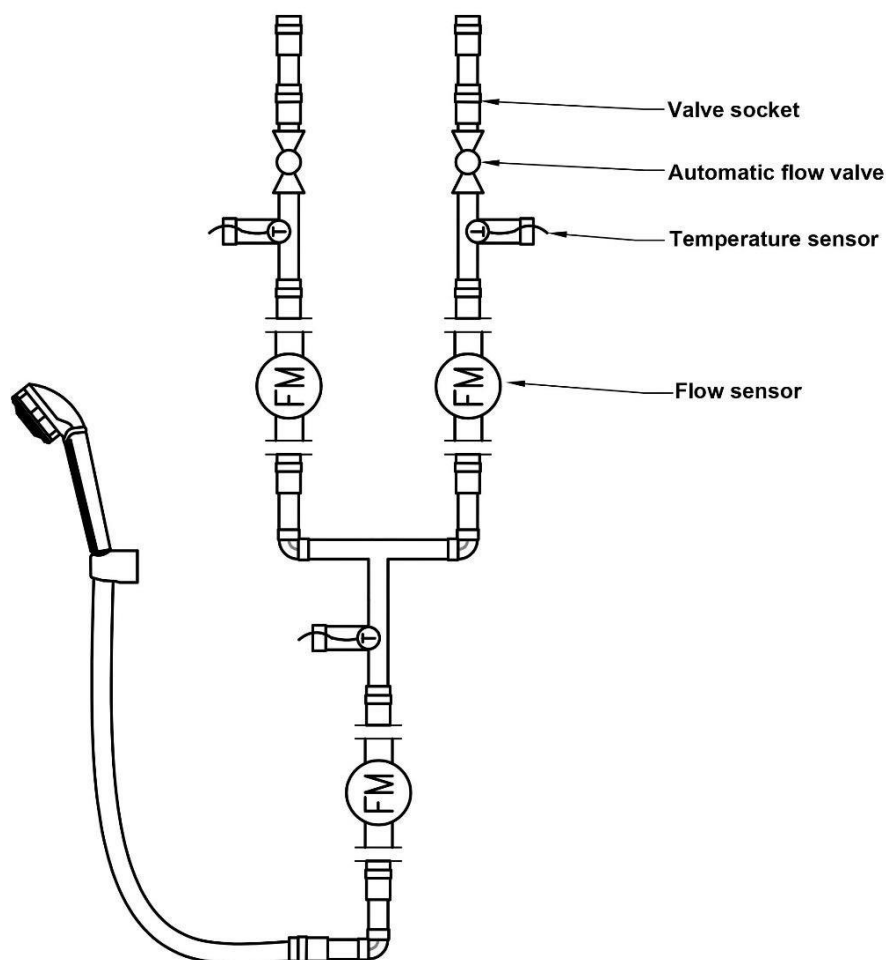
Figure 1 Automated hot water mixture design

After the design was developed, the priority was given to constructing the Neural Network architecture by investigating the parameters of the hot water mixture system, and by identifying the input and output parameters of the system the architecture of the Neural Network was fabricated. The parameters for the ANNinput layer were considered as output temperature and output flow rate. The parameters of the output layer were considered as hot and cold-water flow rates and temperatures. Figure 2 illustrates the architecture of the constructed ANN model here the number of neurons in the first hidden layer was declared as $n^{(1)}$ and the term l denotes the number of hidden layers in the

ANN model. The values of the number of neurons in hidden layers and the number of hidden layers were given in the arbitrary form. This was due to the hyperparameter optimization technique utilized in the script developmentstage to identify these hyperparameter values.

Figure 2 Architecture of Artificial Neural Network model

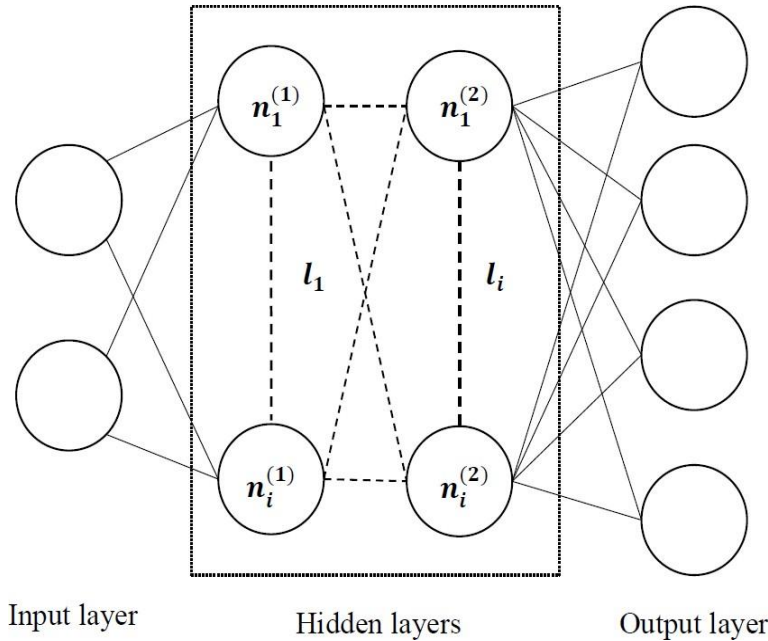## 2.2 ANN and physical model implementation stage

The list of components selected is illustrated in Table 1. These components are essential to fabricate the modelrequired for data collection and the final proposed system of the study.

Table 1 List of selected components of the final model of study

Component name	Model Number
Microcontroller	Raspberry Pi 4 Model B (2gb ram)
Power Supply	Switch mode power supply (SMPS)
Servo motor	DS3230 Metal gear servo
Temperature Sensor	DHT22/AM2302
Flow sensor	YF-S201 hall effect sensor
Ball valve	SLON two pieces ball valve

The system is based on an Artificial Neural Network model, and in order to train the model, a significantamount of dataset must be acquired to obtain accurate predictions. Initially, an automatic and custom flow valve must be designed and tested prior to the collection of datasets. The custom flow comprises two key components, which are the servo motor and the ball valve. Figure 3 illustrates the fabrication of the automated flow valve which includes the other essential components such as brackets and metal plates for mounting purposes to ensure the proper functioning of the automated flow valve.

Figure 3 Automated flow valve

Due to the novel approach being performed by employing an Artificial Intelligence embedded systemintegrated into a hot water mixture system, the relevant dataset was not readily available. Hence, to collect relevant and accurate data, the hot water mixture system was fabricated, and data was acquired by executing the developed data collection script to collect the data at the main locations of a pipeline whichare hot, cold, and output lines.

The data collection script typically comprises the setup of the temperature sensors, flow rate sensors, and servo motors. After the setup, the primary loop of the script was developed to acquire readings at 3 main locations of the system which are hot water temperature and flow rate (hot pipeline), cold water temperature and flow rate (cold pipeline), output water temperature and flow rate (output pipeline). When the script was executed, the instruction was given to both servo motors at hot and cold pipelines to rotate between the specified range of 30 to 90 degrees. Then at each iteration, the servo motor regulates the volume of water flowing in both hot and cold pipelines, and the temperature and flow rates at input pipelines were measured after 3 seconds of waiting time after the servo motors rotate.The output temperature and flow rates were measured after 4 seconds of waiting which includes the delay of the readings measured by the hot and cold flow sensors since the sensors read the pulse withinthe 1-second timeframe when the counter is activated and deactivated. Hence the system was functioningto collect data until the script was terminated. Furthermore, the readings were written to a file after the completion of each iteration of the primary loop. In addition, the file consists of a comma-separated value(CSV) format.

The overall fabricated model of the study is illustrated in Figure 4 which indicates the arrangementof the key devices. Where the custom automated flow valves are initially installed, followed by the temperature and flow sensors in each input pipeline. The flow sensors comprise threaded ends to be easily installed in the hot water mixture system. However, the installation of the temperature sensors was relatively complex comprising fixing a T joint connector and fitting an end cap which was drilled at thecenter to enable the wires to reach out of the system and be connected to the Raspberry Pi. Furthermore,the temperature sensor was installed perpendicular to the flow inside the T joint connector.

Figure 4 Fabricated physical model of study

The Neural network script was developed gradually, and the collected dataset was utilized to train the model. Before training the model, a crucial step was involved in obtaining the best hyperparameters for the model (O'Malley et al., 2019). This was employed by utilizing hyperparameter optimization techniques offered by Keras API. The tuner known as Hyperband was employed in this study along with the Random Search tuner to perform hyperparameter optimization. The best tuner was selected by monitoring the training loss (must be low) of the model since the hyperparameters found from both tuner algorithms are distinct and as a result, provide models with different performances. Hence, the best model was acquired from the tuner which provided the least training loss and then the best model with the ideal set of hyperparameters was trained. The set of hyperparameters this study prioritized to obtain was the number of hidden layers, the number of neurons in those hidden layers, the optimizer, and the dropout. Moreover, several other combinations of hyperparameters were experimented with prior to the final selection of the hyperparameters such as activation functions and learning rate. After the training procedure, the best model was evaluated with the test data, and predictions were made to examine the performance of the model. Furthermore, visualization strategies were utilized to visualize the performance of the model in a graph, particularly the graphs of training and validation losses. The library utilized to visualize was matplotlib.

2.3 Physical model testing stage

A relationship between valve angles and flow rates was established using the data from the acquired data collection process. The respective data of hot and cold angles and flow rates were read utilizing the pandas library. The variables were called to establish two linear equations for the regression graphs utilizing the polyfit function. The linear equation comprises the angles of hot and cold being the independent variables and hot and cold flow rates as the dependent variables. From the equation, the gradients and intercepts were obtained. Hence, when the user inputs the desired temperature and flow rate, the model predicts the hot and cold water flow rates and temperatures considering the new user inputs as new instances. The predicted flow rates are utilized to find the angle required to turn in the hotand cold pipelines. Then the data of hot and cold angles are utilized by the Raspberry Pi to send the controlsignal to the servo motor in the form of pulses to rotate to the angle computed, which will result in deliveringthe desired output flow rate and temperature. The accuracy of delivering the desired parameters depends on the performance of the Neural Network model.

3   RESULTS AND DISCUSSION

3.1   Data collection

Tests conducted with the customized automatic flow valve to check for proper rotation of the ballvalve indicated positive results where both automated flow valves rotated to the specified angle accurately. The data collected from the physical model was successful and a sample of the data collected isillustrated in Table 2.

Table 2 Results of data collected of study

Hot Angle (*degrees*)	Cold angle (*degrees*)	Hot flow (*l/min*)	Cold Flow (*l/min*)	Output Flow (*l/min*)	Hot temp °C	Cold Temp °C	Output Temp °C
53	33	3.6	3.6	7.267	41	27.2	34.1
71	69	3.333	3.467	6.867	41.4	27.2	34.2
39	69	3.733	3.467	7.133	41.6	27.2	34
66	37	3.467	3.6	7	42.4	27.2	35.1
76	71	2.133	3.333	5.533	41.8	27.2	34.4
69	81	2.533	1.73	4.2	42.2	27.2	33.1
40	75	3.733	1.6	5.4	42.2	27.2	37.6
68	44	3.467	3.733	7	47.5	27.2	41.8
88	36	0	4.133	4.067	47.5	27.2	34.5

The sample of collected data in Table 2 indicates the results were within acceptable bounds for flow rate readings with respect to the ball valve angle. However, there were some data points with inaccurate measurements. This can be possibly improved by increasing the waiting time between the devices to measure the reading during each iteration of the loop, which means after the ball valves rotate, a settlingtime of water must be taken into consideration. The waiting time considered in this study for each iteration was roughly 8 seconds and a total of 3000 datasets were collected here for 1 hour only 450 datasets can be collected. Furthermore, during data collection, other factors must also be considered such as giving rest for the system since the devices can possibly fail or overwork, and in this study, a heater unit was utilized as a hot water source as the heating unit also requires substantial time to rest.

3.2   Artificial Neural Network training

The dataset was utilized to successfully train the ANN model and prior to the training, the

Hyperband tuner of KerasTuner library was employed to find the best hyperparameters ideal for this study's ANN model. In addition, the Hyperband tuner algorithm was selected over RandomSearch algorithm due to better training and validation loss provided by Hyperband tuner algorithm. Unfortunately, due to KerasTuner library being released in 2019, false information was provided with respect to the number of neurons in the hidden layers. However, other hyperparameters tuned were provided correctly as illustrated in Table 3.

Table 3 Summary of selected hyperparameters

Hyperparameter	Selected choice or value
Number of hidden layers	8
Optimizer	adam
Loss	Mean Absolute Error (MAE)
Activation function	ReLU
Output layer Activation function	Linear
Dropout in first hidden layer	0.4
Dropout in other hidden layers	0.2

The choices in the tuner search space for optimizer were given as adam, adagrad and rmsprop andthe dropout choice was given between 0.1 to 0.5 in the tuner search space. As illustrated in Table 3 theHyperband tuner algorithm selected adam and other hyperparameters to be the most appropriate choiceor value for this ANN model. Furthermore, the loss and activation function were not tuned since this study comprises a regression model and the type of activation function and loss function were considered asprovided in Table 3. After acquiring the best model from the tuner the best model was trained for 120 epochs to monitor the training and validation loss as illustrated in Figure 5.
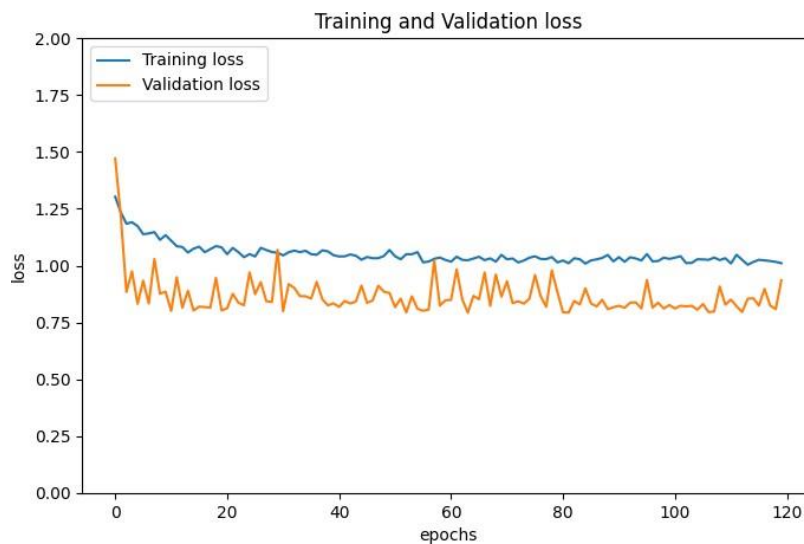
Figure 5 Graph of training and validation loss

The training loss in the last epoch which is 120th epoch was 1.0104 and the validation loss was 0.9354. The graph illustrated in Figure 5 indicates that the training loss (top) and validation loss (bottom)are alleviating and both losses were gradually converging with each other from the starting epoch during training. A factor must also be considered that the tuning algorithm implemented provides us with the best model to train with. Hence, when the best model obtained was trained the

degree of convergence wouldbe less visible. A possible reason the validation loss is less than the training loss is due to the training loss being consistently reported over the period of a complete epoch whereas the validation loss is evaluated over the validation set only once the current training epoch is completed. This suggests on average, training losses are measured half an epoch earlier. Furthermore, the training loss fluctuatesless roughly after 90 epochs. Therefore, the trained model obtained can be considered good when comparing the average difference of both losses was fairly minor. The model was evaluated on the test data to examine the performance and the test loss from the evaluation was 0.938. This indicates that the training loss is relatively higher than the test loss which conveys that there is room for improvement in the ANN model. The most probable reason for the results of the training, validation, and test loss was due to the accuracy or noise comprised in the dataset collected. In addition, the overall dataset was split into20% tests and the test data were split into half to utilize for validation data.

Several strategies were employed to calculate the accuracy since the model is of regression type, the accuracy cannot be computed automatically from the compile method from the Sequential model since it is only available for classification problems. Therefore, the percentage deviation was computed after computing the predicted values of the ANN model with the test data and Figure 6 illustrates the comparison of actual and predicted results along with the deviation of the predicted result with respect to the actual result where the deviations were within 5% range for many of the results illustrating good predictions by the ANN model.

```
Predicted values are:
 [[27.21458   40.248096    3.5891178   3.717945 ]
 [27.21458   40.248096    3.5891178   3.717945 ]
 [27.21458   40.248096    3.5891178   3.717945 ]
 ...
 [27.21458   40.248096    3.5891178   3.717945 ]
 [27.21458   40.248096    3.5891178   3.717945 ]
 [27.21458   40.248096    3.5891178   3.717945 ]]
Actual values are:
 [[26.9       40.2         4.4         4.13333333]
 [27.1       40.6         4.          3.86666667]
 [27.3       40.3         3.73333333  3.06666667]
 ...
 [26.9       38.6         4.26666667  4.         ]
 [27.1       41.          0.66666667  4.66666667]
 [27.1       35.2         3.73333333  3.86666667]]
% deviation [[ 1.15592645  0.11949998 22.592801   11.172522  ]
 [ 0.42102628  0.87433584 11.44800091  4.00010124]
 [ 0.3138739   0.12895898  4.01813418 17.51716108]
 ...
 [ 1.15592645  4.09484326 18.87786765  7.58631162]
 [ 0.42102628  1.86817167 81.42533317 25.51736357]
 [ 0.42102628 12.54244774  4.01813418  4.00010124]]
```

Figure 6 Results of predictions and percentage deviation

3.3   Testing the automated hot water mixture system

The results of the tested system are shown in Figure 7, where the user can input the temperature andflowrate of required and the angles are computed to deliver the user desired parameters by sending the control instruction to the servo motor via the Raspberry Pi.

```
Enter Desired temp and Flow rate:
40.5 8.5
Predicted outputs:
  [[26.650595  40.050434   3.381703   3.7875657]]
Hot side angle:
 53.08414913012051
Cold side angle:
 53.08414913012051
```

Figure 7 Testing the system of automated hot water mixture

The tests performed on the final system indicated that the ANN model performs well for a certainrange of temperatures and flow rates. Table 4 illustrates the time taken for the key procedures of the study where data collection is the time taken to collect the data required for Neural Network training of this study, The training time is the average time utilized to train the best model acquired from the hyperparameter optimization process followed by the training process. Furthermore, the convergence time is the time required for the system to converge the existing output temperature to the required usertemperature and lastly, the response time is the duration the user has to wait for the final automated system to deliver the flow rate and temperature. In summary, the Neural Network approach offers a fasterresponse time which comprises a significant percentage difference of 161% (13 seconds and 120 seconds) in hot water mixing than the existing conventional methods.

Table 4 Comparison between the research study approach and conventional methods

	Neural Network	**Conventional methods**
Data collection (hours)	≥7 hours	-
Training time (seconds)	25 minutes	-
Convergence time	<10 seconds	-
Response time	<13 seconds	60-120 seconds

4   CONCLUSION

The main goal of this study was to develop a system of Neural Network based automated hot water mixture to reduce the time taken for hot water mixing by the current conventional systems of hotwater showers.

The procedure required to develop a path to employ an Artificial Intelligent embedded system consisting of automated and controllable flow valves along with sensors to compute the water temperature and flow rate. The Neural network model performance was significantly dependent on the data collection process and development of the ANN model by utilizing strategies for instance Hyperband tuning algorithm as a hyperparameter optimization technique.

The physical model was successfully fabricated which comprises the salient implementations forinstance the fabrication of the custom automated flow valve, the setup, and installation of DHT22 seriestemperature and YF-S201 flow sensors along with the overall pipework fabrication which includes the valve sockets, T joint, and elbow connections. Moreover, the key findings identified from the study were:the inversely proportional relationship developed between the angle and flow rate of hot and cold waterin experimental results, and the relationship between the predicted and actual results acquired from the trained ANN model.

In conclusion, acceptable results were attained due to the performance of the Neural Network modeland providing predictions to compute the angles essential to rotate the controllable flow valves in instances where the desired shower temperature and flow rate are input by the user. This process was viable due to the successful collection of datasets from the physical model. Although, certain

complications arose during the process of data collection, it can be deduced that a substantial amount of the data collected was within the accepted bounds. Moreover, some potential benefits were identified such as achieving stable temperature with fewer fluctuations and providing good control for users to enter the   desired temperature and flow rate, and faster response rates achieved in contrast to conventional methods. In addition, this study employed a system that ensures user-friendliness and comprises an advancedintelligent system to offer versatility to the system of automated hot water mixture.

REFERENCES

Agrawal, T. (2021). Hyperparameter Optimization in Machine Learning. In *Hyperparameter Optimization in Machine Learning*. https://doi.org/10.1007/978-1-4842-6579-6

Antonio Guili; Amita Kapoor; Sujit Pal. (2019). *Deep Learning with TensorFlow 2 and Keras: Regression, ConvNets, GANs, RNNs, NLP, and More with TensorFlow 2 and the Keras API*. O'Reilly Media, Inc.

Charu C. Aggarwal. (2018). *Neural Networks and Deep Learning. A Textbook*. Springer. https://doi.org/10.7551/mitpress/13811.003.0007

Chollet François. (2019). Chollet - 2018 - Deep learning with Python. In *Manning* (Vol. 53, Issue 9). http://faculty.neu.edu.cn/yury/AAI/Textbook/Deep Learning with Python.pdf

Géron, A. (2019). *Hands-On Machine Learning with Scikit-Learn, Keras, and TensorFlow* (2nd Editio). O'Reilly Media, Inc.

Hoffer, E., Hubara, I., & Soudry, D. (2017). Train longer, generalize better: closing the generalization gap in large batch training of neural networks. *Advances in Neural Information Processing Systems*, *2017-December*, 1732–1742. https://arxiv.org/abs/1705.08741v2

Masters, D., & Luschi, C. (2018). *Revisiting Small Batch Training for Deep Neural Networks*. https://arxiv.org/abs/1804.07612v1

O'Malley, Tom and Bursztein, Elie and Long, James and Chollet, Fran\c{c}ois and Jin, Haifeng and Invernizzi, L. and others. (2019). *KerasTuner*. https://keras.io/keras_tuner/

Patterson, Josh and Gibson, A. (2017). *Deep Learning: A Practitioner's Approach*. O'Reilly.
Shower Systems Explained. (n.d.). Retrieved November 13, 2021, from https://luxehomebydouglah.com/blog/shower-systems-explained/

Soydaner, D. (2020). A Comparison of Optimization Algorithms for Deep Learning. *International Journal of Pattern Recognition and Artificial Intelligence*, *34*(13). https://doi.org/10.1142/S0218001420520138

Vanhoucke, V., Senior, A., & Mao, M. (2011). Improving the speed of neural networks on CPUs. *Proc. Deep Learning and …*, 1–8. http://research.google.com/pubs/archive/37631.pdf

Experimental Identification of Alkali-Aggregate Reaction in Concrete

Rashean Baddeliyanaralalage Don
Curtin University
Perth, Western Australia
r.baddeliy@student.curtin.edu.au

Nihal Somaratna
Sri Lanka Institute of Information Technology
Malabe, Sri Lanka
nihal.s@sliit.lk

ABSTRACT

Several advanced and time-consuming methodologies have been developed to detect Alkali-Silica Reaction (ASR) in suspected structures. The main objective of this research study was to identify a reliable experimental procedure for detecting ASR in existing concrete. A simple staining solution is used here to detect ASR in concrete specimens. The staining reagent employed here is Sodium Cobaltinitrite, which is used in the Los Alamos staining method to detect ASR. Sodium Cobaltinitrite can identify potassium-rich ASR gel by staining it yellow for rapid field screening purposes. Reactive and control concrete specimens were cast to get some experience with this test and to verify whether this test can be used in a suspected concrete structure. Waste white soda-lime glass aggregate was used to cast reactive concrete specimens, whereas natural coarse aggregates were used to cast non-reactive concrete specimens. Testing was carried out in two batches. Each batch consisted of six reactive and six control concrete specimens which were cured in the above-mentioned solutions. The first batch was examined after 44-days and the second batch was tested after 60-days of casting. Results of this test showed that reactive concrete specimens cast using glass displayed yellow stains as expected, demonstrating the presence of potassium-rich ASR gel on the concrete surface. Employing NaOH as a curing medium had accelerated ASR. There is a limitation in the method when utilizing KOH as a curing agent. It is concluded that Sodium Cobaltinitrite can be used as a method for rapid identification of ASR in the preliminary stages of experimental identification of the alkali-aggregate reaction in an existing concrete structure.

KEYWORDS: *Alkali-Silica Reaction, Sodium Cobaltinitrite, Aggregates, Waste glass, Cement, Potassium hydroxide, Sodium hydroxide*

1   INTRODUCTION

The first alleged case of Alkali-Silica Reaction (ASR) was discovered when the premature decay of many concrete structures in California, USA were investigated (Stanton, 1940). This investigation was done by testing the aggregates and cement used in the concrete in a laboratory. Stark (1991) discussed the macroscopic symptoms of Alkali-Silica Reaction. Often the first noticeable indication of ASR is randomly directed cracking at the surface, also known as map cracking due to the irregular pattern of the cracks (Stark, 1991). These cracks progress over time by interconnecting and expanding the cracked surface. This is a slow process that can take many years to reach noticeable levels.

The main factors that influence ASR are water, temperature, reactive aggregate forms, aggregate size, alkali content, stress level, and also, air entrainment and porosity. Alkalis react with the silica in susceptible aggregates to form a gel. This silica gel swells only when moisture is present. Swelling of the gel is the cause of cracking which can lead to degradation of concrete quality and properties. Moisture content plays a major role in the progress of ASR.

A similar process involving carbonates in aggregates has also been identified. It is called an alkali carbonate reaction (ACR). Together, ASR and ACR are referred to as alkali-aggregate reactions (AAR). Of these two ASR is by far the more common form.

One of the most important issues related to AAR is the detection of Alkali Aggregate Reaction in existing concrete structures. Several techniques for detecting the presence of products of the alkali-

aggregate reaction in concrete have been introduced. The majority of these techniques are based on the microscopic examination of affected concrete. Because of the complexities of these microscopic examination methodologies, two simpler staining test methods, viz. Uranyl Acetate test and Los Alamos test, also have been proposed to identify potential AAR by examining the staining pattern produced by certain chemicals on the surface of suspected concrete. These staining tests have the advantage of being simple procedures that can be implemented with basic facilities even in the field.

In Sri Lanka, like in many other countries, certain important concrete structures are suspected to be suffering from ASR. The objective of the present work was to explore the feasibility of using one of these staining tests – the Los Alamos test – as a rapid screening procedure for the detection of possible ASR in the Sri Lankan context.

2   LITERATURE REVIEW

All alkali gels are hygroscopic, which means they absorb moisture. As they absorb moisture, they tend to expand. This can cause damage to the surrounding concrete or mortar if the gel exerts pressure while expanding (Nilsson, 1983). There are two possible mechanisms for concrete in a structure to get exposed to moisture. The first is the structure's exposure to the ambient humid atmosphere, which does not directly involve liquid water. The second involves structures that are actively exposed to liquid water. This refers to the vulnerability of structures to rainfall or river streams with cyclic fluctuations of water levels (Steffens, Li, & Coussy, 2003).

Environmental factors such as temperature have a significant impact on the Alkali-Silica Reaction (ASR), which induces the expansion of concrete and harms long-term durability. An exposure experiment was conducted by Fournier et al. (2009) by using similar types of concrete blocks taken from various exposure locations. It was observed that the rate of ASR expansion after 3–4 years of exposure increased in warmer regions than under cooler temperature conditions (Fournier et al., 2009). Regarding the effect of temperature on the expansion rate and the final expansion, previous works have demonstrated contradictory evidence. According to a study done by Larive (1997), the temperature does not affect the final expansion but has a significant impact on expansion kinetics. Furthermore, the temperature dependence of the kinetics of ASR expansion follows Arrhenius' rule (Larive, 1997).

As not all aggregates are susceptible to ASR, the severity of the symptoms is frequently dependent on the type of aggregate present. Though many rock types have silica as a mineral, ASR is generated only by some siliceous aggregates. Mineral quartz does not display ASR signs as it is stable but Opal is a reactive mineral. Opal, volcanic glass, cristobalite, strained quartz, and various types of cryptocrystalline, microcrystalline, and tridymite are examples of reactive minerals (Thomas et al., 2011). Many variables, such as the modulus and silicate and alkali content, must be investigated concurrently to comprehend the activity of the materials under consideration. The majority of prior experiments for alkali reactive aggregates employed quartz glass and opal (Shi et al. 2015). Waste glass can be utilized as an aggregate in concrete in the form of fine or coarse aggregates. Earlier studies about the use of glass aggregates in mortars indicate that the reactivity of glass is affected by the size of the particles, with finer particles of glass aggregate resulting in lower ASR expansions. Increasing the surface area of glass particles can accelerate the ASR (Rajabipour, Maraghechi, & Fischer, 2010).

The size of the aggregates influences the rate of reaction as well as the expansion of concrete. Hobbs & Gutteridge (1979) investigated the effect of the size of aggregates by using opaline rocks as the aggregate type with fractions ranging from 150 µm to 4.72 mm. They concluded that expansion increases as opaline aggregate particle size decreases (Hobbs & Gutteridge, 1979).

Multon and Toutlemonde (2006) performed and analysed tests on concrete samples exposed to various forms of stress along three different directions. The calculated volumetric expansions of ASR samples that are damaged under 3D phases of stress are minimized, however, the classical analysis cannot conclude actual ASR-induced strains. They carried out this experiment to analyse the actual ASR-imposed strains. Deformations for these ASR-induced expansions are more representative of the ASR imposed expansions on weaker and mortar aged structures and enable volume expansions to be evaluated for the nine various states of stresses (1D and/or 3D). The quantity of axial ASR imposed strain added to twice the radial-imposed strain is equivalent to the volumetric applied strain for the cylinders. The volumetric applied strain was computed on the 400th day to assess the results depending on the level of stress (Multon & Toutlemonde, 2006).

When the concrete matrix contains well-distributed pores, the ASR-induced expansion is substantially reduced. Even though the reaction rate may be unaffected, the pores relieve the swelling of the gel, resulting in lower concrete expansion (Hobbs, 1988). The expansion of both air-entrained and plain mortar bars was measured by Jensen et al. (1984). A decrease of 40% in expansion was found when 4% air was added into the mortar specimen (Jensen et al. 1984).

ASR exhibits similar microscopic behaviour to other deterioration mechanisms including D-Cracking and freeze-thaw. A detailed examination of microscopic characteristics can be used to identify the basic degradation process and to evaluate the existence of ASR gel in a concrete structure. Some smooth, lapped concrete surfaces with reaction rims over coarse aggregate particles, microcracks across particles, and white in colour products of ASR gel could be seen. Verified gel deposits can prove that ASR has occurred (Stark, 1991).

Staining fractured concrete surfaces using Uranyl Acetate solution is another approach for detecting ASR. According to Stark (1991), this technique could be used to identify ASR gel on any concrete surface. Using this approach on formed and sawed concrete surfaces that have been exposed for years has revealed that this does not always produce satisfactory results with such concretes. It is better to use this method on fresh and newly formed concrete surfaces. Some instances for newly formed concrete surfaces include fresh fractures, cores, and sawed surfaces. The existence of ASR gel will be confirmed by a yellowish-green fluorescent glow under ultraviolet (UV) light (Stark, 1991).

Another potential staining technique is the geochemical method for the identification of ASR Gel, which was developed in the Los Alamos National Laboratory and often referred to as the dual staining process or Los Alamos Staining Method (Guthrie & Carey, 1997). It relies on the composition of ASR gel and one of its properties which is the capacity of a fluid to exchange cations. The stained concrete surface can be viewed in normal lighting conditions. In the treatment procedure, two different types of reagents are used. The first is a saturated aqueous solution of sodium cobaltinitrite [$Na_3Co(NO_2)_6$] also known as Sodium hexanitrocobaltate(III), that reacts with soluble potassium and forms a yellowish precipitate staining potassium-rich ASR gel. The other aqueous solution used in this procedure is saturated Rhodamine B solution. It can react with ASR components other than potassium-rich ASR and stain the concrete in a pinkish colour. Calcium ions contained in the ASR gel are identified using this. This dual staining method enables researchers to test concrete for ASR in-laboratory and also in the field like the uranyl acetate approach. However, unlike the uranyl acetate approach, this does not involve the use of Ultraviolet light in a light-tight setting. More significantly, it does not involve the use of variants of uranium which is a radioactive element. The dual staining method is preferable to the uranyl acetate approach not only because it provides more detail, but also as it can improve standard petrographic analysis of the concrete (Guthrie & Carey, 1997).

Field case studies have been done employing the Los Alamos staining method. Tests have also been carried out using different Rhodamine dyes such as rhodamine B base, Rhodamine B, and Rhodamine 6G solutions. Sodium Cobaltinitrite and Rhodamine have been applied on different concrete structures and chips to detect the presence of ASR. Those concrete structures which gave positive results to Los Alamos dual staining technique were subsequently examined via microscopic petrography to verify the existence of ASR gel (Guthrie & Carey, 1998).

In 2019 a research study was conducted to analyse the alkali-aggregate reaction in concrete dams in India. They recommend some extensive investigations to understand the distress mechanism due to ASR. This includes a combination of methodologies such as visual inspection of the interior concrete core, the staining approach proposed by Guthrie & Carey (1997) which involves water-soluble compounds known as Concentrated solutions of sodium cobaltinitrite and rhodamine, Petrographic examinations of aggregates and mineral composition. They also recommend conducting x-ray diffraction and SEM study (Arora et al., 2019).

3   METHODOLOGY

3.1   Introduction

The present work is primarily concerned with the investigation of existing concrete structures suspected of being impacted by Alkali Aggregate Reaction. The objective was to check the feasibility of using an experimental procedure to detect potential AAR in such structures within the limited

laboratory facilities available in a typical situation in Sri Lanka. After comparing the two staining tests discussed above it was decided to use the Los Alamos test because of its simplicity and applicability in field testing. Even though this test uses two different reagents separately, it was decided to confine the present work to one reagent: sodium cobaltinitrite which would be able to detect the vast majority of ASR cases.

The limitations that had to be considered were twofold: lack of extensive laboratory facilities and lack of experience in interpreting results of staining tests. The simplicity of the selected test addressed the former. The present study intended to address the latter by conducting a series of staining tests on concrete made with reactive aggregates as well as on control specimens made with non-reactive aggregates. If the tests, when interpreted by the authors (who do not have special expertise in such interpretations), can correctly identify potential AAR in the test specimens then it may be concluded that it would be feasible to use the selected test method for the detection of potential AAR in existing concrete structures.

The testing was done in two steps.
- Samples of reactive and non-reactive concrete specimens were cast and cured in different curing solutions for different time periods.
- Samples were tested for Alkali-Silica Reaction using staining solution.

There are several commonly available alkali reactive aggregates. In the present work waste white glass was used as the reactive aggregate. The white glass shows the highest expansion which is greater than that for Amber and Green glass (Christian, 2003). Natural coarse aggregate was used in control (non-reactive) specimens.

Three curing solutions were utilized to cure concrete specimens.
1. Water

In the Standard test for compressive strength of cylindrical concrete specimens-ASTM C 39, water is employed as a curing medium. In this research project also, distilled water was used as a curing solution.
2. 1M NaOH solution

This is widely used to accelerate ASR in aggregate identification tests such as ASTM C 1260 (Mortar-Bar Method), accelerated version of ASTM C 1293 (Concrete Prism Test) also known as the accelerated concrete prism test, and ASTM C 1567 (Accelerated Mortar-Bar Method). The NaOH solution provides a high alkaline media to accelerate ASR in concretes.
3. 1M KOH solution

To provide a more potassium-rich high alkaline medium.

These three different curing solutions, namely: water, 1 M NaOH, and 1 M KOH, were used to cure concrete specimens. KOH was primarily used as a curing solution in this study to determine whether the test results are altered by an external potassium medium in the absence of an alkali aggregate reaction. Another motivation for using potassium hydroxide is to test how this methodology reacts to different alkali kinds.

3.2   Experimental Procedure

When deciding on the design grade of concrete specimens, the capability of the specimen to provide a clean concrete surface was primarily evaluated. No strength testing, such as compression or tensile tests, were required in the methodology described. It was decided to cast reactive and control specimens with nominal Grade 25 concrete using the volume mix proportions shown in Table 1.

Table 1. Volume mix ratio for concretes

Specimen Type	Cement	River Sand	Glass Coarse Aggregates	Natural Stone Coarse Aggregates
Control	1	1	-	2
Reactive	1	1	2	-

Two batches of concrete were tested after curing for different time periods. Each batch consisted of non-reactive and reactive concrete specimens cured in respective curing agents. Timber moulds of 50 mm X 50 mm X 200 mm were used to cast the concrete specimens.

The concrete specimens were demoulded after 24 hours. They were kept for 24 hours in water and then moved to the three curing solution baths which were at room temperature.

3.3 Application of Sodium Cobaltinitrite

3.3.1 Preparation of Specimens

There are several methods for preparing the concrete specimen surface in the field, such as bush hammering, fracture of a core or hand sampling, and sawing/polishing to create a smooth surface for petrographic examination or preparation of a thin section. This stain testing is more efficient on fractured surfaces since fracturing causes the minimum amount of chemical change to ASR gel than surfaces created by bush hammering, sawing, or polishing. Chemical compounds that may interfere with the ASR gel resulting from methods like sawing, polishing lubricants etc. must be avoided (Guthrie & Carey, 1997). A crack was produced on the surface of the concrete specimen using a bursting wedge with a small force from a hammer. Then the concrete specimen was fractured. The fractured surface was then treated with the reagent.

3.3.2 Surface Treating

The specimen surface was rinsed with distilled water to remove any loose dust particles and to wet the surface before treating with the Sodium Cobaltinitrite solution. Then Sodium Cobaltinitrite solution was applied to the fractured surface of the concrete. After 60 seconds the surface was rinsed again with distilled water. Following the final rinse, stained regions were slightly visible on some concrete surfaces. Specimens were dried to see the clearer yellow stains. The specimens were first examined with the naked eye to determine whether any discolouration or yellow stains were present. After observing the stains with the naked eye, the specimens were examined with a 10X hand lens to obtain a more magnified view of the stains.

4 RESULTS AND DISCUSSION

The results observed after treating with Sodium Cobaltinitrite are discussed under a few categories.
- Depending on the type of aggregate used to cast concrete specimens
- Depending on the curing solution used
- The difference in observations according to the curing duration.

4.1 Observations and Discussion According to the type of the Aggregate

Reactive and Non-Reactive Concrete Specimens cured in water were treated with Sodium Cobaltinitrite to see the reactivity of the aggregate types. It was observed that yellow stains appeared in concrete specimens produced with glass aggregates. As shown in Figure 1, Yellow stains were not evident in concrete specimens cast using non-reactive natural coarse aggregates. The same observations were made in the second batch according to Figure 2.
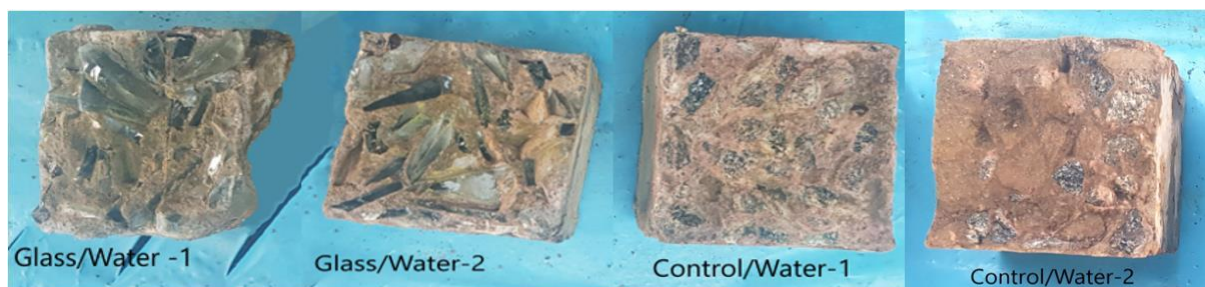

Figure 1. Concrete specimens cured in water (Batch 1)

Figure 2. Concrete specimens are cured in water (Batch 2).

In the case of curing in 1M solution of NaOH also it was observed that in both batch 1 and batch 2 yellow stains appeared in concrete specimens produced with glass aggregates, but according to Figure 3 yellow stains were not evident in concrete specimens cast using natural coarse aggregates.
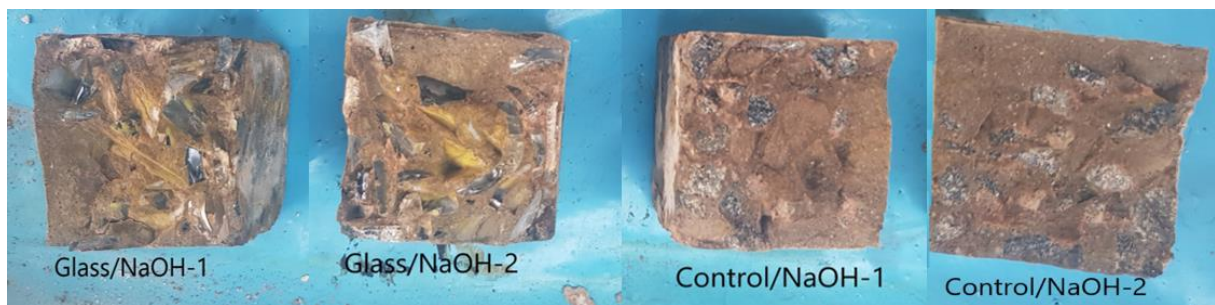

Figure 3. Concrete specimens cured in 1M NaOH (Batch 1)

Figure 4 shows the second batch of concretes. In both batches, the staining was noticeable along the edges, inside the aggregate, and in the composite at the contact in broken sections of the reactive aggregate. The staining was most visible where the glass particles had been in contact before breaking the concrete specimen. The intensity of the reaction of aggregates to the curing solution is described in a different section of this paper. The amount of ASR in the concrete corresponds with the severity of yellow stains present. (Guthrie & Carey, 1998)

Figure 4. Concrete specimens cured in 1M NaOH (Batch 2)

The results in the case of curing in 1M solution of KOH were different. Both reactive and non-reactive concrete specimens had yellow stains. This was observed in both batches as shown in Figure 5 and Figure 6. This anomaly has been addressed further under the type of curing solution.
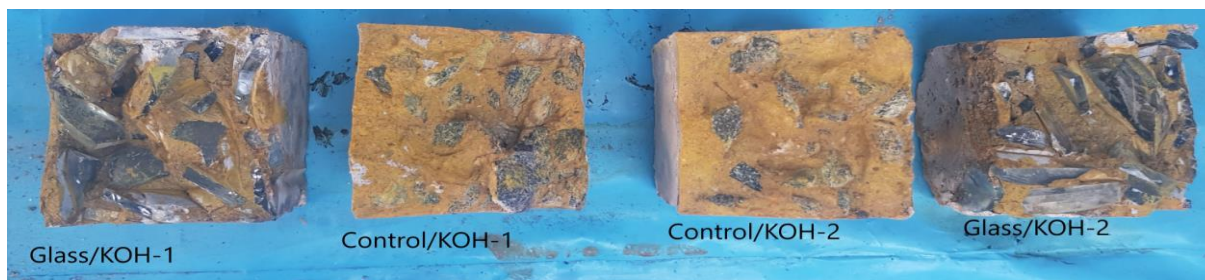
Figure 5. Concrete specimens cured in 1M KOH (Batch 1)

Figure 6. Concrete specimens cured in 1M KOH (Batch 2)

4.2 Observations and Discussion According to the type of the Curing Solution

4.2.1 Water

The concrete specimens of the first batch made using glass can be seen with slight yellow stains around the aggregates and the concrete surface. In both batches, yellow stains on concrete made with glass aggregates indicate that the AAR was likely to take place in concrete containing reactive aggregates even when cured in water, which does not contain any alkalis such as sodium and potassium. The absence of stains in control specimens of both batches suggests that the concrete cast using non-reactive aggregates was not subjected to the Alkali-Silica Reaction when cured in water.

4.2.2 1M solution of NaOH

NaOH is used here to accelerate ASR in the concrete specimens. There were no clear traces of yellow stains on the fractured surfaces of concretes containing non-reactive aggregates.

Glass aggregate concrete specimens of the first batch which were cured in 1M NaOH displayed more prominent yellow stains than those cured in water. ASR is accelerated by immersing concrete or mortar specimens in a strong alkaline solution such as 1M NaOH. These accelerated methods have been developed to minimize the length of tests and to enhance the practicality of testing.

The intensity of yellow stains in glass aggregate specimens cured in 1M NaOH is greater than that in glass aggregate concrete specimens cured in water. This confirms that the availability of alkalis in curing solution can accelerate AAR. A significant increase in yellow stain severity can be observed in batch 2 when compared with batch 1.

4.2.3 1M solution of KOH

It was observed that, when cured in KOH solution, specimens cast using control aggregates as well as reactive aggregates in both batch 1 and batch 2 displayed yellow stains all over the fractured surface of the concrete specimen. In the previous cases of curing in water and NaOH, the concrete specimens cast using control aggregates did not show any visible signs of yellow stains. The intensity of yellow colour in the two batches appear to be similar.

In this study, a simple spot test was carried out to check whether Sodium Cobaltinitrite might produce a false-positive result in the presence of K+ ions from the KOH solution even without any ASR. A concrete specimen made of non-reactive aggerates and cured in water was fractured. A few

drops of KOH were added using an eyedropper onto the fractured surface of the concrete specimen. The other surface of this same specimen was not applied with KOH. When tested with sodium cobaltinitrite the surface treated with a few drops of KOH showed yellow stains as shown in Figure 7 while the surface not treated with KOH did not show any stains. This suggests that stains in the specimens immersed in KOH were caused by the alkali solution and not any ASR. The reason for yellow stains might be the reaction of Sodium Cobaltinitrite with the K+ ions available in the KOH solution.

Figure 7. Control/Water specimen treated with Sodium Cobaltinitrite after applying KOH drops on the surface

The results seen from the concretes immersed in KOH is a limitation of this method. The original expectation was observations similar to those in concretes cured in NaOH. But it appears that K+ ions from other sources can produce false-positive results.

4.3 Observations and Discussion According to the curing duration.

Batch 1 specimens were cured for 44-days while those of batch 2 were cured for 60-days. It was observed that the intensity of yellow stains in the specimens containing reactive aggregates is higher in batch 2 compared to batch 1 as shown in Figure 8.
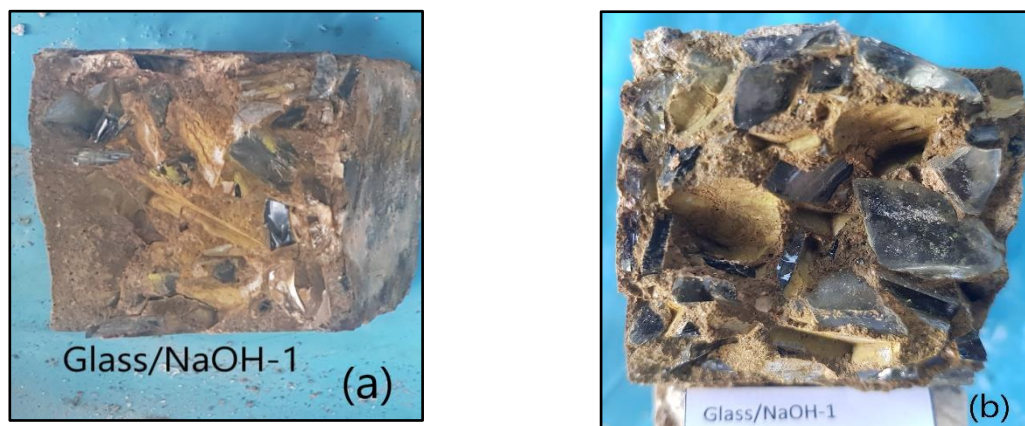

Figure 8. Glass/NaOH specimens of (a) batch 1 and (b) batch 2

AAR reaction typically continues over a long time (Swamy, 1991). Mortar Bars tests-ASTM C 1567, using recycled glass as the aggregate had been performed by Serpa et al. (2013). They observed that the expansion of mortars was greater in 28-days than in 14-days (Serpa, Silva, De Brito, Pontes, & Soares, 2013). Other researchers such as Christian (2003), Rajabipour et al (2010) have also done similar studies using mortar bar testing. They also confirm that the reaction becomes greater with exposure time (Rajabipour et al., 2010). As the intensity of yellow stains is higher in batch 2 than in batch 1, it can be concluded that the ASR has taken place in batch 2 more than in batch 1.

5   CONCLUSION

The testing outcomes were sufficient to draw some conclusions from this investigation. Sodium Cobaltinitrite staining can be used even by people without extensive experience and training to detect the presence of Alkali-Silica Reaction. The appearance of yellow stains on fractured concrete surfaces offers a rapid indication of the presence of ASR. Staining using sodium cobaltinitrite allows testing of concrete for alkali-silica reaction in a laboratory or even in the field. Using sodium cobaltinitrite to identify ASR is a viable test in the early phases of assessing a suspected structure for ASR. However, it is best to confirm any positive test results with a second test such as petrographic analysis under the supervision of an expert.

If this test does not provide a positive result on a concrete surface, it can be concluded that the Alkali-Silica Reaction is unlikely to occur in the concrete concerned.

The Los Alamos staining test examined in this study has only minimum environmental and health impacts in comparison with the uranyl acetate staining methods involving radioactive elements (Guthrie & Carey, 1997).

The Los Alamos test using sodium cobaltinitrite can be utilized as a rapid screening test in the preliminary stages of experimental identification of alkali-aggregate reaction in existing concrete structures.

6   ACKNOWLEDGEMENTS

REFERENCES

Arora, V., Singh, B., Patel, V., & Mohapatra, B. (2019). Diagnosis of alkali aggregate reaction in concrete dams: an Indian case study. *Journal of Asian Concrete Federation, 5*(2), 27-36.

Christian, M. (2003). Glass Concrete. *Concrete International, 25*(6).

Fournier, B., Ideker, J. H., Folliard, K. J., Thomas, M. D. A., Nkinamubanzi, P.-C., & Chevrier, R. (2009). Effect of environmental conditions on expansion in concrete due to alkali-silica reaction (ASR). *Materials Characterization, 60*(7), 669-679. doi:10.1016/j.matchar.2008.12.018

Guthrie, G., & Carey, B. (1998). Detection of alkali-silica reaction swelling in concrete by staining.

Guthrie, G. D., & Carey, J. W. (1997). A simple environmentally friendly, and chemically specific method for the identification and evaluation of the alkali-silica reaction. *Cement and Concrete Research, 27*(9), 1407-1417. doi:10.1016/s0008-8846(97)00123-3

Hobbs, D. W. (1988). *Alkali-silica reaction in concrete.*: Institution of Civil Engineers.

Hobbs, D. W., & Gutteridge, W. A. (1979). PARTICLE-SIZE OF AGGREGATE AND ITS INFLUENCE UPON THE EXPANSION CAUSED BY THE ALKALI-SILICA REACTION. *Magazine of Concrete Research, 31*(109), 235-242. doi:10.1680/macr.1979.31.109.235

Jensen, A. D., Chatterji, S., Christensen, P., & Thaulow, N. (1984). Studies of alkali-silica reaction — part II effect of air-entrainment on expansion. *Cement and concrete research, 14*(3), 311-314. doi:10.1016/0008-8846(84)90046-2

Larive, C. (1997). Apports combinés de l'expérimentation et de la modélisation à la compréhension de l'alcali-réaction et de ses effets mécaniques. In: Ecole Nationale des Ponts et Chaussées.

Multon, S., & Toutlemonde, F. (2006). Effect of applied stresses on alkalisilica reaction-induced expansions. *Cement and Concrete Research*.

Nilsson, L.-O. (1983). Moisture effects on the alkali-silica reaction.

Rajabipour, F., Maraghechi, H., & Fischer, G. (2010). Investigating the Alkali-Silica Reaction of Recycled Glass Aggregates in Concrete Materials. *Journal of Materials in Civil Engineering, 22*(12), 1201-1208. doi:10.1061/(asce)mt.1943-5533.0000126

Serpa, D., Silva, A. S., De Brito, J., Pontes, J., & Soares, D. (2013). ASR of mortars containing glass. *Construction and Building Materials, 47*, 489-495.

Shi, C., Shi, Z., Hu, X., Zhao, R., & Chong, L. (2015). A review on alkali-aggregate reactions in alkali-activated mortars/concretes made with alkali-reactive aggregates. *Materials and Structures, 48*(3), 621-628. doi:10.1617/s11527-014-0505-2

Stanton, T. E. (1940). Expansion of Concrete through Reaction between Cement and Aggregate. *Transactions of the American Society of Civil Engineers*.

Stark, D. (1991). *Handbook For The Identification Of Alkali-SIica Reactivity In Highway Structures*. Washington: Strategic Highway Research Program.

Steffens, A., Li, K. F., & Coussy, O. (2003). Aging approach to water effect on alkali-silica reaction degradation of structures. *Journal of Engineering Mechanics-Asce, 129*(1), 50-59. doi:10.1061/(asce)0733-9399(2003)129:1(50)

Swamy, R. N. (1991). *The alkali-silica reaction in concrete*: CRC Press.

Thomas, M. D. A., Fournier, B., Folliard, K. J., & Resendez, Y. A. (2011). *Alkali-Silika reactivity field identification handbook*.

Data Science to Determine Mechanical Properties of Low Carbon Steel During In-Process Inspections

K. G. Alahapperuma, D. D. D. Suraweera & N. Nandhakumar
University of Vocational Technology
Ratmalana, Sri Lanka.
University of Vocational Technology
Ratmalana, Sri Lanka.
Ashok Steel Private Limited Company
Waththala, Sri Lanka.
kgalahapperuma@uovt.ac.lk, dddsuraweera@uovt.ac.lk, nandha.watttala@gmail.com

ABSTRACT

Carbon steel is a widely used category of engineering metal, mainly due to its attractive mechanical and fabrication properties and low cost. The chemical composition, physical parameters, and mechanical properties of carbon steel are maintained as per the specified standards, and local steel should be complied with Sri Lankan Standard 375: 2009. Generally, the chemical composition is tested during melt stages, and mechanical properties are tested for finished products. Since it is necessary to ensure products comply with the standard, mechanical properties are tested during in-process inspections as well. When the results are not within the acceptable range, a considerable amount of production has to be rejected, causing a loss to the manufacturers. If the results of the in-process inspection are instant, it will help make suitable adjustments to process conditions and thereby prevent rejection of products, while reducing quality assurance costs, as well. Therefore, the objective of this study is to predict tensile properties with chemical composition, as input variables, to be used for in-process inspections. Forty mechanical test reports were collected from a steel manufacturing factory for 12 mm diameter, thermo-mechanically treated (TMT) steel bars. Each test report is of 15 samples from the respective batch, and consists of corresponding chemical composition and physical parameters. Multiple linear regression analysis was applied to each batch, using Statistical Package for the Social Sciences (SPSS) software, to predict yield strength (YS), ultimate tensile strength (UTS), elongation at break (EB) with carbon equivalent value (CEQ) and percentage of Sulphur as inputs. Relationships between variables were not significant, even though those relationships can be used to predict tensile properties. The predictions may not be reliable, due to the limited conditions of the study and assumptions made. It is therefore recommended to apply multivariate regression analysis or Artificial Neural Network (ANN) techniques, with other chemical elements, process temperature and water flow rate etc. also as input variables.

KEYWORDS: *Chemical composition, In-process inspection, Low carbon steel, Multiple linear regression analysis, Tensile properties*

1   INTRODUCTION

Plain carbon steel is regarded as a universal engineering metal, due to its many attractive properties during processing as well as usage. Superior strength properties, adaptability to multiple fabrication techniques, amenable to various heat treatments, environmentally favored characteristics, and recyclability are among them. It is also an economically reasonable material. In 2019, the value of the global market size of carbon steel was USD 887.7 billion, and as a reinforcing metal carbon steel finds various structural applications, such as walls, fencing, frames, and pipelines etc. (Grand View Research, 2020). Carbon is the main alloying element that controls the properties of carbon steel, and other elements such as Silicon, Manganese, Sulphur and Phosphorus are also present in it in minor amounts (Pakirappa, 2004). Properties of carbon steel should be maintained within prescribed ranges, according to the specified standards. In Sri Lanka, the chemical composition, physical parameters and

mechanical properties of carbon steel should be confirmed with the SLS 375:2009 standard (Sri Lanka Standard Institution, 2009). The chemical composition of steel is tested during the melting stage, and mechanical properties are tested for manufactured bars. The tensile properties of carbon steel are highly essential components of the tested mechanical properties. YS is regarded as the main property which determines the grade of steel. According to the standard, UTS is also highly important, and the ratio of UTS/YS should be maintained above 1.05. EB is another essential property that should be maintained above 14%. Even though the specified mechanical and physical properties and chemical composition need to comply with standard requirements, approximate values of mechanical properties are sufficient when a quick analysis is done during in-process inspections.

The production of steel is usually held on a 12-hour shift basis, and mechanical properties are tested at the final inspection process, for manufactured cooled bars. In the case of hot rolling mills with manual or semi-automated systems, it is preferable to analyse the same mechanical properties to be tested for finished products, at some frequency, during the production stage itself. This is done in order to ensure that the product quality is maintained for the entire batch; generally, samples are drawn for testing at one-hour intervals. However, the drawn hot samples have to be cooled to room temperature, to be tested for mechanical properties which approximately takes 40–45 minutes. When the test results are found, the mill approximately completes one hour's production period. When the test results are not acceptable, remedial actions need to be taken by quarantining that particular hourly production quantity. If data science is applicable to estimate the essential mechanical properties, immediately after the samples are drawn, it will be beneficial for steel manufacturers as it prevents production losses as well as man power, cost, and the time spent on experiments.

Use of data science techniques in this type of study is found in the literature. Lim (1991) applied multiple linear regression to determine the mechanical properties of two grades of steel, with chemical composition as the input variables. Examples for the use of advanced techniques such as ANN models are also found. To determine the effect of chemical composition and tensile properties on the hardness and the impact toughness of one micro-alloyed steel, ANN networks were implemented (Faizabadi, *et al.*, 2014). In a similar study, to predict tensile properties of austenitic stainless steel, ANN models were applied (Wang *et al.*, 2020) using chemical composition, test temperature and heat treatment as the input variables. Seven data science techniques of Random Forest, Neural Network, Linear regression, K- Nearest Neighbor, Support Vector Machine, Decision Tree, and Ensemble methods were applied (Sandhya *et al.*, 2019) in another study to determine the tensile strength, with carbon percentage, bar diameter, processing temperature and manufacturing technique as the input variables.

The specific purpose of this analysis is to approximate the mechanical properties of final steel products, while they are still in the production progress, using chemical composition as inputs. Since the effect of certain chemical elements is not regarded as independent, carbon equivalent value was considered as one variable, instead of considering individual elements. Advanced techniques of data science such as non-linear regression models or ANN models are preferred for this type of studies. Since the study is an initial step, multiple linear regression analysis was selected as the technique. Thus, the objective of the study was to observe the usefulness of the selected input variables of carbon equivalent value and Sulphur content, to predict the tensile properties of YS, UTS and EB, using multiple linear regression analysis.

2   METHODOLOGY

Forty reports possessing physical parameters and mechanical properties based on the SLS 375:2009 standard were collected from a steel manufacturing factory[1]. The reports were of 12 mm nominal diameter, TMT concrete reinforcing bars of 12RB500 grade, and each test report was of 15 samples from the respective batch. The corresponding chemical composition of each batch was also

---

[1] Test reports of 12 mm nominal diameter, TMT concrete reinforcing bars of grade12RB500, low carbon steel, supplied by a steel manufacturing factory in Sri Lanka were the source of data. Each test report consisted of mechanical properties, physical parameters and chemical composition belonging to 15 samples from the respective batch.

available in each test report. The readings of the mechanical properties of each batch were averaged before applying for the analysis. The flow rate of water used for the thermo mechanical treatment, inlet and outlet temperatures of water, billet temperature, and other process parameters were assumed to be the same for all batches.

The data related to 40 batches of samples were analysed with SPSS software using multiple linear regression technique analysis. Percentages of carbon equivalent value and Sulphur were the two independent variables to predict the tensile properties of YS, UTS and EB. Carbon equivalent value is based on all elements of Carbon, Manganese, Chromium, Molumdenum, Vanadium, Nickel and Copper, as per the SLS standard (Sri Lanka Standard Institution, 2009). However, only the Carbon and Manganese amounts are analysed during chemical inspections of this grade of steel, assuming the presence of other elements is insignificant. Table 1 shows the input and output parameters with their relevant statistics used for the analysis.

Table 1. Input and Output Parameters and Their Statistics Used for
Multiple Linear Regression Analysis

Parameter	Unit	Maximum	Minimum	Average	Standard Deviation	Median	Variance
Input							
CEQ, %	% by weight	0.357	0.282	0.319	0.019	0.32	0.000337
S, %	% by weight	0.04	0.02	0.0293	0.0083	0.03	0.000066
Output							
YS	$Nm^{-2}*(10^6)$	564	545	555.7	4.2317	556	17.46
UTS	$Nm^{-2}*(10^6)$	637.6	613.6	627.54	5.9831	627	34.9025
EB	% of original Length	28	22	24.95	1. 2393	25	1.4975

3   RESULTS

The regression equation for YS is given in Eq. (1).

$$YS = 55.524 + 16.49(CEQ\%) - 36.784(S\%) \tag{1}$$

The two graphs of expected values and experimental values of YS are shown in Figure 1.
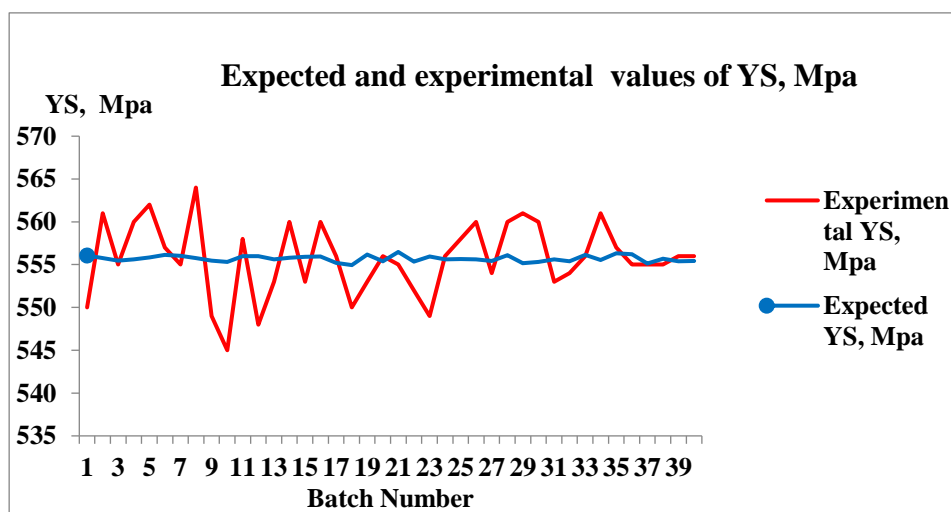

Figure 22. Expected and experimental values of yield strength (YS)

The regression equation for UTS is given by Eq. (2).

$$UTS = 634.566 - 17.213(CEQ\%) - 52.612(S\%) \tag{2}$$

Figure 2 indicates the graphs of expected values and experimental values of UTS.
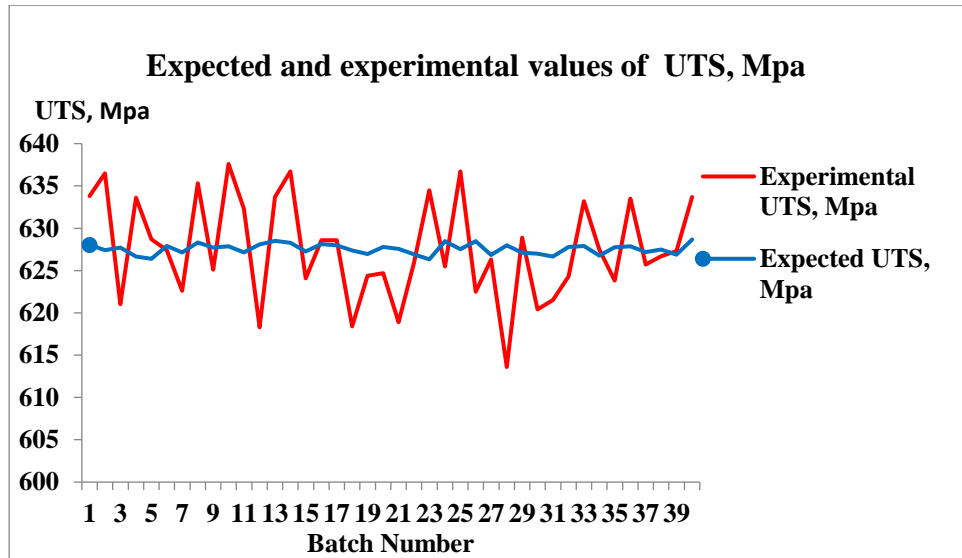

Figure 2. Expected and experimental values of ultimate tensile strength (UTS)

The regression relationship for EB is given by Eq. (3).

$$EB = 26.512 - 5.169(CEQ\%) + 2.893(S\%) \tag{3}$$

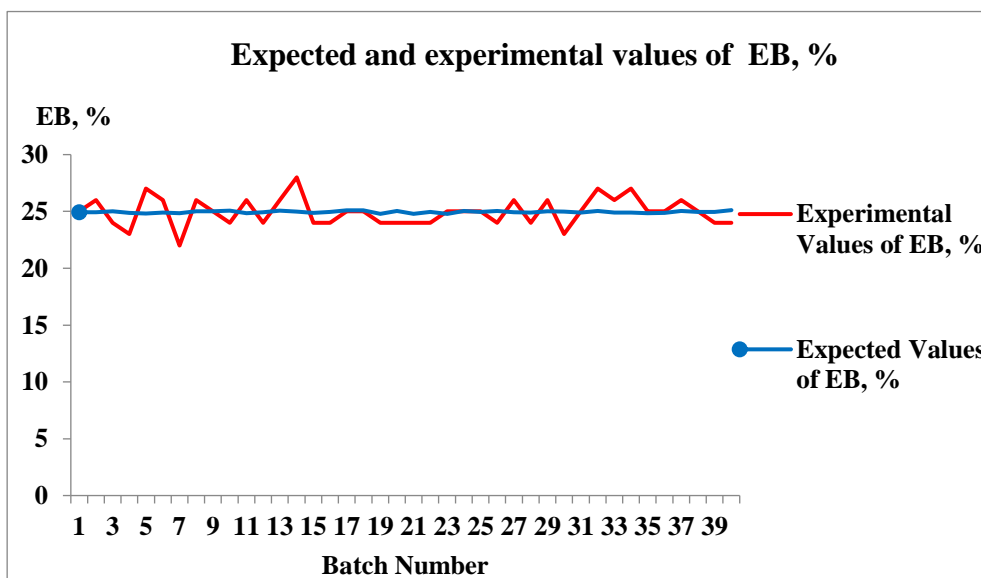Figure 3 shows the expected values and experimental values of EB.

Figure 3. Expected and experimental values of percent elongation at break (EB)

4   DISCUSSION

As per the derived linear relationships for the tensile properties, the obtained P (probability) value in each case was greater than 0.05, and the obtained R^2 values for YS, UTS and EB were 4.8, 5.0 and 5.4, respectively. These details imply that the association of the variables in each relationship is not significant.

The yield strength shows a moderately positive correlation with CEQ%, and highly negative correlations with S%. UTS shows negative correlations with both CEQ%, and S%. Its correlation with CEQ% is moderate while its correlation with S% is considerably high. EB shows a somewhat moderate and negative correlation with CEQ% and a low, positive correlation with S%. There may be other variables which affect these parameters, and the fact that the effects of which were assumed as negligible in the study   could be the reasons for the observed correlations.

Since this was an initial attempt to predict the association of the known variables with the expected properties, only average experimental values of properties were applied in order to make the task easy. Additionally, only 40 reports were used, even though a large number of reports are preferable for this sort of analyses. Further, the chemical composition was available only batch-wise; not for the individual samples.

According to the operational manual of semi-automated hot rolling mills, production process conditions such as the flow rate of the water used for the thermo-mechanical treatment, inlet, and outlet temperatures of water, and billet temperature can be varied in the timeline. However, for the analysis, those parameters were considered to be constant and maintained preferably for the process operations.

Even though the major chemical elements, whose presence is regarded as significant, were considered for the evaluation, several other elements which were not considered for this analysis, are also present in this particular steel. Those neglected elements include Cr, Cu, V, Mo and P etc.

This study was focused on only 12 mm nominal diameter bar samples, though there is a preferred range of products available for this grade steel, such as 10 mm, 16 mm, 20 mm, 25 mm, 32 mm, and 40 mm.
This analysis was an initial approach to observe the effectiveness of chemical composition during in process inspections. The derived relationships can be used to approximate the tensile properties, provided the other process conditions are not varied throughout the entire process, which may not be generally plausible. Therefore, for more reliable relationships for the expected properties, actual variation of other process conditions must be considered during the analyses.

5   CONCLUSION

Data science techniques are used nowadays to predict the details of material science techniques. Therefore, mechanical properties obtained by conventional experimental methods can be predicted through the application of proper data science models. The accuracy of data science-based approaches will be dependent on the input of sufficient accurate details.

This study was an initial attempt to analyse the possibility of applying the available data to obtain the results of mechanical tests, done for finished products of a selected low carbon steel, using linear regression models. The study was conducted under certain limitations and assumptions. The obtained results will be helpful to predict the properties, provided all other process conditions are not changed throughout the entire production process. Therefore, to obtain more reliable results, the study needs to be redesigned with more input variables of actual process conditions.

6   RECOMMENDATIONS

In future studies, models developed with more input variables are recommended, expecting improved accuracy. Contents of other available chemical elements, process parameters, and heat treatment conditions can be applied as other inputs. Other preferable ranges of products with different bar diameters may be considered with a higher number of test records. Another suggestion is to use chemical element contents obtained sample-wise, instead of the contents obtained batch-wise.

The analysis can also be focused on non-linear multivariate relationships or more advanced techniques, such as ANN models and grey theory models etc.

REFERENCES

Faizabadi, M. J., Khalaj, G., Pouraliakbar, H., & Jandaghi, M. R. (2014). Predictions of toughness and hardness by using chemical composition and tensile properties in micro alloyed line pipe steels. *Neural Computing and Applications-December 2014, volume* 25, pg1993–pg1999. DOI: 10.1007/s00521-014-1687-9.

Grand View Research. (2020, April). *Market analysis report, Carbon steel market size, share and trends analysis report by type (low carbon steel, medium carbon steel, high carbon steel), by application (shipbuilding, automotive, construction), by region, and segment forecasts, 2020 – 2027.* https://www.grandviewresearch.com/industry-analysis/carbon-steel-market

Lim, W. T. (1991). *Statistical analysis of reinforcing steel properties.* Thesis (MSc). University of Canterbury. https://ir.canterbury.ac.nz/handle/10092/6461

Pakirappa. (2004). *Metallurgy and material science* (2nd edition). Premier Publishing House.

Sandhya, N., Sowmya, V., Bandaru, C.R., & Babu, G. R. (2019). Prediction of mechanical properties of steel using data science techniques. *International Journal of Recent Technology and Engineering, volume 8*(issue 3).

Sri Lanka Standard Institution. (2009). *Sri Lanka standards 375:2009 (specification for ribbed steel bars for the reinforcement of concrete-publication no. UDC 669.14- 122.4:691.714:691.328)*(4th edition). No.17, Victoria Place, Elwitigala Mawatha, Colombo 08.

Wang, Y., Wu, W., Li, X., Xie, Z., Liu, R., Liu, W., Zhang, Y., Xu, Y.,& Liu, C. (2020). Prediction and analysis of tensile properties of austenitic stainless steel using artificial neural network. *Metals, volume 10* (issue 234). Doi:10.3390/met10020234

Efficient Ventilation Configurations for an Isolation Ward in View of Reducing the Potential Contamination of Its Occupants

Hasitha Durage , Prof. Rahula Attalage
Sri Lanka Institute of Information Technology, New Kandy Road, Malabe, Sri Lanka.
rahula.a@sliit.lk

Dr R.M.P.S. Bandara
General Sir John Kotelawala Defence University, Kandawala Rd., Ratmalana, Sri Lanka
bandara@kdu.ac.lk

ABSTRACT

The rise of respiratory infections, such as the SARS epidemic in 2003, and the H1N1 influenza epidemic in 2011, highlighted the importance of efficient ventilation in healthcare facilities. The novel SARS -Cov-2 disease has sparked many concerns over the ventilation performance of multi-bed isolation wards and their ability to suppress airborne infectious contamination. The study is primarily based on suggesting ventilation improvements for a locally acquired multi-bed intensive care isolation unit. The study via ANSYS -fluent incorporates a k-ε turbulent model that is used to analyze exhaled CO_2 particle tracks of 4 human models. Three ventilation strategies, namely, Displacement, Stratum, and Curtain -Air-jet are initially considered and evaluated based on two indoor air quality indices (IAQs), namely, air change efficiency and contaminant removal effectiveness. Stratum ventilation comfortably exhibits unidirectional flow characteristics with an air change efficiency of 0.946, which was obtained through ANSYS -CFX while each suggested configuration is capable of achieving a contaminant removal effectiveness value greater than 1 which depicts that the contamination source is not in a perfect mixing zone. Results provided inconclusive evidence to draw correlations between the two IAQ indices and thus it is confirmed that these indices solely depend on the type of ventilation strategy. Contaminant concentration on health care worker breathing plane and exhaled particle tracking for 4 minutes in each analyzed configuration revealed that both Stratum and Curtain air-jet models improve the escaped particle efficiency by 25% and 29% respectively compared to the base model. These models are further compared against reference values specified by guidelines to evaluate their suitability for real-world operation.

KEYWORDS: *Ventilation, efficiency, ANSYS, isolation, airborne particles, Displacement, Stratum, Curtain -Air-jet*

1. INTRODUCTION

Airborne infectious diseases such as severe acute respiratory syndrome (SARS) in 2003, H1N1 influenza in 2009, droplet infectious diseases such as Ebola (2013-2014) in Africa, and the novel SARS - CoV- 2 diseases originating from Wuhan, China has sparked major concerns over the disease control actions implemented in recent years even with the development of technology. Implementation of proper ventilation strategies that mitigates pathogen transmission via droplets or airborne should be initiated only after extensive experimental or simulation-based studies and research. Aerobiology is the study involving aerial diffusion, biological material deposition, and aerosolization (Pepper & Dowd, 2009). Unlike droplet transmission, individuals are susceptible to airborne particles by inhalation or close contact with secondary infectious sources (VG et al., 1993). Disease-carrying droplets so far have proven to be contagious within a radius of approximately 3 -feet from the infectious source (WELLS, 1934). In enclosed or indoor spaces, the potential threat of infection caused by respiratory and nuclei droplets is considerably high since the velocity, which is dictated by the mass aids in trapping onto surfaces at various distances from the source (Cole & Cook, 1998). In addition, as outlined by (Gralton

et al., 2011), Individuals at a distance from the source are also at a high risk of exposure to airborne particles.

Isolation wards/rooms or negative pressure rooms are mainly designed to control the contamination due to airborne and droplet transmission mentioned above. One of the main causes of developing a positive or neutral ventilation pressure gradient is the action of door-opening and closing of the AIIR (Saravia et al., 2007). A comparative study carried out by (Adams et al., 2011) compared the contaminant containment efficiency of AIIRs using fluorescent microspheres as infectious droplets. It was identified that air traffic caused by healthcare providers reduced the suppression efficiency of droplets. AIIRs provided with anterooms, however, limited the net particle escape during the action of door-opening and closing and thus mitigating hospital-acquired infections (HAIs) for inpatients. The latest studies related to isolation rooms and mechanical ventilation are intended to find effective methods of controlling contaminated air inside AIIR and between the outer environments. Most of these studies are aided by software implementing Computational fluid dynamics (CFD). An analysis completed by (Khankari, 2017) used a 3-dimensional CFD model of a typical isolation room. The impact of HVAC designs on thermal comfort, airflow patterns, and velocity was determined using CFD simulations employing airflow patterns, PMV distribution, temperature distribution, and flow path lines within the room. The study concluded that the case where the supply diffuser is above the patient's head and the return grill behind the supply diffuser offered the best path for infectious particles to exhaust out of the return air grill without causing considerable recirculation.

The implementation of novel ventilation configurations in an isolation ward is the main objective of this study. In a typical displacement ventilation model, a thin layer of air is developed above the ground due to the floor supply and the relatively hot contaminated air rises and mixes with the ambient air due to its higher energy and less density (Ren et al., 2015). Stratum ventilation is a concept that is developed to primarily cater for elevated room temperature and undesired thermal comfort. This configuration is designed in a way that the occupant zone is subjected to horizontal fresh air supply and return (Lin, 2017). Curtain–air–jet configuration is also a potential improvement for ventilation performance in AIIRs. While the primary objective of implementing air curtains is to separate the contaminated zone from the clean zone, several other benefits such as reducing or balancing the cooling requirement in a healthcare environment are also achieved by air curtains. The study uses these configurations to improve a base configuration of an isolation ward using ANSYS -Simulation-based conclusions.

2. MATERIALS AND METHODS

Local survey results

Figure 1 represents the HVAC plan of isolation unit A obtained from the survey conducted locally. The isolation room is a 4–bed patient ward with an anteroom. The dimensions of the isolation room are 6.9 x 5.6 x 2.6 m.

Indices for quantification

1. Air exchange efficiency (ε_a)

As the name implies, it measures the efficiency between the predicted air replacement time and the actual age of air in the space. It measures the ratio between the shortest path possible for air replacement in a time reference (τ_n) and the actual time needed for air exchange (τ_{exe}) as shown in the equation below.

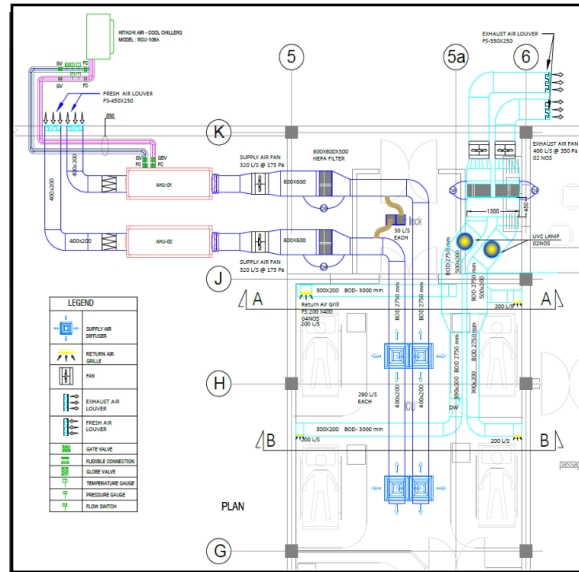$$\varepsilon_a = \frac{\tau_n}{\tau_{exe}} \tag{1}$$

Figure 23 - HVAC Plan of Isolation unit A (Source – survey ABANS

2. Air exchange efficiency (ε_a)

As the name implies, it measures the efficiency between the predicted air replacement time and the actual age of air in the space. It measures the ratio between the shortest path possible for air replacement in a time reference (τ_n) and the actual time needed for air exchange (τ_{exe}) as shown in the equation below.

$$\varepsilon_a = \frac{\tau_n}{\tau_{exe}} \tag{2}$$

It is identified that the shortest possible time for air replacement (τ_n) is the inverse value of the air exchange rate in the space which is given by the following formula.

$$\tau_n = \frac{V}{Q} \tag{3}$$

Where V is the volume of the indoor space and Q is the ventilation flow rate.

- Mean age of Air -MAA ($\bar{\tau}$)

As defined by (Simons et al., 2016) mean age of air refers to the time air has spent in a space or a point in the space accumulating potential contaminants. It is defined that the actual time needed for air exchange, τ_{exe} is twice the value of the mean age of air in the room, $\bar{\tau}$. Hence, obtaining the mean age of air through CFD simulations enables the calculation of air exchange efficiency which is one objective of this study. In conclusion, air exchange efficiency in this study is calculated using the combination of Equations 1 and 2 as shown below.

$$\varepsilon_a = \frac{\tau_n}{\tau_{exe}}$$
$$= \frac{V/Q}{2\,\bar{\tau}} \tag{4}$$

3. Contaminant removal effectiveness ε_c

In contrast to ventilation efficiency, contaminant removal effectiveness is an indicator based on the contaminant concentration at the exhausts, C_e to the average contaminant concentration in the indoor space $\bar{C}$ ("ASHRAE_Standard62-01_04_," n.d.) as shown in the following formula.

$$\varepsilon_c = \frac{C_e - C_s}{\bar{C} - C_s} \tag{5}$$

Here, C_s refers to the contaminant concentration at the supply which is usually considered as 0 in negative pressure isolation rooms analysis. This parameter is applied in this study using the plane basis approach where the average contaminant concentration in the breathing plane of healthcare workers (HCWs) is taken as the indoor space concentration.

CFD Simulation Setup

Solid Works Model

The Simulation study is carried out in ANSYS to improve the mechanical ventilation efficiency of the base configuration that was modelled using SOLIDWORKS as shown in figure 2.
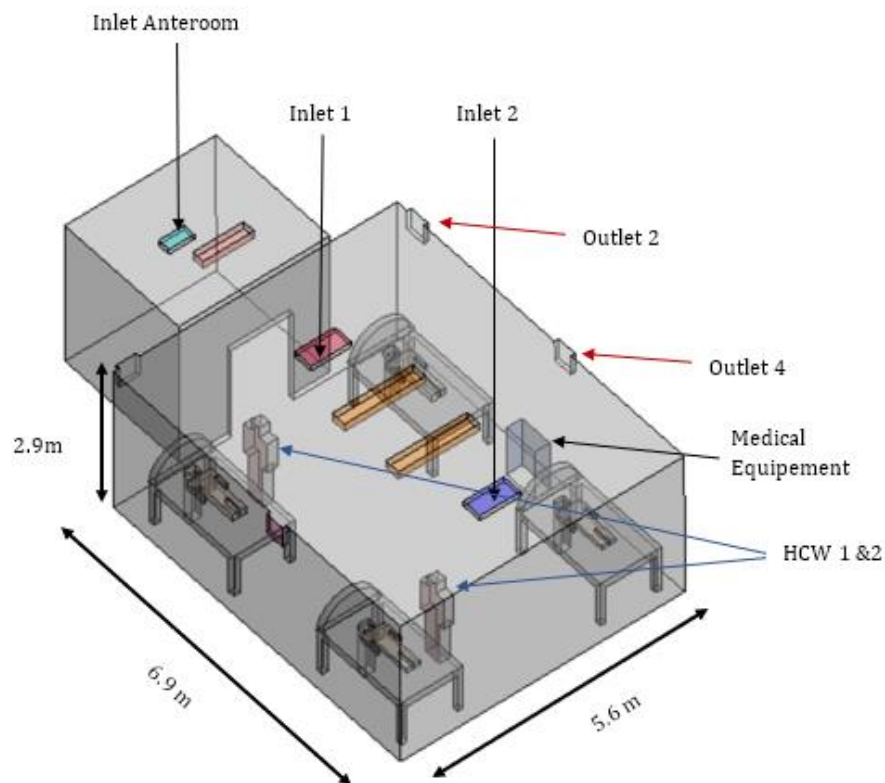

Figure 24 - Isolation unit A- 3-D geometry Model

The proposed design also includes the Anteroom for accurate simulation of airflow patterns in cases where the door room is unintentionally kept open. In addition to the components illustrated in the HVAC plan, the 3-D isolation unit also consists of models representing 4 patients, 2 healthcare workers, lamps, and medical equipment. Three ventilation configurations are suggested in view of improving the ventilation performance of the base configuration based on the analyzed indoor air quality indices and other vital measures.

Ansys Boundary conditions

The simulation study is carried out in both ANSYS – CFX and FLUENT. The air change efficiency ε_a is obtained via ANSYS -CFX using an "AgeOfAir" variable. The expression was turned on in the continuous fluid model. The age of air was calculated by specifying the age of air at the inlet to be 0. Then, a subdomain was created as the source term for the analysis and the age of air was increased by 1 second. The table below shows the initial condition for each ventilation configuration used in ANSYS -CFX.

Table 5- Boundary Conditions Ansys CFX solver

Boundary Conditions – CFX –Pre			
Mass flow Inlet	**Applicable Case**	**NOS**	**Value**
	Base case	2	0.362 kg/s
	Case-1-Displacement ventilation	4	0.181 kg/s
	Case-2- Stratum ventilation	2	0.362 kg/s
	Case-3- Air-jet -curtain	2	0.362 kg/s
Exhaust Outlet	Base case	4	-6 Pa
	Case-1-Displacement ventilation	4	
	Case-2- Stratum ventilation	4	
	Case-3- Air-jet -curtain	4	
Velocity inlet	Case-3- Air-jet -curtain	4	0.5 m/s, 1 m/s

The simulation carried out in ANSYS-FLUENT was utilized to obtain the contaminant removal effectiveness and several other vital results which aided in evaluating efficient ventilation configurations. The following tables represent the boundary conditions used for the simulation study in ANSYS – FLUENT.

I.   Initial conditions

An airflow velocity *of 0.617m*/s for the two inlets in the isolation space and *0.24m/s* supply for the anteroom diffuser is created using the values obtained from the HVAC Plan. All four exhausts in the domain are designed as pressure – outlets in order to generate the target value of negative pressure in the room which is -5pa compared to adjacent spaces.

Table 6 - Boundary Conditions- Fluent Solver

Boundary conditions				
Type	**Geometry**	**Temperature (K)**	**Velocity Magnitude (m/s)**	**Gauge Pressure (Pa)**
Inlet	Inlet (1 and 2)	288	0.62	0
	Inlet - Anteroom	288	0.24	5
	Patient Mouth	315	1.30	0
Outlet	4 Pressure Outlets	300	N. A	-6
	Geometry	**Temperature(K)**	**Heat Flux(W/m²)**	**Convection**
Walls	HCW	309	60	N. A
	Manakin	315	60	N. A
	Lamps	320	160	N. A
	Medical equipment	305	149	N. A
	Wall solid	N. A	N. A	14.7

II.   DPM Boundary conditions

Discrete phase particles in the continuous fluid domain should be assigned with particular behaviour in the vicinity of certain boundaries in order to simulate accurate tracks and obtain results that depict the real condition in such environments. Table 3 shows the DPM boundary conditions used for simulations.

Table 7 - DPM Boundary conditions – Ansys Fluent

Property	Type /value	
Injection type	Surface	
Surface options	Face normal direction	
Material	Carbon -dioxide	
Particle type	Inert	
Velocity Magnitude	1.3 m/s	
Total flow rate	4.183×10^{-4} kg/s	
Particle treatment	Unsteady	Interaction with continuous phase

The two supply inlets to the isolation room are assigned with a DPM boundary of "reflect" to ensure that exhaled particles do not leave the domain through any air supply inlet. Patient manikins, HCWs, medical- equipment, lamps, and walls are modelled as DPM boundary of "trap" to attach particles upon contact. "Escape" condition is used for patient mouth and exhausts to ensure particles in these boundaries escape in the direction specified.

Suggested Ventilation configurations
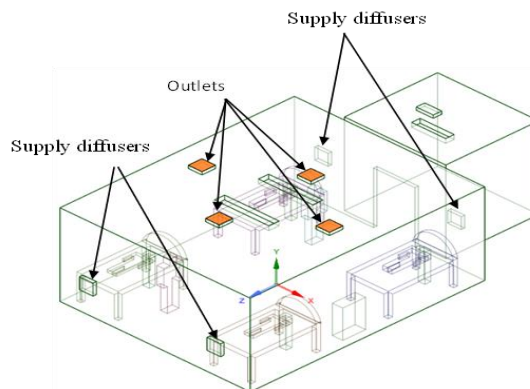I.   Displacement Ventilation

Figure 25 – Displacement Ventilation

The two supply diffusers in the base modal are replaced by 4 diffusers with cross-sections of 0.4 x 0.4m using a lower flow rate in view of reducing the inlet velocities. This is done in order to sweep contaminated air surrounding the patient and HCWs to the 4 exhaust vents on the ceiling without causing induction or air mixing. Two supply diffusers are placed on the west wall of the room while the remaining are placed on the entrance wall as shown in Figure 3.
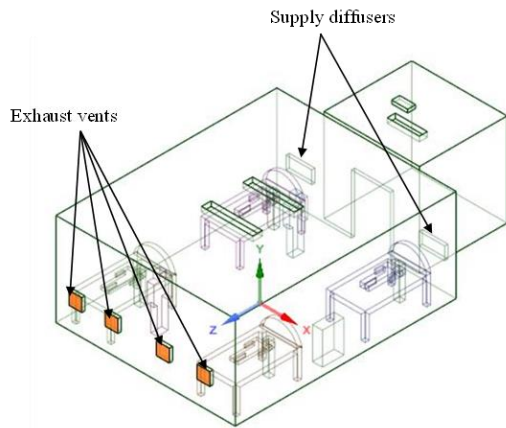
II.   Stratum Ventilation   III Curtain - Air- jet Ventilation
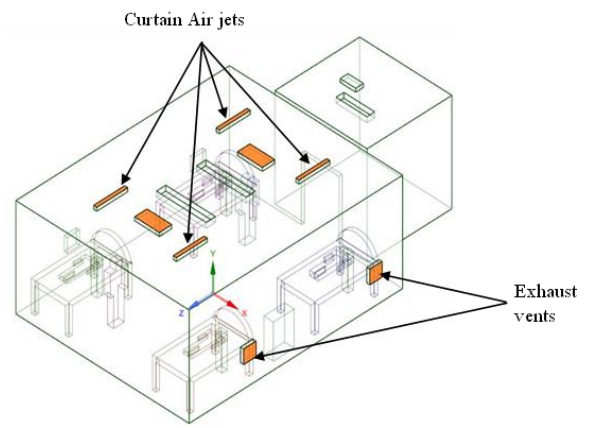

Figure 27 – Stratum Ventilation

Figure 26 – Curtain Air-Jet Ventilation

Stratum ventilation is a novel technology that targets only the occupied zone of an indoor environment. A stratum ventilation system mainly addresses thermal comfort, energy consumption and efficiency, and indoor air quality (IAQ). In the geometry shown in Figure 4, four exhaust vents are placed at the west wall of the isolation room, elevated just above the breathing plane of all 4 patients. The two supply diffusers are placed on the east wall (Entrance boundary wall) above the patient bed. In the Curtain air-jet model shown in Figure 5, the AII room is modified by adding 4 Air-jet curtains with a (1 m x 0.1m) cross-section on the ceiling in line with the available gap between the patient and the still position of HCWs. The supply diffuser size and location of the base geometry are unchanged to ensure sufficient airflow and cooling in the room.

4. RESULTS AND DISCUSSION

Grid Independence Test

Parametric analysis is carried out by defining Edge sizing for selected geometries and using the type of definition to be "Number of divisions" as the input parameter in ANSYS Mesh. Results variation for Volume- weighted- mean- velocity is calculated in the volume inside the solid boundaries of the geometry whereas Average -facet – velocity is calculated using the variations observed on the faces of each assigned exhaust. The convergence test results are plotted below.
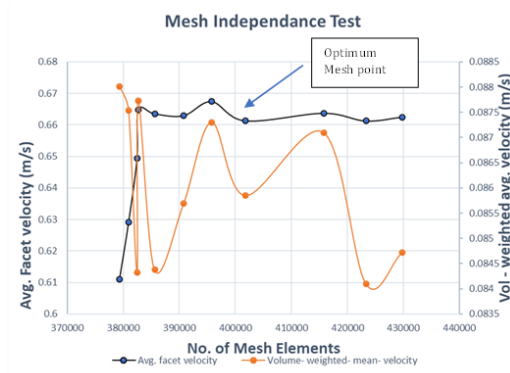

Figure 28 - Grid Independence test results

For a volume-weighted study, refinement in geometrical edges does not provide accurate improvements as expected. The optimum mesh size of 401809 elements with 78069 nodes is chosen for future simulations.

Air change efficiency

A steady-state simulation was carried out in ANSYS- CFX for each suggested ventilation configuration including the base model. The resulting age of air plots on the health care worker breathing plane is shown in the following figures.

A) Base Model

B) Displacement Ventilation

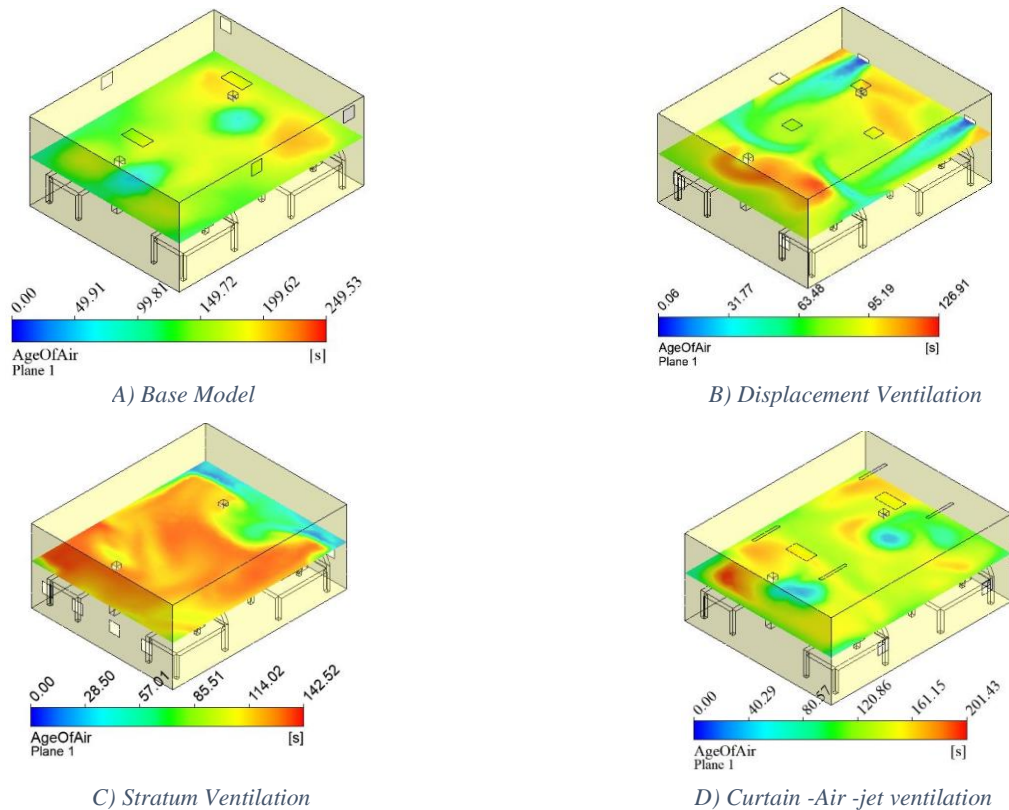*C) Stratum Ventilation*

D) Curtain -Air -jet ventilation

Figure 29 – Age of Air contour plots HCW breathing plane

In Figure 7 A), the age of air in the region of each patient mouth is considerably high compared to other regions of the room. This may increase the chances of possible accumulation of exhaled infectious particles in those regions. A potential stagnation region with 180 – 220s age of air (Orange colour) is created near-patient 2. This could happen due to air recirculation combined with exhausts unable to draw supplied air through a laminar flow. In contrast, case 1 in Figure 7 B) employing a displacement ventilation configuration exhibits a maximum age of air of only 128 seconds compared to the base model that yielded 249 seconds. Potential infectious particles exhaled from either patient 1 or 2 will be swept away in less than 50 seconds as observed in the colour bar shown in Figure 7 B). However, it is observed that a relatively low diffusive region occurs between patients 3 and 4 resulting in an open cavity like behaviour. (Lawson & Barakos, 2011) . Such regions are undesirable in the context of contaminant suppression. In contrast, one major advantage of the stratum ventilation configuration is that fresh air tends to continuously concentrate on the anteroom door region. Beyond this region, the age of air constantly lies between the range of 100 – 125 seconds (See Figure 7 C)). This regular age of air in the vicinity of HCW s and patients could diminish any zones of recirculation. Figure 7 D) is a representation of the curtain air-jet model with 0.5m/s air jet velocity. In contrast to an air jet velocity of 1m/s, the current configuration is capable of improving the age of air in the HCW breathing plane.

The table below represents the mean age of air obtained from ANSYS -CFX POST and the calculated air change efficiency of each corresponding configuration.

Table 8 – Summary – Mean age of air and Air change efficiency

	Configuration			
	Base Model	**Displacement Ventilation**	**Stratum Ventilation**	**Air -jet Curtain**
Mean age of Air (s)	172.3	76.3	91.7	133.2
Air change Efficiency (ε_a)	0.503	0.568	0.946	0.505

Contaminant removal effectiveness (ε_c)

Contaminant removal effectiveness can be obtained via several methods depending on the region of interest. Where there is a specific region or an area considered on the domain relative to the exhaust concentration, it is then referred to as the local contaminant removal effectiveness. Where there is no such location specified, it is referred to as the global contaminant removal effectiveness. The local contaminant removal effectiveness was obtained using the facet average on the exhaust and the HCW breathing plane.

Table 9 – Results - Global contaminant removal effectiveness

Ventilation Strategy	Area weighted avg exhaust (x1000) (kg/m³) (x10³)	Volume Avg contaminant concentration (kg/m³) (x10³)	Contaminant removal effectiveness
Base	0.036	0.149	0.243
Displacement	2.915	1.258	2.317
Stratum	0.929	0.677	1.371
Air jet	0.977	0.612	1.596

The mixing ventilation strategy implemented in the base model resulted in a low ε_c value of 0.243. This depicts that the contamination source and HCW breathing plane is in the zone of air circulation and hence increased the risk of direct exposure to exhaled contaminant particles. In contrast, each of the suggested configurations represented the upper limit ($\varepsilon_c > 1$) of the characteristic flow type for contaminant removal effectiveness and thus reducing the exposure to potential contamination by occupants in the facility.

Identifying correlations between air change efficiency and contaminant removal effectiveness enables accurate prediction of exhaled particle behaviour in the design stage of an AII room. Figure 8 represents the correlation between the two IAQ indices.
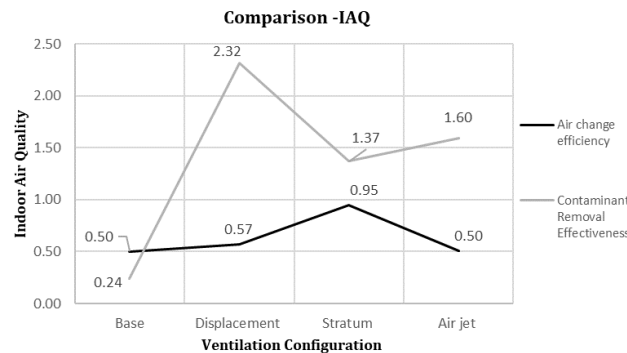

Figure 8 - Comparison of obtained indoor air quality indices

The base model, which represented a perfect mixing model with ε_a of 0.503, have also resulted in the lowest contaminant removal effectiveness of 0.252. Although similar mixing ventilation

configurations are required to validate this statement, the CFD study carried out by (Novoselac and Srebric 2003) has also provided factual results highlighting that an increase in air change efficiency, ε_a for a mixing ventilation system is directly followed by an increase in contaminant removal effectiveness as underlined in the current study. Such a correlation is not noticeable in other ventilation configurations namely, displacement and stratum where the air change efficiency is 0.568 and 0.946 respectively. Based on these results, developing correlations by equations or specific criteria solely based on these two tools is therefore considered unsuitable.

Exhaled particle tracking

Exhaled particle tracking was carried out using the DPM boundary conditions shown in Table 3. A time-based approach is used for each path line model. This approach in contrast to a domain length-based approach will provide more clarity when comparing each ventilation configuration since particle residence time with reference to its relevant position is vital in AII rooms.

| A) Base Model | B) Displacement | C) Stratum | D) Curtain Air -Jet |

pathlines-1
Time [s]

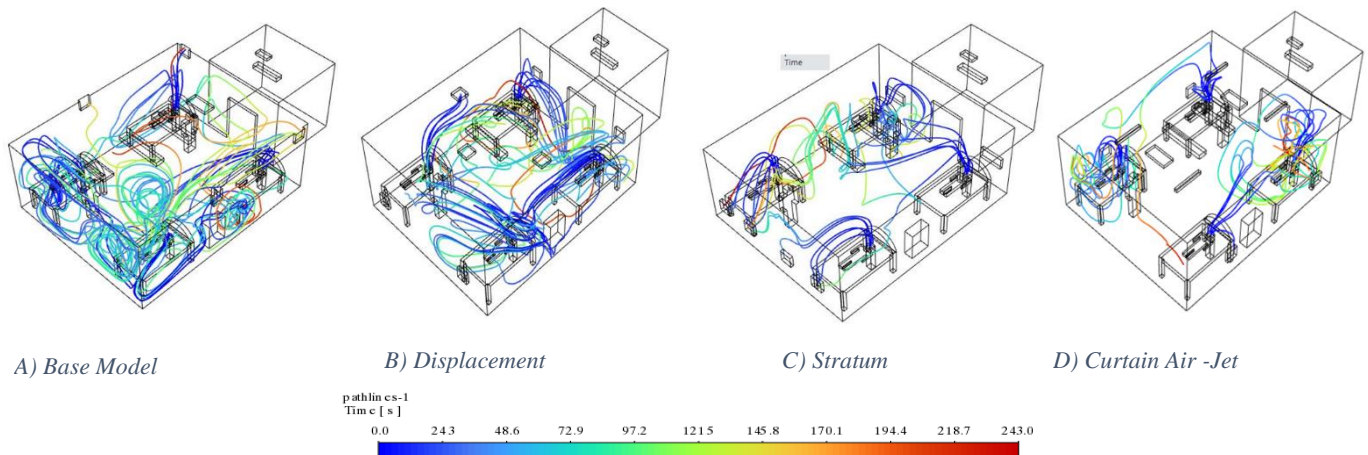| 0.0 | 24.3 | 48.6 | 72.9 | 97.2 | 121.5 | 145.8 | 170.1 | 194.4 | 218.7 | 243.0 |

Figure 9 – Exhaled particle tracking – Path line models

In the base model in Figure 9 A), pathlines surrounding HCW 2 is entrained in the supply air current entering the domain from supply inlet 2. Particle circulation is therefore dominant in this region for a time range of approximately 0 – 96 seconds. In the displacement ventilation model shown in Figure 9 B), it is observed that exhaled particles from each patient except for patient 3 reside at a lower level upon exhalation. It is considered beneficial when the airborne contaminant particle density is less than the room air density (*Engineering Guide Displacement Ventilation*, 2016a). The capability of upward motion of contaminants is strictly affected by its relative density. Since the exhaled CO_2 particle density is higher than the surrounding air density, contaminant escape efficiency is reduced in this model. In stratum ventilation, it is observed that HCW 1 is surrounded by newly released particles from patient 1 or 2. One possible flaw of this configuration is that exhaled particles of patients 1 and 2 do not reach the outlets in a streamlined path. However, the characteristic of stratum ventilation has been able to avoid two of the main challenges faced in AII rooms, namely: Air short-circuiting and Stagnation. (Lin et al.,2009) . In comparison with the simulation study results by (F. Wang et al. 2021), which concluded that a curtain air jet velocity of 0.5 m/s is best suited for contaminant containment, the current study also indicates better ventilation with a 0.5 m/s air jet velocity as seen in Figure 9 D).

Figure 10 summarizes the escaped particle efficiency for each configuration in the simulated time frame of 4 minutes.
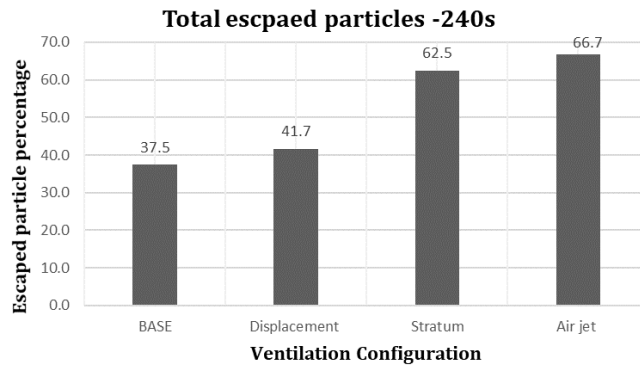
Figure 10 - Total escaped particle *percentage*

Temperature and Pressure distribution

The practical suitability of these configurations can be evaluated by analyzing the average temperature and pressure values as shown in the figures below and comparing them against specified values by guidelines.
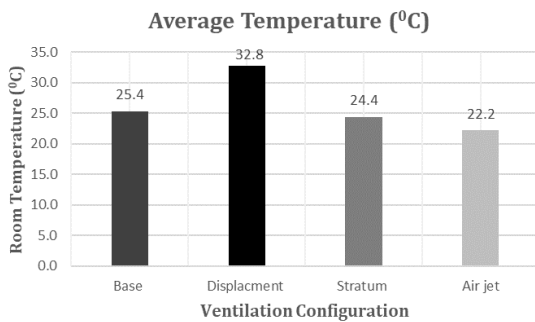

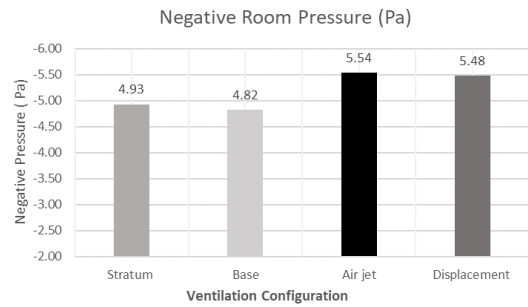Figure 11 – Temperature Distribution of each ventilation configuration

Figure 30 - Pressure differential of each ventilation configuration

ASHRAE Standard implemented guideline ("Engineering Guide Displacement Ventilation" 2016) specifies a temperature of 68F or 20^0C for the supply air temperature. Furthermore, it is specified that a displacement ventilation configuration with floor-level supply is most efficient when *'contaminant particles are warmer and lighter than the supplied air'*. Although exhaled particles are significantly warmer than the supply air, their higher density makes them heavier compared to the continuous airflow. This can be concluded as the pivotal factor for the increased temperature in the AII room. It should be noted that although Anteroom airflow can reduce the pressure differential, it is not capable of regulating the AIIR pressure towards a positive pressure. Therefore, it is predicted that AIIR differential pressure could be slightly higher when the Anteroom door is closed.

5. CONCLUSIONS

The main objective of this study was to support the ongoing multi-disciplinary efforts of understanding particle behaviour in isolation wards to minimize the spread of infectious airborne diseases. Air change efficiency values of both displacement and stratum ventilation configurations showed unidirectional flow characteristics while the base model showed a perfect mixing flow type.

Results revealed that there is negligible to no correlation between the two indices and possible correlations could exist only within a specific type of ventilation strategy. Furthermore, path line models showed that total escaped particles efficiency was significantly improved by 25 % and 30 % in both stratum and curtain-air-jet models respectively compared to the base model. Finally, these two models

could maintain a room temperature in the region of $21 - 25\ ^0C$ and negative pressure of -5 Pa as required by the original configuration confirming their suitability for actual operation.

6. ACKNOWLEDGEMENTS

REFERENCES

Adams, N. J., Johnson, D. L., & Lynch, R. A. (2011). The effect of pressure differential and care provider movement on airborne infectious isolation room containment effectiveness. *American Journal of Infection Control*, *39*(2), 91–97. https://doi.org/10.1016/j.ajic.2010.05.025

Cole, E. C., & Cook, C. E. (1998). Characterization of infectious aerosols in health care facilities: An aid to effective engineering controls and preventive strategies. *American Journal of Infection Control*, *26*(4), 453–464. https://doi.org/10.1016/S0196-6553(98)70046-X

Engineering Guide Displacement Ventilation. (2016a).

Gralton, J., Tovey, E., McLaws, M. L., & Rawlinson, W. D. (2011). The role of particle size in aerosolised pathogen transmission: A review. *Journal of Infection*, *62*(1), 1–13. https://doi.org/10.1016/J.JINF.2010.11.010

Khankari, K. (2017). Airflow dynamics of a patient room. *REHVA*, 52–58

Lawson, S. J., & Barakos, G. N. (2011). Review of numerical simulations for high-speed, turbulent cavity flows. *Progress in Aerospace Sciences*, *47*(3), 186–216. https://doi.org/10.1016/J.PAEROSCI.2010.11.002

Lin, Z. (2017). Stratum ventilation - a low-carbon way to thermal comfort and indoor air quality. *International Journal of Low-Carbon Technologies*, *12*(3), 323–329. https://doi.org/10.1093/ijlct/ctw020

Lin, Z., Chow, T. T., Tsang, C. F., Fong, K. F., & Chan, L. S. (2009). Stratum ventilation – A potential solution to elevated indoor temperatures. *Building and Environment*, *44*(11), 2256–2269. https://doi.org/10.1016/J.BUILDENV.2009.03.007

Novoselac_ASHRAE_Transactions_2003. (n.d.).

Pepper, I. L., & Dowd, S. E. (2009). Aeromicrobiology. *Environmental Microbiology*, 83–102. https://doi.org/10.1016/B978-0-12-370519-8.00005-5

Ren, S., Tian, S., & Meng, X. (2015). *Comparison of Displacement Ventilation, Mixing Ventilation and Underfloor Air Distribution System*.

Saravia, S. A., Raynor, P. C., & Streifel, A. J. (2007). A performance assessment of airborne infection isolation rooms. *American Journal of Infection Control*, *35*(5), 324–331. https://doi.org/10.1016/j.ajic.2006.10.012

Simons, M., Waters, J. R., & White, P. R. S. (2016). Local mean age of air: Predictive techniques compared: *Http://Dx.Doi.Org/10.1177/014362449902000409*, *20*(4), 211–218. https://doi.org/10.1177/014362449902000409

VG, C., CM, B.-S., MD, H., BJ, D., P, N., C, V., CL, W., JO, K., JT, C., & TR, F. (1993). Transmission of multidrug-resistant Mycobacterium tuberculosis among persons with human immunodeficiency virus infection in an urban hospital: epidemiologic and restriction fragment length polymorphism analysis. *The Journal of Infectious Diseases*, *168*(4), 1052–1055. https://doi.org/10.1093/INFDIS/168.4.1052

Wang, F., Chaerasari, C., Rakshit, D., Permana, I., & Kusnandar. (2021). Performance Improvement of a Negative-Pressurized Isolation Room for Infection Control. *Healthcare*, *9*(8), 1081. https://doi.org/10.3390/healthcare9081081

WELLS, W. F. (1934). ON AIR-BORNE INFECTIONSTUDY II. DROPLETS AND DROPLET NUCLEI. *American Journal of Epidemiology*, *20*(3), 611–618. https://doi.org/10.1093/OXFORDJOURNALS.AJE.A118097

FACULTY OF ENGINEERING

SLIIT UNI
THE KNOWLEDGE UNIVERSITY